UNIVERSITAT POLITÈCNICA DE VALÈNCIA

Department of Mechanical and Materials Engineering

PhD Thesis

Pantograph-catenary dynamic models and their implementation in hardware-in-the-loop tests

December 2022

Author: Jaime Gil Romero

Supervisors: Dr. Manuel Tur Valiente
Dr. F. Javier Fuenmayor Fernández

PhD Thesis

Pantograph-catenary dynamic models and their implementation in hardware-in-the-loop tests

for the degree of

Doctor in Industrial Engineering and Production

presented by

Jaime Gil Romero

at the

Department of Mechanical and Materials Engineering

of Universitat Politècnica de València

Supervised by

Dr. Manuel Tur Valiente
Dr. F. Javier Fuenmayor Fernández

Valencia, December 2022

PhD Thesis

Pantograph-catenary dynamic models and their implementation in hardware-in-the-loop tests

Author: Jaime Gil Romero

Supervisors: Dr. Manuel Tur Valiente
Dr. F. Javier Fuenmayor Fernández

QUALIFYING TRIBUNAL

President: Dr. _____

Vocal: Dr. _____

Secretary: Dr. _____

Valencia, December 2022

Abstract

There is an extensive network of electrified railway lines over the world. Most of them use overhead contact lines or catenaries to provide the trains with electrical power. Catenaries consist of electrified wires placed over the rail track, designed to contact the pantograph placed on the roof of the train. The proper operation of the system is very demanding, especially at high speed, when the continuity of the contact is compromised.

The most predominant tool for studying and designing the pantograph-catenary system is the use of numerical simulations. Notably, the Finite Element Method (FEM) is the most popular technique for modelling and simulating the dynamic interaction of the pantograph and the catenary. This method allows modelling catenaries with outstanding fidelity and without any loss of generality.

After the simulation stage, the pantograph and the catenaries have to be assessed by in-line experimental tests. However, there is an alternative that can replace those tests with a significant reduction in costs. The alternative method, called Hardware In the Loop (HIL), allows testing pantographs in the laboratory with a test rig that emulates the interaction with a virtual catenary. Different research groups have implemented HIL; however, in every attempt, a compromise solution has been adopted, demonstrating the challenging nature of HIL. This Thesis aims to advance in the field of HIL tests, pushing forward the capabilities of the technique and solving some of the limitations found in the literature. This Thesis proposes two different kinds of catenary models for their use in HIL tests.

The first is an analytical model based on a string of periodic geometric profile that accounts for the steady state. It reduces the complexity of the catenary but keeps the main features involved in the dynamic. The model has proven useful in explaining the fundamental dynamics of the catenary, helping understand the interference between two pantographs. This analytical model is suitable for HIL because of its low computational cost. An iterative algorithm is proposed to use the analytical model in HIL. The fact that the model is periodic permits a specific strategy to compensate the control loop delay. This strategy has excellent performance and accuracy, validated by comparing HIL tests with numerical simulations and getting an agreement. This agreement will not be possible if the pantograph model of the simulations is inaccurate. Therefore, the validation is carried out with a weight or mass model in place of the pantograph to eliminate potential differences. Even though the precision achieved is good, the analytical catenary model lacks fidelity, which has motivated the development of a more advanced periodic model.

The second catenary model for HIL tests is the Periodic Finite Element Model (PFEM), discretised with FEM to avoid further topological and structural simplifications. The model includes the periodicity condition, and the dynamics are solved by frequency analysis. Furthermore, the catenary non-linearities are considered in the formulation. An iterative algorithm, similar to the one used for the HIL tests with the analytical catenary, is used to realise HIL tests with PFEM catenaries. The previous strategy with a mass model is used to validate the test, confirming great precision. The results are gratifying due to the sophistication of the model, the accuracy of the tests and the cancellation of the delay. The tests simulate the response of realistic catenaries with the simplifying periodicity hypothesis. They are adequate for the dynamic of equal-span catenary at the central zone of every section, but future efforts have to be made to get rid of the periodicity condition while keeping the accuracy of the results.

Resumen

Existe una extensa red de líneas ferroviarias electrificadas en todo el mundo. La mayoría de ellas utilizan líneas aéreas de contacto o catenarias para suministrar electricidad a los trenes. Las catenarias son estructuras de cables ubicadas sobre las vías ferroviarias, diseñadas para ser contactadas por los pantógrafos que se encuentran sobre la parte superior de los trenes. El correcto funcionamiento del sistema requiere un alto nivel de exigencia, especialmente a alta velocidad, cuando la continuidad del contacto se ve comprometida.

La herramienta más empleada para el estudio y diseño del sistema pantógrafo-catenaria es el uso de simulaciones numéricas. En particular, el Método de los Elementos Finitos (MEF) es la técnica más extendida para modelar y simular la interacción dinámica del pantógrafo con la catenaria. Este método permite modelar catenarias con fidelidad y sin pérdida de generalidad.

Después de la etapa de simulación, el pantógrafo y la catenaria tienen que ser testados mediante ensayos experimentales en vía. Sin embargo, existe una alternativa que puede reemplazar esos ensayos con una reducción significativa de costes. Dicha alternativa, llamada Hardware In the Loop (HIL), permite testar pantógrafos en el laboratorio mediante un banco de ensayos que emula la interacción con una catenaria virtual. Diferentes grupos de investigación han implementado HIL; sin embargo, en todos los intentos se han adoptado soluciones de compromiso, lo que demuestra el reto que supone la aplicación de HIL. Esta Tesis pretende avanzar en el campo de ensayos HIL, impulsando las capacidades de la técnica y solventando algunas de las limitaciones encontradas

en la literatura. Para ello se proponen dos tipos diferentes de modelos de catenaria para su uso en ensayos HIL.

El primero es un modelo analítico basado en un cable tensado con perfil geométrico periódico que proporciona la solución estacionaria del sistema. Este enfoque reduce la complejidad de la catenaria, pero mantiene las principales características que intervienen en la dinámica. El modelo ha demostrado ser útil para explicar el comportamiento fundamental de la catenaria, ayudando a comprender el fenómeno de interferencia entre dos pantógrafos. Este modelo analítico es adecuado para HIL debido a su bajo coste computacional. En el presente trabajo se propone un algoritmo iterativo para utilizar el modelo analítico en HIL. El hecho de que el modelo sea periódico permite la aplicación de una estrategia específica para compensar el retraso del lazo de control. Esta estrategia tiene un excelente rendimiento y precisión, validados al comparar ensayos HIL con simulaciones numéricas y obtener coincidencia entre los resultados. Esta coincidencia no se podrá conseguir si el modelo de pantógrafo de la simulación es impreciso. Por lo tanto, la validación se realiza con un peso en el lugar del pantógrafo para eliminar las potenciales diferencias en el modelo. Si bien la precisión alcanzada es buena, el modelo analítico de catenaria carece de fidelidad, lo que ha motivado el desarrollo de un modelo periódico más avanzado.

El segundo modelo de catenaria para ensayos HIL es el Modelo Periódico de Elementos Finitos (MPEF), discretizado con el MEF para evitar adicionales simplificaciones topológicas y estructurales. En la formulación se incluye la condición de periodicidad y la dinámica se resuelve mediante análisis en frecuencia. Además, las no linealidades de la catenaria se consideran en la formulación. Un algoritmo iterativo, similar al utilizado para los ensayos HIL con catenaria analítica, es usado para realizar ensayos HIL con catenarias MPEF. La estrategia anterior de utilización de un peso se emplea para validar el sistema de ensayos, resultando tener una gran precisión. Los resultados son gratificantes debido a la sofisticación del modelo de catenaria, la precisión de los ensayos y la cancelación del retraso. Los ensayos realizados simulan la respuesta de catenarias realistas con la hipótesis simplificativa de periodicidad. Son adecuados para la dinámica de catenarias de vanos iguales en la zona central de cada cantón, sin embargo es necesario seguir realizando esfuerzos para eliminar la condición de periodicidad sin comprometer la precisión de los resultados.

Resum

Existeix una extensa xarxa de línies ferroviàries electrificades a tot el món. La majoria d'elles utilitzen Línies Aèries de Contacte o catenàries per a subministrar electricitat als trens. Les catenàries són estructures de cables situades sobre les vies ferroviàries, dissenyades per a ser contactades pels pantògrafs que es troben sobre la part superior de la locomotora. El correcte funcionament del sistema requereix un alt nivell d'exigència, especialment a alta velocitat, quan la continuïtat del contacte es veu compromesa.

L'eina majoritària per a l'estudi i disseny del sistema pantògraf-catenària és l'ús de simulacions numèriques. En particular, el Mètode dels Elements Finits (MEF) és la tècnica més usada per a modelar i simular la interacció dinàmica del pantògraf amb la catenària. Aquest mètode permet modelar catenàries amb fidelitat i sense pèrdua de generalitat.

Després de l'etapa de simulació, el pantògraf i les catenàries han de ser testats en assajos experimentals en via. No obstant això, existeix una alternativa que pot reemplaçar eixos assajos amb una reducció significativa de costos. Aquesta alternativa, anomenada Hardware in the Loop (HIL), permet testar pantògrafs en el laboratori amb un banc d'assajos que emula la interacció amb una catenària virtual. Diferents grups d'investigació han implementat HIL; no obstant això, en tots els intents s'han adoptat solucions de compromís, la qual cosa demostra el repte que suposa l'aplicació de HIL. Aquesta Tesi pretén avançar en el camp dels assajos HIL, impulsant les capacitats de la tècnica i solucionant algunes de les limitacions trobades en la literatura. Aquesta Tesi

proposa dos tipus diferents de models de catenària per al seu ús en assajos HIL.

El primer és un model analític basat en un cable tens amb perfil geomètric periòdic que proporciona la solució estacionària del sistema. Aquest model redueix la complexitat de la catenària, però manté les principals característiques que intervenen en la dinàmica. El model ha demostrat ser útil per a explicar la dinàmica fonamental de la catenària, ajudant a comprendre el fenomen d'interferència entre dos pantògrafs. Aquest model analític és adequat per a realitzar assajos HIL a causa del seu baix cost computacional. Aquest treball proposa un algoritme iteratiu per a utilitzar el model analític en assajos HIL de pantògrafs. El fet que el model siga periòdic permet l'aplicació d'una estratègia específica per a compensar el retard del llaç de control. Aquesta estratègia té un excel·lent rendiment i precisió, validats en comparar assajos HIL amb simulacions numèriques i obtenir coincidència entre els resultats. Aquesta coincidència no es podria aconseguir si el model de pantògraf de la simulació no és el correcte. Per tant, la validació es realitza amb una massa en el lloc del pantògraf per a eliminar les potencials diferències en el model. Si bé la precisió aconseguida és bona, el model analític de catenària manca de fidelitat, la qual cosa ha motivat el desenvolupament d'un model periòdic més avançat.

El segon model de catenària per a assajos HIL és el Model Periòdic d'Elements Finits (MPEF), discretitzat amb el MEF per a evitar simplificacions topològiques i estructurals addicionals. El model inclou la condició de periodicitat i la dinàmica es resol mitjançant anàlisi en freqüència. A més, les no linealitats de la catenària es consideren en la formulació. Un algoritme iteratiu, similar a l'utilitzat per als assajos HIL amb catenària analítica, és usat per a realitzar assajos HIL amb catenàries MPEF. L'estratègia anterior d'utilització d'una massa s'empra per a validar el sistema d'assajos, resultant tindre una gran precisió. Els resultats són gratificants a causa de la sofisticació del model de catenària, la precisió dels assajos i la cancel·lació del retard. Els assajos realitzats simulen la resposta de catenàries realistes amb la hipòtesi simplificativa de periodicitat. Són adequats per a la dinàmica de catenàries de vans iguals en la zona central dels seccionaments, no obstant això és necessari continuar fent esforços per a eliminar la condició de periodicitat sense comprometre la precisió dels resultats.

Acknowledgements

I feel really grateful for having encountered the research group in which I have developed my Thesis for the last four years. I want to thank my supervisor Manuel Tur, for directing my Thesis with enthusiasm and brightness. My supervisor F. Javier Fuenmayor, for his vast experience, integrity and support. My colleague Santiago Gregori, for his great understanding of the word cooperation, his determination, his constant awareness of the latest scientific developments and his rigour.

I want to make mention of Antonio Correcher, for the support provided in the control field.

I want to thank all my colleagues with whom I share the workplace, for the great environment and charming company. I want to thank all the staff and professors of the Department of Mechanical and Materials Engineering, especially José Martínez, for his disinterested attention and contagious joy.

I would like to acknowledge the importance of the support of my family, friends and girlfriend. Were it not for them, these years would have been much harder.

Preface

During the development of this Thesis, a global pandemic struck the world, significantly impacting transport and public funds. Also, a war has begun, prompting an energetic crisis. This is said without forgetting all the harm and pain that the previous facts have certainly caused to the world population in other more important fields unrelated to this work. Nevertheless, the aim of this Thesis has remained the same: improving a means of transport, the train, that has been and will be very beneficial for society.

Contents

Part I

Thesis report

Chapter 1

Introduction

1.1 Motivation

Only 30% of railway lines are electrified in the world. And knowing the global tendency towards decarbonisation, it is not surprising the high market volume of rail electrification and the fact that it is predicted to increase in the following years. Although about 60% of world electricity comes from fossil fuels, some countries have demonstrated to be able to produce more clean electricity, such as Norway, where just a 0.5% comes from this source. In the case of Spain, this data reaches a value of about 30%, having reduced by half the figure from 2005 [1].

Electrification is not the only development in the railway sector. The vast growth of high-speed lines in the last decades has changed the strategic position of train transportation in many countries, providing citizens with a fast option that, in many cases, beats air transportation. Since the first Spanish high-speed line three decades ago, Spain has adopted a strategy of expansion, becoming the second bigger network in the world with about 3700 km. The economic investment so far has been 56000 M € and another 73000 M € to be spent in order to achieve the final aim of 8740 km [2].

Among all the electrification systems, the Overhead Contact Line (OCL), broadly called catenary, is the most widely used, especially at high-speed lines

where almost the entire network is provided with catenaries. Catenaries consist of electrified wires placed over the rail track so that the trains can collect current. The connection between the catenary and the train is sustained via a pantograph that tries to keep a sliding contact with the contact wire of the structure. The OCL system allows great interoperability that is ensured via the European standard EN-50367 [3]. The system good performance is critical for the sustainability of high-speed railways and for achieving higher running speeds. From a mechanical point of view, the best current collection is achieved when the dynamic interaction between the catenary and the pantograph provides an uninterrupted contact. The main tool for studying the pantograph-catenary interaction, in the earliest stages of the design process, is the use of numerical simulations. The European standard EN-50318 [4] states the requirements for validating numerical simulations. Later, the pantograph-catenary system has to be proven in line, and the standard EN-50317 [5] regulates the measurement system for the experimental tests.

The motivation of this Thesis is to enhance the tools for studying the pantograph-catenary interaction; with the prospect that these tools will be helpful in improving the installations in the future and in achieving new challenges. Specifically, this work is aimed at nearing the latest technologies and the computational power to the experimental techniques used in the pantograph-catenary testing system.

1.2 The pantograph-catenary system

The OCL is a structure mainly composed of wires responsible for providing the trains with electric current. The design of the catenaries is subjected to the European Standard EN-50119 [6], which approaches safety, reliability, durability and maintenance. In Fig. 1.1, a high-speed catenary is represented where the main components are tagged. There are diverse catenary configurations, but essentially they have a similar arrangement.

The contact wire is the ultimate element of the OCL; it keeps contact with the pantograph and suffers wear. Besides the electrical design, from the mechanical point of view, the catenaries are designed to have proper dynamic behaviour and keep the contact wire within defined limits. The dynamic performance requires the contact wire to be tensioned, ensuring that the wave propagation speed in the wire is higher than the train speed. The tension also reduces the convexity of the catenary curve that the contact wire follows due to gravity, leading to a more uniform configuration. To manage the contact wire height

profile, the contact wire is supported by spatially-distributed variable-length droppers, which are attached to an auxiliary wire called messenger wire. To distribute the wear over the pantograph contact strip, the contact wire must follow a zig-zag trajectory in-plant layout. The zig-zag or staggering is achieved with steady arms, which laterally pull the contact wire, while avoiding any risk of collision with the pantograph. The structure that sustains the previous wires in the air consists of supports and brackets. Besides holding the steady arms, the brackets bear the weight of all the wires by the support points at the messenger wire. Due to the catenary topology, an increase in stiffness occurs close to the supports; thus, some catenaries mitigate this by including a stitch wire between the droppers and the messenger wire adjacent to supports.

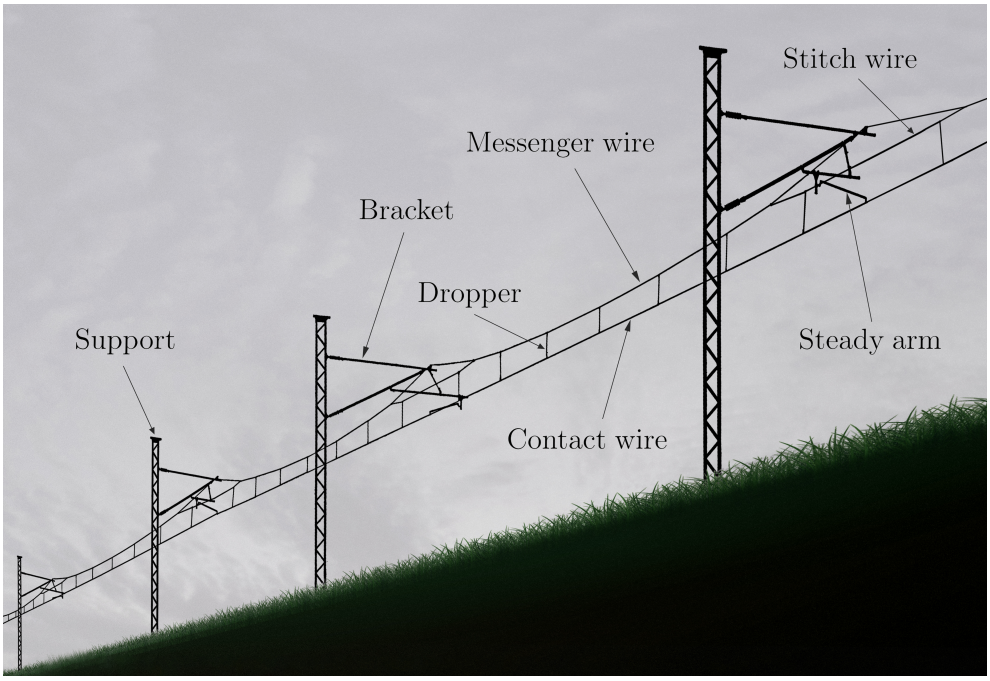

Figure 1.1: High-speed stitched catenary

The portion of the catenary between two supports is called span, which can be considered as the elemental cell of which the catenaries are made up. On a larger scale, the catenary is also split into sections; a section consists of several consecutive spans which share the same contact and messenger wires. At the outer supports of the section, there is a compensation system of weights and pulleys that ensures constant tension in both wires. The different sections of

the catenary have an overlap zone where the pantograph transitions between two consecutive sections. The section division facilitates installation and maintenance and allows better control of tensions and thermal deformations.

The pantograph is the mechanism responsible for contacting the catenary by pushing upward and absorbing the vibration of the contact wire that oscillates very quickly from the pantograph point of view. A DSA-380 pantograph is shown in Fig. 1.2; it consists of a mechanical linkage, a two-strip head, and an uplift system. The mechanical linkage is composed of the upper and the lower arms and allows the pantograph to adapt to the catenary height variations. The uplift system extends the mechanical linkage and pushes the entire mechanism against the contact wire. The pantograph head is responsible for following the height profile of the contact wire and thus is suspended by two pairs of v-shape springs connected to the upper-arm extreme in order to absorb the vibrations.

Figure 1.2: DSA-380 pantograph

1.3 Numerical simulations

The use of numerical simulations is a widely used tool for evaluating the pantograph-catenary dynamic performance during design. A multitude of aspects can be obtained and analysed from simulations, for example, the steady-arm uplift is vital for safety, and the contact force between the pantograph and the catenary is the most relevant magnitude for the current collection quality.

In most cases, the catenary is modelled via the Finite Element Method, whereby good fidelity and generality are achieved. Commonly, the generation of the dynamic model of the catenary consists of two separate problems: the static configuration problem and the dynamic problem. The initial configuration problem is devoted to solving the static equilibrium, where the large displace-

ments of the wires imply solving non-linear equations. After solving the initial configuration, the linearisation of the equations is suitable for the displacement range of the dynamic problem. Nonetheless, other non-linearities of the catenary, precisely the non-linear behaviour of droppers and contact loss, are considered in the dynamic problem [7, 8].

Diverse options are used to model the pantograph with different degrees of complexity. Multi-body models include the non-linear behaviour of the mechanical linkage, and FEM models additionally consider the deformation of the bars. However, more simple pantograph models, like lumped parameter models (Fig. 1.3), are broadly used for their simplicity and acceptable accuracy in the 0-20 Hz frequency range required in EN-50318 [4].

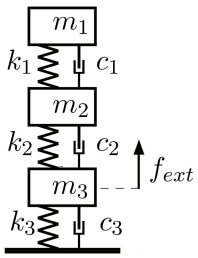

Figure 1.3: Lumped parameter model of the pantograph

It is necessary to define a contact model to couple the interaction of the pantograph and the catenary dynamic models. Generally, the *penalty* method is used to emulate the non-penetrability restriction. The *penalty* method replaces the mentioned restriction by penalising the penetration with a constant called contact stiffness. A high contact stiffness has to be tuned to achieve good precision while avoiding compromising numerical stability and ill conditioning of the system.

1.4 Hardware in the loop tests

Numerical simulations compute the interaction between the pantograph and the catenary virtual models. However, the real equipment has to be proved via in-line experimental tests, implying a higher investment. Hardware In the Loop (HIL) allows testing the pantograph in a laboratory while interacting with a virtual catenary model at a certain velocity. For instance, new pantograph systems or active control equipment could be tested with HIL. Compared to numerical simulations, these tests eliminate the uncertainty of the pantograph

model. Even though the pantograph models can be fitted by experimental adjustments, the presence of non-linearities makes the experimental data difficult to match.

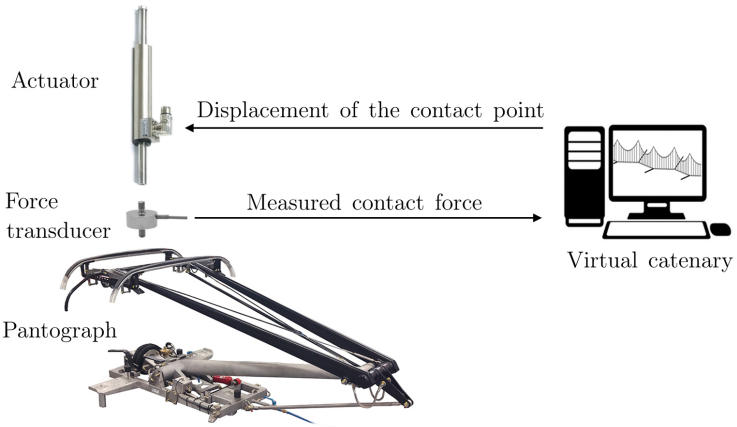

Figure 1.4: Schematic representation of HIL test

The implementation of HIL implies the interaction between a physical model and a virtual one; this makes HIL a technological challenge. A schematic representation of HIL tests of the pantograph-catenary is depicted in Fig. 1.4 with the main elements: the pantograph, the virtual model of the catenary, the actuator and the force transducer. The virtual catenary is a dynamic model that produces a displacement response and requires a force excitation to compute it. Specifically, the displacement of the contact point, which is the point along the contact wire travelling at the velocity set for the test. This displacement has to be transferred to the pantograph head through an actuator, imposing the response of the virtual catenary to the real pantograph. This causes a force between the pantograph and the actuator that is measured by a force transducer; the measured force value is used as input force for the virtual catenary model, where it is applied at the contact point.

There are strict requirements for the proper operation of the whole system. The virtual model has to be computationally efficient enough to be computed in real time. Furthermore the mentioned response should be transferred to the pantograph with immediacy to avoid affecting the dynamic of the catenary. The implementation of HIL requires the inclusion of compensatory and control techniques to mitigate the error produced by the transference of the virtual catenary displacement to the hardware.

1.5 Objectives

This work has been developed for a better understanding of the pantograph-catenary system and for the practical application of the improvements achieved in the theoretical field. The main objectives of the Thesis can be summarised as follows:

- **Development of simplified models.** The FEM is a well-established method for the simulations of the pantograph-catenary system with good accuracy and generality. However, analytical models can be helpful for a better understanding of the physical phenomena involved in the problem and for some applications that require a certain degree of simplicity.
- **Models for HIL.** Hardware in the loop tests entail the availability of numerical models of the catenary. This Thesis aims to define suitable models for the particular needs of HIL. This part includes: simplifications/adaptation of catenary models, algorithms for applying the previous models in HIL and computational strategies for increasing the accuracy of the tests.
- **Practical application of HIL.** The ultimate aim of this work is to accomplish HIL tests of a real pantograph effectively. The development and improvement of a HIL test rig and the troubleshooting tasks are carried out in this Thesis.

1.6 Thesis layout

Due to the fact that this Thesis includes a compendium of publications, the document is split into two parts. The first one is an overview of the work realised and the second one contains the publications that have been produced.

Part I includes this introduction, where the main subjects related to the Thesis have been presented. Immediately after this chapter, a review of the relevant publications found in the literature is presented in Chapter 2. In Chapter 3 the contributions of this Thesis are exhibited by summarising the publications of Part II. To conclude this overview, the discussion of the results, conclusions and future works are summarised in Chapter 4.

Part II includes four papers produced during the Thesis period. In Paper A, an analytical model composed of an infinite string and a visco-elastic support is used to study the behaviour of the catenary and the results are contrasted with

more accurate numerical simulations. In Paper B, an algorithm is proposed to perform HIL tests with the catenary model of Paper A. In Paper C, a formulation is developed to solve the dynamics of infinite periodic structures modelled by FEM; the formulation is used to model the catenary, and a similar algorithm to the used in Paper B is proposed to adapt the model for HIL tests. Utilising the formulation of Paper C, in Paper D, HIL tests with periodic catenary models are accomplished with proven accuracy.

Chapter 2

State of the art

As has been discussed in the previous Chapter, the pantograph-catenary dynamic interaction is a problem worth studying due to its extensive use. In this work the modelling of the system, the simplification of the models and the experimental technique of HIL are investigated. Therefore in this Chapter a literature review on those topics is presented.

2.1 Pantograph-catenary modelling

There are different techniques for the mechanical study of OCL as described in [8]. The alternatives are divided into computational simulations, hardware-in-the-loop tests and in-line testing. This section features the models found in the literature for simulations of the pantograph-catenary system.

The finite Element Method is a well-established technique for modelling catenaries and is the most frequently used. The benchmark exercise [7] features ten different software for solving the pantograph-catenary interaction, most of them based on FEM. The software PACDIN [9, 10], which participated in that benchmark exercise, has been developed in the same research group where this Thesis takes place. PACDIN is a FEM pantograph-catenary simulator based in Absolute Nodal Coordinate Formulation [11] that has been enhanced for a high computational performance [12].

In recent years, the catenary models have been enriched to incorporate more features initially not considered. In [13] and [14], the effect of catenary irregularities is considered and proved to affect the pantograph-catenary operation negatively. Specifically, in [13], the study includes realistic measurements of installed catenary. The deformation produced by temperature in a three-dimensional curved catenary is considered in the FEM model of [15]. Another factor that can affect the operation of the OCL is the crosswind. In [16], a FEM catenary is enhanced by the addition of stochastic fluctuating wind described by empirical spectrum. Also, the aerodynamics of the pantograph can affect its performance; a numerical simulation of the pantograph is carried out in [17] to study its dynamic effect, and the results are contrasted in the wind tunnel. A distinct feature included in the simulations is vehicle-track vibration. In [18], the pantograph base reproduces the translations and rotations of the train caused by random rail irregularities. Also, [19] is endowed with track-induced vibration, and it is concluded that only the low-frequency vibration will affect the dynamic interaction between the pantograph and catenary. Nevertheless, the effect of track irregularities has not been demonstrated to strongly influence the pantograph-catenary interaction.

The pantograph modelling also plays an important role in the system dynamics. There is a wide variety of pantograph models with different degrees of complexity, but the experimental behaviour of the pantographs is hard to match. In [20], the dissipative parameters of the pantograph joints are identified to adjust a pantograph model. In order to tune those parameters, the joints are tested disassembled, and good agreement between simulation and experiment results is claimed for the assembled model. In [21], a multi-body pantograph model with non-ideal joints and flexibility is developed with proper calibration. Additionally, the performance of the pantograph-catenary interaction is optimised using a inertance-integrated damping at the pantograph, achieving a significant improvement.

2.2 Simplified and periodic models of the catenary

FEM models have proved to be very suitable for modelling the catenary; they provide good accuracy and a limitless capacity for adapting to different catenary topologies. However, simplified models that assume a certain reduction of the system features can be helpful in some determined applications. In [22], the catenary is modelled as a single and two-degrees-of-freedom system with periodically time-varying mass and stiffness to obtain a method of relating the speed limit of the catenary to the parameters of the catenary. A dynamically

more complex model is presented in [23], where an infinite string with viscoelastic support is used to obtain the stationary response of lumped-parameter moving models coupled to the string.

The dynamic behaviour of the catenary can be characterised by the dynamics of periodic infinite structure when specific hypotheses are satisfied. This feature can be helpful to simplify the catenary models and is exploited for HIL test in this work. This periodic approach is used in diverse structures such as rails or bridges in the literature. The first attempt to solve this problem was made with analytic models based on a periodically supported infinite string/beam [24, 25, 26]. In all these references, the domain of the problem is reduced to the basic cell of the structure, and proper boundary conditions are set; besides that, some differences are found between them. The model of [24] considers an infinite periodic Euler-Bernoulli beam subjected to a uniform moving harmonic pressure field to model the rail. The modal approach is used in [25] to solve a set of finite repeated substructures, and the limit when the length tends to infinity is applied for the case of a moving constant load. The problem is also solved in [26], using the Fourier Transform. The previous solutions do not fit well the topology of the catenary due to the simple geometry. However, the approach given in [26] is extended in [27], where a two-level infinite catenary model, composed of an upper and lower string and equidistant dampers that connect both strings, is proposed. The wave equation provides the dynamic behaviour of the string, and a harmonic point load excitation is employed. Other similar models can also be found in the literature, such as that in [28], which is composed of several finite strings and is used to study the wave propagation and reflection phenomena in the catenary. The review of [29] can be consulted for a broad collection of analytic approaches for different structures under moving loads.

Another different approach is the so-called two-and-a-half dimensional (2.5D) finite element models, which allows to model structures with constant cross-sections. This strategy is found in [30] to model a rail. Fourier Transform with respect to space and time is performed to solve the problem, which allows the application of the periodicity condition on the reactions of the supports in the frequency domain. The same authors presented an improved model in [31] where the dynamic interaction of multiple wheels with the periodic model is computed through Fourier series decomposition of the contact force.

The previous periodic models have some topological limitations; a more general method is the so-called Wave Finite Element Method (WFEM) which provides more freedom thanks to the FEM discretisation. WFEM allows modelling finite and infinite periodic structures in the frequency domain [32, 33]. In [34],

some additional formulation is stated to compute the response of a WFEM model excited by a moving load. Additionally, this technique allows considering structures with a different cell in the periodic arrange [33].

2.3 HIL test

The HIL laboratory tests have been used in many fields to evaluate large structures that can not be held in conventional installations. The accomplishment of the tests depends on strict requirements, and researchers are making a considerable effort to increase the capabilities of HIL. A review of recent HIL achievements in diverse fields is collected in [35] and, in this Section, the HIL state of the art is revised for pantograph-catenary systems.

The early works on pantograph-catenary HIL test rig are found in the installations of the University of Southwest Jiaotong [36, 37] where the significant size reduction of the catenary model and truncated modal approach is employed for the high computational requirement of this real-time application. The test implementation is carried out by a hydraulic actuator controller with a servo valve. In the research group of Politecnico di Milano [38], the tests also rely on a hydraulic system and a moving window strategy is employed to simulate a periodic catenary model including three active spans. This model was enhanced in [39] with the consideration of the non-linear dropper behaviour, which is crucial for the fidelity of the catenary dynamics. This facility was tried out in [40] to test the active control system of the pantograph. Another upgrade was carried out by the same group in [41], where a more complex test rig allows the contact point to move over the surface of the pantograph strips to emulate the catenary stagger.

The models used in every HIL installation must be computed in real-time. Additionally, their response has to be transferred to the physical device with enough fidelity, and the presence of a delay is a challenge for this aim. In the literature, this problem is addressed using different ideas. In the Institute of Engineering Mechanics of China [42], the HIL technique is applied to the vehicle-bridge interaction, where a Recursive Prediction Optimal (RPO) compensator is utilised for dealing with the delay of HIL. RPO algorithm requires the transfer function of the actuator system to design an optimum control architecture in which an entire order observer provides the state of the system to feed an LQR controller and a recursive predictor compensator. In the results provided, the previous strategy outclasses three different methods. One of them is Polynomial Extrapolation [43] that consists of the extrapolation

of an n^{th}-order polynomial function, the method uses current and past target values to make a prediction that replaces the original target to compensate the delay. The second one is Inverse Compensation [44], in which the discrete transfer function of the actuator is inverted to counteract the actuator response, especially the delay. The last one is the Differential Feed-forward Compensator [45], where the PID controller of the actuator is augmented with a feed-forward scheme for delay compensation. This method assumes that the displacement control errors will not change so much in a few future time steps, in consequence, the feed-forward scheme is enhanced with the inclusion of the anticipated error.

An interesting approach of the control system is considered in the University of Bristol [46, 47] for the benefit of HIL tests of the pantograph-catenary system. This simulation is denominated DSS (Dynamically Substructured System) due to the proposed architecture of the control system. Most HIL tests are realised in an open-loop strategy, requiring an ideal transference system and strict technical specifications. Therefore, DSS suggests an interface that entails a closed loop, in which the response of the virtual model is compared with the current status of the actuator, leading to a control action for reducing the differences. In the work [46] proposed by the same group, DSS is implemented with a very elementary catenary model of one degree of freedom and variable stiffness. Linear Substructuring Control (LSC) is implemented to control the actuator, and the tests run with a shock absorber replacing the pantograph. The results are satisfactory for the control field but are still far from a proper pantograph-catenary characterisation. Thus, this approach is enhanced in [47] utilising a sliding window approach for the catenary but testing the same simplified pantograph model. The results achieved in [47] show that the accuracy of HIL of the catenary is still a challenge by comparison with emulated HIL test. Finally, in [48], the DSS strategy is tested with a real pantograph in the same installation with a relatively good agreement in the frequency domain. The work conducted at the University of Wien [49] employs a moving mesh formulation in combination with absorbing boundary layers; its strategy can be classified as DSS since it also develops a control algorithm based on the energy equation to limit the error in the controlled position of the catenary and avoid the instability produced by delays.

Chapter 3

Contributions

This Thesis includes a compendium of four articles in Part II, where the contributions that have been published or submitted are presented. This Chapter summarises the four papers and fundamentally discusses the main results achieved; for further details, the papers can be consulted. Papers A and C are devoted to developing models of the catenary. In contrast, Papers B and D include experimental work on Hardware-in-the-loop tests.

3.1 Paper A

This paper develops a new analytical pantograph-catenary model to get a closed-form expression of the contact force. The catenary is governed by the telegraph equation and the pantograph by a lumped parameter model. The proposed model is based on a previous model presented in [23], here denominated Analytical String Model 1 (ASM1). In [23], a explicit solution of the telegraph equation is proposed and analysed in different cases. In Paper A, the governing equation is modified by including a Kelvin-Voigt damping model to get a dissipative behaviour similar to that incorporated into the FE model. This leads to a different equation from [23] with higher order, which is solved in this work. In [23], the contact wire height profile is not included, but it plays an essential role in the dynamic behaviour of the pantograph-catenary system [50, 51, 14, 52]. Therefore, in this work, the height profile of a real catenary contact wire is incorporated into the model.

The interaction contact force obtained with the analytical model is compared with a verified FE model solution [9, 10]. To obtain a response as similar as possible to that of FE models, the stiffness and mass parameters of the analytical model are properly tuned by following a proposed methodology based on static equilibrium and wave propagation.

3.1.1 Analytical model of the catenary

The proposed Analytical String Model (ASM2) is composed of an infinite string prestressed with tension T and supported by a continuous visco-elastic layer, as shown in Fig. 3.1, with $\overline{k}$ and μ being the stiffness and linear density coefficients per unit of length, respectively.

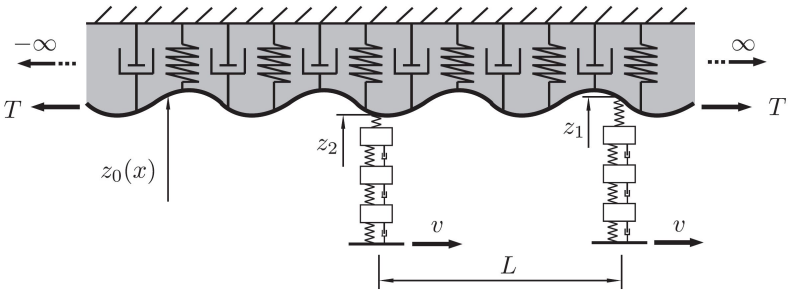

Figure 3.1: Two pantographs coupled to the ASM2 with initial height $z_0(x)$.

The string subjected to a load $p(x,t)$ is governed by the equation:

$$\mu\frac{\partial^2 w}{\partial t^2} - T\frac{\partial^2 w}{\partial x^2} + \left(\alpha\mu + \beta\overline{k}\right)\frac{\partial w}{\partial t} - \beta T\frac{\partial}{\partial t}\left(\frac{\partial^2 w}{\partial x^2}\right) + \overline{k}w = p(x,t) \qquad (3.1)$$

where $w = w(x,t)$ is the vertical displacement of the contact wire and for this case $p(x,t) = F_0 e^{i\Omega t}\ \delta(x - vt)$ because harmonic moving load is considered with frequency Ω and velocity v. Note that a Kelvin-Voigt damping model is included in the differential equation, where the damping terms are a linear combination of the inertial and elastic terms.

The solution to Eq. (3.1) is given by:

$$w(x,t) = \frac{1}{2\pi}\int_{-\infty}^{\infty} \frac{F_0\ e^{-i(k(x-vt)-\Omega t)}}{\lambda k^3 + \eta k^2 + \tau k + \sigma}\mathrm{d}k \qquad (3.2)$$

where:

$$\begin{aligned}\lambda &= i\beta T v \\ \eta &= T - \mu v^2 + i\beta T \Omega \\ \tau &= i\left(\alpha\mu + \beta\overline{k}\right) v - 2\mu v \Omega \\ \sigma &= \overline{k} + i\left(\alpha\mu + \beta\overline{k}\right)\Omega - \mu\Omega^2\end{aligned} \tag{3.3}$$

Applying the residue theorem to Eq. (3.2), the string vertical displacement is:

$$w(x,t) = \begin{cases} iF_0 \sum\limits_p \dfrac{e^{-i\left(k_p^\Omega (x-vt) - \Omega t\right)}}{\lambda \prod\limits_{r\neq p}\left(k_p^\Omega - k_r^\Omega\right)}; & x - vt \leq 0 \\ -iF_0 \sum\limits_q \dfrac{e^{-i\left(k_q^\Omega (x-vt) - \Omega t\right)}}{\lambda \prod\limits_{r\neq q}\left(k_q^\Omega - k_r^\Omega\right)}; & x - vt > 0 \end{cases} \tag{3.4}$$

where k_p^Ω are the poles of the integrand of Eq. (3.2) with a positive imaginary part and k_q^Ω are the poles with a negative imaginary part. The analytical expressions of the poles are found in Paper A.

Additionally, the contact wire initial height profile is included. Then, the total string height can be written as:

$$z(x,t) = z_0(x) + w(x,t) \tag{3.5}$$

where $z_0(x)$ is the initial height, which depends on the position x.

3.1.2 Frequency response function

Due to the linearity of the system, the problem can be solved first in the frequency domain, after which Fourier Transform can be used to get the solution of a general problem. The dynamic interaction of two pantographs coupled to ASM2 is solved by getting first the Frequency Response Functions (FRFs) of every system independently.

Given two points 1 and 2 over the string, located at a distance L and both moving at the same speed v (see Fig. 3.2), the FRF of the string H_{12} is defined as the ratio between the vertical displacement of 1 and the harmonic force applied at 2:

$$H_{12}(\Omega) = \frac{w(vt + L, t)}{F_0 e^{i\Omega t}} \tag{3.6}$$

Replacing the expression (3.4) in Eq. (3.6) and considering the signs of the poles, the FRF is:

$$H_{12}(\Omega) = \frac{-ie^{-ik_1^\Omega L}}{\lambda\left(k_1^\Omega - k_2^\Omega\right)\left(k_1^\Omega - k_3^\Omega\right)} \tag{3.7}$$

Similarly, H_{21} can be defined as the ratio between the displacement produced in 2 and the excitation applied at 1:

$$H_{21}(\Omega) = \frac{ie^{ik_2^\Omega L}}{\lambda\left(k_2^\Omega - k_1^\Omega\right)\left(k_2^\Omega - k_3^\Omega\right)} + \frac{ie^{ik_3^\Omega L}}{\lambda\left(k_3^\Omega - k_1^\Omega\right)\left(k_3^\Omega - k_2^\Omega\right)} \tag{3.8}$$

When the displacement is measured at the force application point, the direct FRF is:

$$H_{11}(\Omega) = H_{22}(\Omega) = \frac{-i}{\lambda\left(k_1^\Omega - k_2^\Omega\right)\left(k_1^\Omega - k_3^\Omega\right)} \tag{3.9}$$

On the other hand, the FRF of the pantograph model:

$$H_{\mathrm{p}}(\Omega) = \frac{1}{k_{\mathrm{h}}} + \left[-\Omega^2\mathbf{M}_{\mathrm{p}} + i\Omega\mathbf{C}_{\mathrm{p}} + \mathbf{K}_{\mathrm{p}}\right]^{-1}_{(1,1)} \tag{3.10}$$

where $\mathbf{M}_{\mathrm{p}}$, $\mathbf{C}_{\mathrm{p}}$ y $\mathbf{K}_{\mathrm{p}}$ are the mass, damping and stiffness matrices of the pantograph respectively, and k_{h} the contact stiffness. Additionally, the operator $[\ ]_{(1,1)}$ extracts the first row first column element of the matrix which refers to the upper mass degree of freedom of the pantograph.

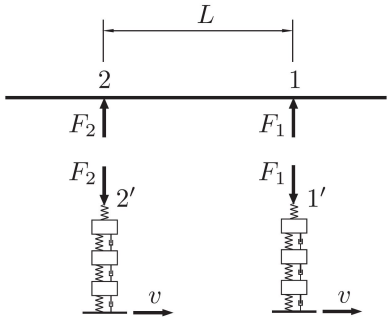

Figure 3.2: Contact forces in the coupled string model with two pantographs.

The contact forces F_1 and F_2 between each pantograph and the string, represented in Fig. 3.2, are the unknowns of the problem. The linearity of Eq. (3.4) allows writing the vertical displacement of the points 1 and 2 as the superposition of the displacement produced by each force acting separately and the geometric profile z_0. The height of points 1 and 2 should be equalled to the height of the points $1'$ y $2'$ which belong to the pantograph (see Fig. 3.2) to set the equations for solving the interaction forces. Finally, an expression is obtained that relates the forces in the frequency domain $\tilde{F}_1$ and $\tilde{F}_2$ to the geometric profile of the contact wire $\tilde{z}_0$ in the frequency domain:

$$\begin{bmatrix} -H_{\mathrm{p}}(\Omega) - H_{11}(\Omega) & -H_{12}(\Omega) \\ -H_{21}(\Omega) & -H_{\mathrm{p}}(\Omega) - H_{22}(\Omega) \end{bmatrix} \begin{Bmatrix} \tilde{F}_1 \\ \tilde{F}_2 \end{Bmatrix} = \begin{Bmatrix} 1 \\ e^{i\frac{\Omega L}{v}} \end{Bmatrix} \tilde{z}_0 \quad (3.11)$$

Supposing $z_0(x)$ can be expressed as a sum of harmonic functions, the Eq. (3.11) and the superposition principle allow the computing of the different harmonic components of the CF.

3.1.3 Parameter setting

The parameters of the analytical model are adjusted to get a static and dynamic behaviour similar to the precise FEM catenary model. The damping parameters, α and β, and the tension T, are also defined in the FEM model and do not need to be adjusted. The value of $\overline{k}$ is tuned to match the static equilibrium response of both the ASM2 and FE models. Additionally, the value of μ is adjusted to find similar wave propagation behaviour in both ASM2 and FE models. More details about this setting is found in Paper A.

3.1.4 Pantograph interference

Understanding the multiple pantograph interference is a complex task, [53, 54]. In this work, the ASM2 is used to get an expression for evaluating the optimal distances between pantographs.

The CF of the trailing pantograph is analysed with respect to the pantograph separation L. To simplify the analysis, the initial height of the contact wire $z_0(x)$ is considered a pure harmonic function with frequency Ω. As the trailing pantograph has a negligible effect on the leading pantograph [55, 53], it is assumed here that $H_{12}(\Omega) = 0$, which implies that the CF of the leading pantograph is not modified with respect to the single operation scenario. In addition, the exponential term which includes k_3^{Ω} can be neglected in $H_{21}(\Omega)$

(Eq. (3.8)) due to this wave being strongly damped for velocities lower than v_c.

The best performance of the trailing pantograph, or the minima of $\left|\tilde{F}_2\right|$, is found when the displacement created by the leading pantograph at the trailing one is in phase opposition with respect to the geometric profile. For every frquency Ω, there is a group of equidistant optimal values of L that minimise the amplitude of the trailing pantograph CF:

$$L_{\min} = \frac{2\pi n - arg(C_a)}{\Omega/v + k_{2R}^{\Omega}} \; ; \qquad n = 0, 1, 2, ... \tag{3.12}$$

where C_a is a constant that can be consulted in Paper A. This indicates that by placing the pantographs at one of those distances away, a specific frequency of the second-pantograph contact force is attenuated by the presence of the first pantograph.

3.1.5 Numerical results

The ASM2 implies important simplifications compared to the more complex FE models. The continuous visco-elastic support does not strictly describe the complex dynamics of the droppers and the messenger wire. Thus, the analytical model lacks of variable stiffness, wave reflections and non-linearities. Additionally, the analytical model includes the periodicity hypothesis and only serves to compute the steady state.

The Contact Force (CF) of the ASM2 is compared with a catenary modelled by the FEM model. The FE catenary model is defined long enough to get a quasi-steady response in its central spans. The CF is filtered by a 20 Hz low-pass filter, following the guidelines in [3]. For the single pantograph operation, the contact force obtained by ASM2 is compared in Fig. 3.3 (in the frequency domain) and Fig. 3.4 (in the temporal domain) with that computed by the FE model for excitation frequencies ranging from 0 to 20 Hz and the pantograph running at 200, 250, 300 and 350 km/h. There is a reasonable similarity between the results of both models since the magnitude of the analytical results is not too far from the FE results. However, significant discrepancies are found at 350 km/h in the first two harmonics.

The CF standard deviation σ is the variable most often used to quantify current collection quality. The standard deviation σ is plotted versus train velocity in Fig. 3.5. As σ depends on the mean CF in the FE model, FEM results are shown with a mean CF of 70, 80, 90 and 100% of the maximum mean CF

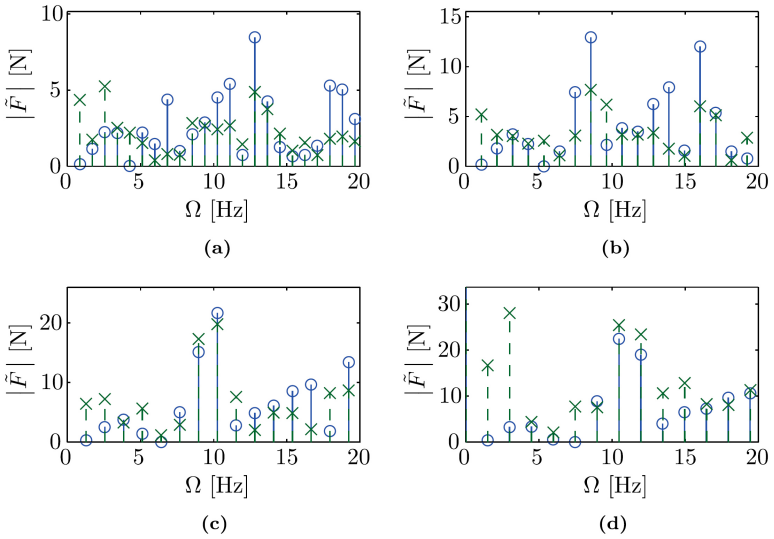

Figure 3.3: CF in the frequency domain at (a) 200 km/h, (b) 250 km/h, (c) 300 km/h and (d) 350 km/h. ○ ASM2 ×FEM.

allowed by EN-50367 [3]. However, for the ASM2 the mean value of the CF (F_{m}) does not have any influence on σ; therefore, F_{m} is not indicated in the figure. Despite all the simplifications introduced in the analytical model, it is able to give a good approximation of σ with respect to the more accurate results obtained from the FE model. Especially the similarity for the maximum mean contact force allowed by the standard is remarkable. Note that the mean CF effect is negligible for velocities smaller than 250 km/h for the studied pantograph-catenary system.

For a double pantograph operation, the standard deviation of the CF of the trailing pantograph σ_2 is compared with the FEM results in Fig. 3.6 for a wide range of L at the operating speeds of 200, 250, 300 and 350 km/h. Considering all the differences between the models, the approximation obtained by the analytical model has reasonable accuracy for the three first cases. Still, a bigger standard deviation is predicted with ASM2 as in the single pantograph operation at 350 km/h.

In Eq. (3.12), it has been stated that every harmonic component of the contact force of the trailing pantograph is attenuated at specific periodic values of L. In Fig. 3.6, since $z_0(x)$ contains several harmonics, the fluctuating σ_2 behaviour

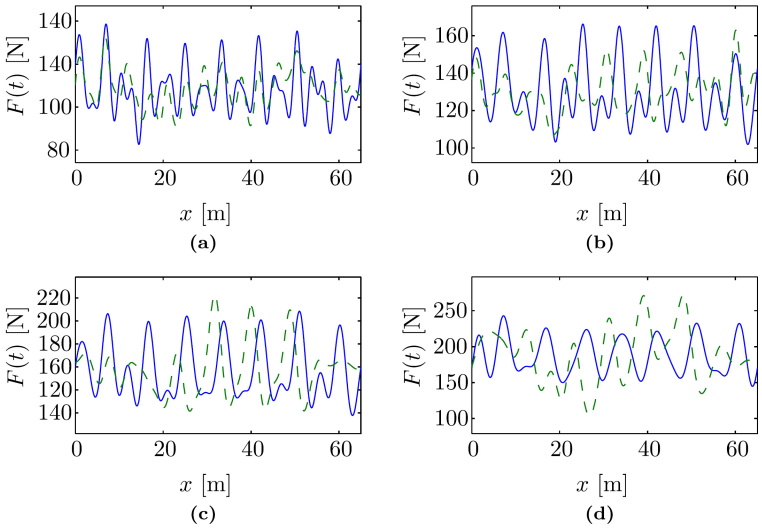

Figure 3.4: CF in the time domain at (a) 200 km/h, (b) 250 km/h, (c) 300 km/h and (d) 350 km/h. —ASM2 – – FEM for a central span.

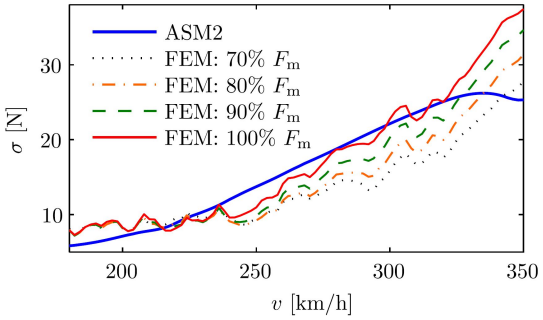

Figure 3.5: Comparison of the standard deviation of the CF between the ASM2 and the FE model for different pantograph velocities and different values of the mean CF.

is produced by the contributions of all the CF harmonics, which are minimised at $L_{\min}(\Omega)$.

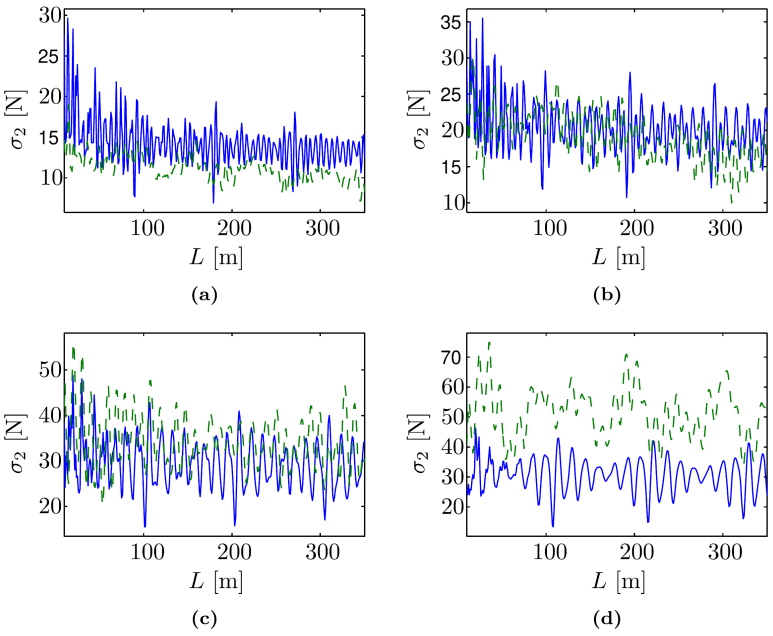

Figure 3.6: SD of the trailing pantograph CF with respect to the distance between pantographs at (a) 200 km/h, (b) 250 km/h, (c) 300 km/h and (d) 350 km/h. —— ASM2. – – FEM.

3.2 Paper B

In Hardware-In-the-Loop (HIL) tests, the catenary model should be as realistic as possible but, at the same time, must be solved in real-time, which is usually achieved by using simplified catenary models instead of more complex finite element models. In this work, we propose a new method for performing pantograph HIL tests using the proposed model in Paper A, which considers the main dynamic features of the catenary and the initial contact wire height profile.

A catenary with equal-length spans is illustrated in Fig. 3.7. In the central spans of the catenary section, the pantograph contact force reaches a quasi-stationary regime characterised by its repetition in every span. In that zone, the catenary can be considered a periodic catenary. Thus, the contact force $f_c(t)$, the geometric profile $z_0(t)$ and the height of the contact point of the catenary $z_c(t)$ are considered T-periodic functions of period $T = L/v$, where L is the span length and v is the train speed.

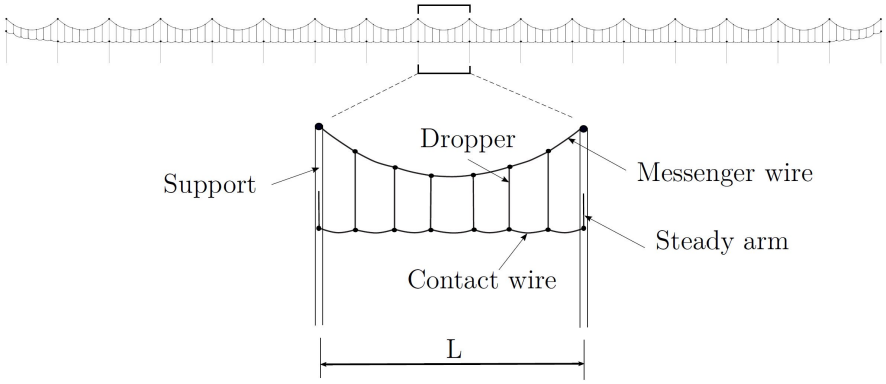

Figure 3.7: Scheme of a catenary section and detail of a single span.

Let us assume that the periodic interaction force is discrete (as in HIL tests) and known for a whole span, $f_c(t_n)$ with $n = 0, \ldots, N-1$, in which $N = L/(v\Delta t)$. This discrete force can be shifted to the frequency domain $F_c(\omega_k)$ by applying the Discrete Fourier Transform (DFT). Following, the receptance found in Eq. (3.9) allows getting the displacement of the contact point in the frequency domain $U_c(\omega_k)$:

$$U_c(\omega_k) = H_{11}(\omega_k)F_c(\omega_k) \tag{3.13}$$

The total height of the contact point is obtained by adding the DFT of the geometric profile $Z_0(\omega_k)$ to the displacement produced by the force:

$$Z_c(\omega_k) = Z_0(\omega_k) + U_c(\omega_k) \tag{3.14}$$

This holds for:

$$\omega_k = k\frac{2\pi}{N\Delta t} \quad k = 0, \ldots, N-1 \tag{3.15}$$

Finally, the Inverse Discrete Fourier Transform (IDFT) is used to return to the time domain, $z_c(t_n)$

The static configuration of the catenary $z_0(x)$ can be obtained by different methods. For example, semi-analytical methods are used in [56], or a method based on a Finite Element (FE) model was proposed in [9]. Here we use a non-linear FE model [57] to obtain the height of the contact wire $z_0(x)$. The representation of a 65-meter-span geometric profile in the spatial domain, $z_0(x)$, and in the frequency domain, $Z_0(\omega_k)$, is found in Fig. 3.8.

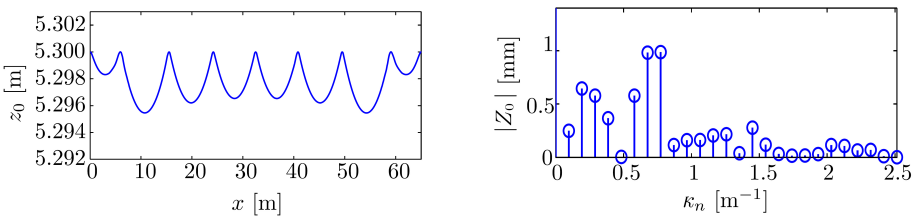

Figure 3.8: Contact wire height profile (a) Space domain (b) Frequency domain

3.2.1 Iterative algorithm

The height of the contact point in a whole span of the catenary $z_c(t_n)$ can be calculated if the periodic contact force is known in advance. In a HIL test, the force is measured every time step t_n and, in general, it is not periodic. Here we propose an iterative method to find the steady solution of the problem using the periodic formulation of the analytic catenary in HIL.

As in HIL tests, the basic premise is that a contact force value is obtained every instant, and the model has to provide a displacement value of the contact point. In this method, the contact force is measured in consecutive instants that can be grouped in sets of N values corresponding to one span. Every set b is considered as a block or span of the catenary and the force values of the set are named $f^b(t_n)$. The contact force in the frequency domain is obtained by the DFT of the contact force of a block. To avoid waiting until the completion of a span to compute the displacement of the contact point, the contact force of block b is built with measures of the previous span and the current one. Thus, at any instant t_n, the contact force in the frequency domain is calculated as:

$$F_c^n(\omega_k) = \sum_{m=0}^{n} f_c^b(t_m) e^{-i\omega_k m\Delta t} + \sum_{m=n+1}^{N-1} f_c^{b-1}(t_m) e^{-i\omega_k m\Delta t} \tag{3.16}$$

Finally, the Eqs. (3.13) and (3.14) and the IDFT allows obtaining $z_c(t_n)$ to be sent to the actuator in a HIL test. In this application of the IDFT, the frequency content can be reduced to take off the higher involved frequencies in the test that are not in the range of interest and can cause instabilities.

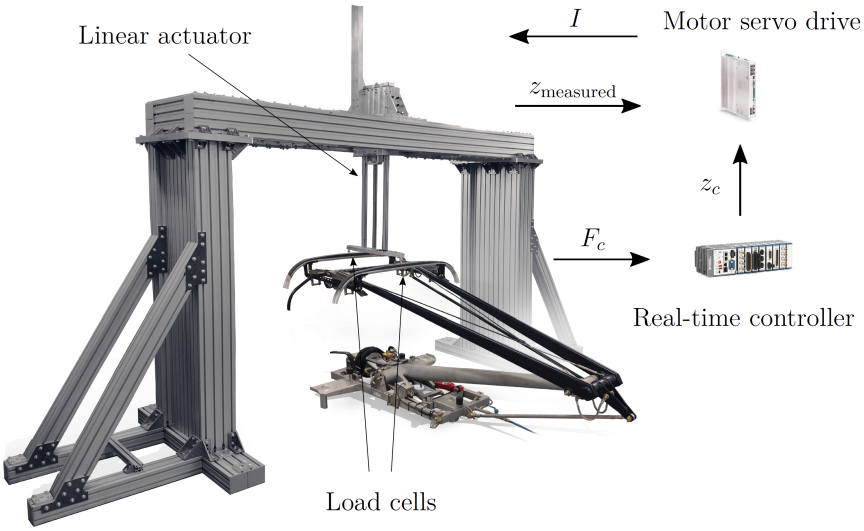

Figure 3.9: HIL test rig.

3.2.2 HIL test rig

The main components of the HIL test rig are depicted in Fig. 3.9. The contact force on each collector strip of the pantograph is measured employing a load cell. This signal is filtered and conditioned and finally acquired by the National Instruments® cRio-9040 real-time controller in which the analytical catenary model runs to provide the contact-point height to be followed by the linear actuator (LinMot® 70x400U), simulating the catenary movement.

All the tasks are shown schematically in Fig. 3.10. The contact force f_c between the linear actuator and the pantograph is measured, filtered and sampled to feed the catenary model, which provides the contact point height z_c every $\Delta t = 1$ ms. However, communications between the real-time controller and the motor servo drive (LinMot® E1400) cannot take place at this rate, so one value out of every N_{com} values of z_c is sent, via Ethernet UDP communication, to LinMot servo drive. The value received by LinMot z_{com} is set as the new reference, and the controller tries to reach this reference by generating a set of intermediate reference points linearly interpolated from the previous reference z_{old} to z_{com}. The LinMot servo drive uses a PID controller, which works at a higher rate, to fulfil these intermediate references. The whole loop described requires a certain time to be accomplished. Compensating the test rig delay in the HIL tests is crucial because omitting this step could modify the final

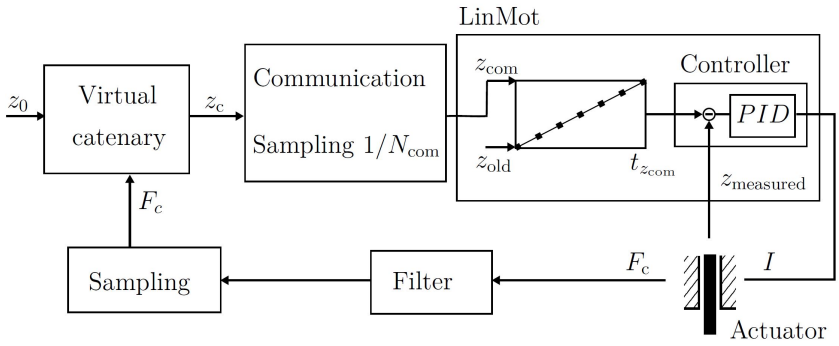

Figure 3.10: Simulation cycle of tasks in HIL test.

response or make it unstable. Due to the fact that the response is always defined in the domain of a period, an advanced position can be sent to the actuator to counteract the delay.

3.2.3 Experimental results

To validate the control system and the operation of the HIL test rig, an experimental validation test was carried out in which the pantograph was replaced by a mass of 5.29 kg directly attached to the linear actuator, as shown in Fig. 3.11. The objective is to eliminate the uncertainty of the physical model tested to match the HIL test with a computational simulation.

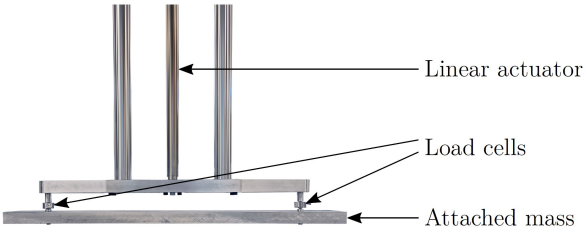

Figure 3.11: Mass attached to the linear actuator for the validation test.

In Fig. 3.12, experimental results of a HIL test with the mass are compared with the same problem computationally solved. The frequency range considered in the results is up to 25 Hz. The experimental results are almost identical to the analytical solution, indicating satisfactory experimental validation.

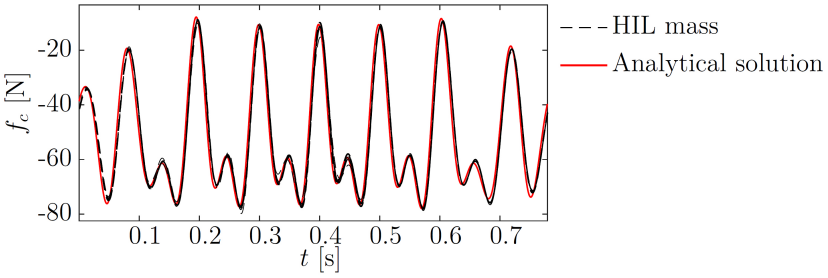

Figure 3.12: Comparison of the contact force in the mass HIL test (10 spans overlapped) at 300 km/h with the analytical solution.

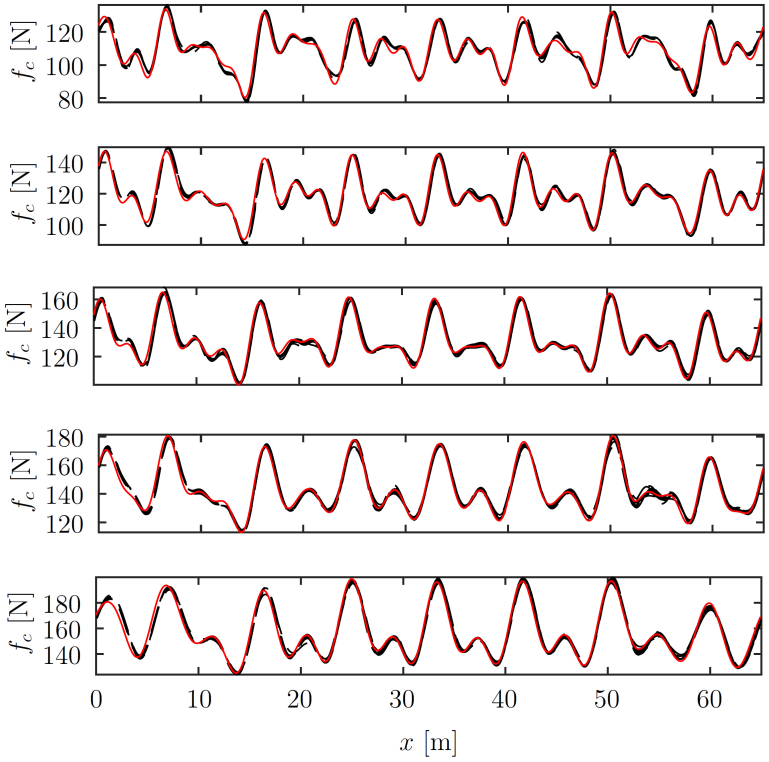

Figure 3.13: Comparison of the contact force obtained from the pantograph HIL test (10 spans overlapped in black) and the analytical solution with a linear pantograph model (red curves). Tests performed at 200, 225, 250, 275 and 300 km/h from top to bottom.

Once the test has been validated, a pantograph is placed in the test rig to be tested. The contact force up to 25 Hz obtained is shown in Fig. 3.13 with the pantograph running at 200, 225, 250, 275 and 300 km/h. This contact force is also compared in Fig. 3.13 with the analytical solution obtained using a linear lumped-parameter pantograph model showing remarkable similarity between them.

3.3 Paper C

This work aims to provide an entire framework to realise HIL tests with a periodic catenary model. This paper has two different tasks; the first one is devoted to solving the steady-state interaction of constant velocity moving loads with periodic structures modelled by the FEM. The developed model is denoted Periodic Finite Element Model (PFEM). The second part presents a strategy for using PFEM in HIL tests. The global objective is to perform high-fidelity HIL pantograph tests dealing with the usual control-loop delay in this type of test.

An infinite periodic railway catenary is shown in Fig. 3.14. As a periodic structure, the catenary is subdivided into consecutive blocks b of length L, which are repeated infinitely in the x axis. The pantograph moves at a constant speed v, and the interaction with the catenary will be indefinitely repeated at every block if the stationary state is achieved. Therefore, the external contact force applied to the catenary is a periodic moving load of period $T = L/v$.

Let us define the field of displacement in specific direction as $u(x, y, z)$. In this particular problem, the displacement field is repeated in each block. Thus, the periodicity condition reads as follows:

$$u(t, x, y, z) = u(t - bT, x + bL, y, z) \tag{3.17}$$

which allows the description of the response of the entire catenary with one single block so that the response of the reference block $b = 0$ will be considered from now on. This reference block is discretised by the Finite Element Method (FEM), and the displacements of its N_{dof} nodal degrees of freedom are denoted by $\mathbf{u}(t)$. The nodes of the FE mesh of the reference block can be divided into left (L) and right (R) boundary nodes and inner (I) nodes, as shown in Fig. 3.14.

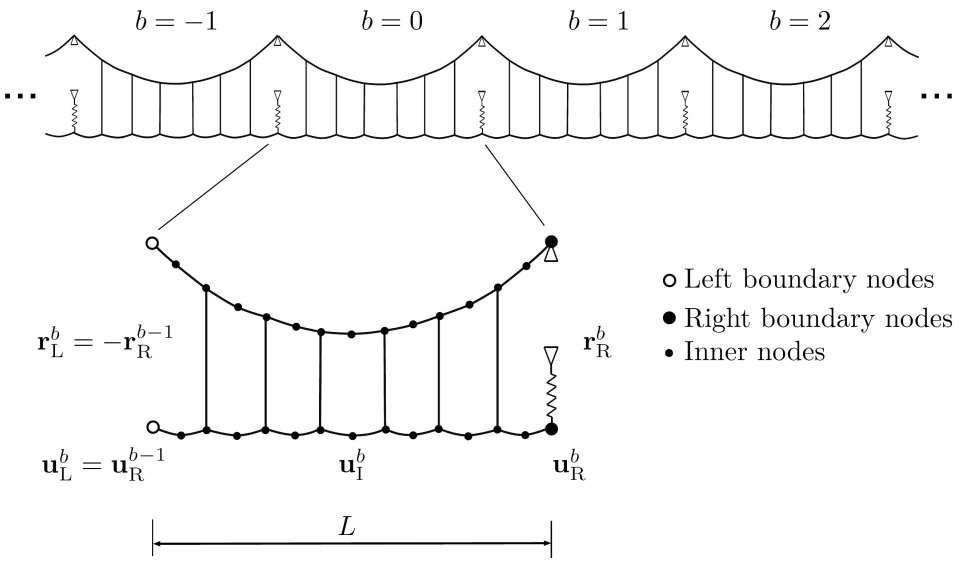

Figure 3.14: Catenary as a periodic infinite structure and Finite Element discretisation of block $b = 0$.

3.3.1 Frequency Response Function

The strategy entails shifting the problem to the frequency domain in which the periodicity condition is more easily stated.

Displacements of the left boundary nodes $\mathbf{u}_{\mathrm{L}}$ must fulfil Eq. (3.17), that is:

$$\mathbf{u}_{\mathrm{L}}(t) = \mathbf{u}_{\mathrm{R}}(t+T) \tag{3.18}$$

Which, after applying the Fourier Transform, becomes:

$$\mathbf{U}_{\mathrm{L}}(\omega) = e^{i\omega T}\mathbf{U}_{\mathrm{R}}(\omega) \tag{3.19}$$

being $\mathbf{U}_{\mathrm{L,I,R}}(\omega)$ the Fourier Transform of $\mathbf{u}_{\mathrm{L,I,R}}(t)$, respectively.

The nodal equivalent external force vector $\mathbf{F}$ can be divided into left, inner and right nodal degrees of freedom, namely $\mathbf{F}_{\mathrm{L}}$, $\mathbf{F}_{\mathrm{I}}$ and $\mathbf{F}_{\mathrm{R}}$, respectively. If the degrees of freedom of left and right boundary nodes are adequately defined (mesh compatibility), $\mathbf{F}_{\mathrm{L}}$ and $\mathbf{F}_{\mathrm{R}}$ are related through the following equation:

$$\mathbf{F}_{\mathrm{L}} = e^{i\omega T}\mathbf{F}_{\mathrm{R}} \tag{3.20}$$

In the reference block, the dynamic equation in the frequency domain is:

$$\begin{aligned} \mathbf{D}(\omega)\,\mathbf{U} &= \mathbf{F} + \mathbf{R} \\ \mathbf{D}(\omega) &= \mathbf{K} + i\omega\mathbf{C} - \omega^2\mathbf{M} \end{aligned} \tag{3.21}$$

where $\mathbf{M}$ is the mass matrix, $\mathbf{K}$ is the stiffness matrix and $\mathbf{C}$ is the damping matrix of the substructure contained in a single block. The reaction force vector $\mathbf{R}$, applied to the left and right boundary nodes $\mathbf{R} = [\mathbf{R}_\mathrm{L},\ \mathbf{0},\ \mathbf{R}_\mathrm{R}]^\top$, is also unknown.

Considering the periodicity condition again and the action-reaction principle, the reaction force vector in the left and right boundary $\mathbf{R}_\mathrm{L}$ and $\mathbf{R}_\mathrm{R}$ are related by:

$$\mathbf{R}_\mathrm{L} = -e^{i\omega T}\mathbf{R}_\mathrm{R} \tag{3.22}$$

Operating with Eqs. (3.21), (3.22) (3.20) and (3.19), the relation between the nodal forces and nodal displacement is obtained:

$$\left\{ \begin{array}{c} \mathbf{U}_\mathrm{L} \\ \mathbf{U}_\mathrm{I} \\ \mathbf{U}_\mathrm{R} \end{array} \right\} = \mathbf{H}(\omega) \left\{ \begin{array}{c} \mathbf{F}_\mathrm{I} \\ \mathbf{F}_\mathrm{R} \end{array} \right\} \tag{3.23}$$

3.3.2 Impulse response

Below, the necessary step to move from the frequency domain to the time domain is stated. As the structure is modelled with FEM, Eq. (3.23) cannot be analytically defined but is computed for a discrete number of frequencies N_f with a frequency increment $\Delta\omega$:

$$\omega_k = k\Delta\omega \qquad k = 0, \ldots, N_\mathrm{f} - 1 \tag{3.24}$$

In addition, time t is also discretised with a time increment Δt:

$$t_n = n\Delta t \tag{3.25}$$

In Eq. (3.23), the receptance $\mathbf{H}(\omega)$ relates nodal displacement with nodal forces. The next step is to create a different operator $I(\omega, \mathbf{x}, \mathbf{y})$ that relates physical points, specifically, the displacement of point $\mathbf{x}$ with the force of point $\mathbf{y}$. To that end, the FEM shape functions, $\mathbf{N}_\mathrm{I}(\mathbf{x})$ and $\mathbf{N}_\mathrm{R}(\mathbf{x})$, are employed:

$$I(\omega, \mathbf{x}, \mathbf{y}) = \mathbf{N}(\mathbf{x})\ \mathbf{H}(\omega)\ \left\{ \begin{array}{c} \mathbf{N}_\mathrm{I}(\mathbf{y})^\top \\ \mathbf{N}_\mathrm{R}(\mathbf{y})^\top + e^{-i\omega T}\mathbf{N}_\mathrm{L}(\mathbf{y})^\top \end{array} \right\} \tag{3.26}$$

where the term $e^{-i\omega T}\mathbf{N}_{\mathrm{L}}(\mathbf{y})^{\top}$ is used to include the excitation produced in elements out of the reference block but sharing nodes with the reference block.

By applying the Inverse Discrete Fourier Transform to Eq. (3.26), the impulse response at time step t_n is obtained as:

$$h(t_n, \mathbf{x}, \mathbf{y}) = \sum_{k=0}^{N_f-1} a_k \mathrm{Re}\left(I(\omega_k, \mathbf{x}, \mathbf{y})\, e^{i\omega_k n \Delta t}\right) \Delta\omega \tag{3.27}$$

being $a_k = 2$ if $k \neq 0$ or $a_k = 1$ if $k = 0$. $h(t_n, \mathbf{x}, \mathbf{y})$ is the displacement of point $\mathbf{x}$ at time t_n when a unitary force is applied at $\mathbf{y}$ at $t_n = 0$.

The pantograph is virtually moving at a constant speed v and applies a vertical contact force $f_{\mathrm{c}}(t_n)$ at the contact point, whose displacement is labelled as $u_{\mathrm{c}}(t_n)$. There are N_{c} virtual contact points in the domain of the block corresponding with the time steps. The impulse response function $h(t_n, \mathbf{x}, \mathbf{y})$ can be used to compute the vertical displacement of the contact point produced by all the values of the contact force:

$$u_{\mathrm{c}}(t_n) = \sum_{\hat{n}=0}^{N_{\mathrm{c}}-1} \mathbb{I}(n, \hat{n})\; f_{\mathrm{c}}(t_{\hat{n}}) \tag{3.28}$$

in which:

$$\mathbb{I}(n, \hat{n}) = h(t_n - t_{\hat{n}}, \mathbf{x}_{\mathrm{cw}}(t_n), \mathbf{y}_{\mathrm{cw}}(t_{\hat{n}}))\Delta t \tag{3.29}$$

where $\mathbf{x}_{\mathrm{cw}}(t_n)$ and $\mathbf{y}_{\mathrm{cw}}(t_{\hat{n}})$ are the coordinates of the contact point in function of the time step.

In addition to the displacement due to interaction with the pantograph, the vertical position of the contact wire depends on the static configuration of the catenary. If $z_{\mathrm{cw}}(t_n)$ is the contact wire height at the initial catenary configuration, the total height of the contact point at time step n can be obtained from:

$$z_{\mathrm{c}}(t_n) = z_{\mathrm{cw}}(t_n) + u_{\mathrm{c}}(t_n) \tag{3.30}$$

3.3.3 Hardware In the Loop test methodology with a linear catenary model

The contact force measured in the test rig is the input of the virtual catenary model, which must supply the contact point vertical position in real time.

Eq. (3.28) condenses in a $N_c \times N_c$ matrix $\mathbb{I}(n, \hat{n})$ the steady-state vertical displacement of the contact point at time t_n as a function of the stationary force applied in all contact points of the block at time $t_{\hat{n}}$ for $\hat{n} = 0, ..., N_c - 1$.

Matrix $\mathbb{I}(n, \hat{n})$ can be precomputed which makes the proposed model very suitable for use in HIL testing because few operations are required to obtain the contact point response. We propose to apply this model in combination with an algorithm by adapting the iterative procedure proposed in Paper B to a periodic catenary model scenario. This procedure allows both the virtual catenary and the physical pantograph to achieve the steady-state regime in a HIL test.

Defining k as the time step or global iteration of the HIL test. The iterative method runs the HIL test for consecutive blocks of N_c time instants. The time step is also labelled as $\overline{n}$ that initialise to 1 at the beginning of every block b. The contact force is measured at a given iteration k (or $\overline{n}$ in the time domain of every block). At this moment the contact force values measured from t_0 to $t_{\overline{n}}$ are available in the current block. To complete the set of N_c measures of contact force required to compute the response of the catenary model, the contact force values from $t_{\overline{n}+1}$ to t_{N_c-1} are taken from the previous block $b-1$. Thus, by combining Eqs. (3.30) and (3.28) the contact point height at iteration k is computed as:

$$z_c^k(t_n) = z_{cw}(t_n) + \sum_{\hat{n}=0}^{\overline{n}} \mathbb{I}(n, \hat{n})\ f_c^b(t_{\hat{n}}) + \sum_{\hat{n}=\overline{n}+1}^{N_c-1} \mathbb{I}(n, \hat{n})\ f_c^{b-1}(t_{\hat{n}}) \tag{3.31}$$

Note that the response $z_c(t_n)$, defined from t_0 to t_{N_c-1}, must be updated for all t_n every iteration k.

Once the contact wire height is available, only the vertical position of the contact point for the next time step $z_c^k(t_{\overline{n}+1})$ is sent to the actuator. The method runs iteratively step by step until the measured contact force in two consecutive blocks matches with a given tolerance. The delay compensation strategy is performed by sending the displacement $z_c^k(t_{\overline{n}+D})$ to advance the response D steps, corresponding to the delay.

3.3.4 Hardware in the loop method with nonlinear catenary model

The consideration of the non-linear behaviour of droppers is detailed in Paper C. The same idea introduced in [10] but adapted to account for the periodic nature of the system is applied in this work. The proposed formulation is developed in two stages. In the first, the response is computed with the linear model described in Subsection 3.3.3. The second is devoted to applying correction forces to the slack droppers. The non-linear correction forces are added by using analogue operators to Eq. (3.29) defined in each dropper. To satisfy the condition of no compression forces, a system is solved in which the non-linear forces are the unknowns. This part computational cost is equivalent to solving a linear system of order equal to the slack droppers at any time step.

3.3.5 Numerical results

In this subsection, the results are displayed; the data of the catenary model can be found in Section 6 of Paper C. The method proposed in [10] is used to build the FE model of the block necessary for the PFEM model. The same method is used to obtain a conventional FEM model of the catenary for validation purposes. We have made a long enough catenary section to assume the steady-state regime on its central spans. In this way, transient effects are negligible due to the notable length of the FEM catenary model and it is expected to obtain the same solution in both the proposed periodic model (PFEM) and the finite length FEM model.

The algorithm proposed is tested in a virtual HIL simulation in which a numerical pantograph model is used to replace the real pantograph used in a true HIL test. The time integration of the pantograph model is carried out independently of the catenary model through the Hilber-Hughes-Taylor (HHT) integration method [58]. In this virtual test, the displacement of the catenary contact point obtained from Eq. (3.31) is imposed on the pantograph model, and the contact force in the next time step is computed.

In the numerical case analysed in this section, the velocity of the pantograph is set at 250 km/h, and the virtual HIL simulation runs until there are no noticeable differences in the computed contact force of two consecutive blocks. The contact force obtained in successive blocks of the virtual test is depicted in Fig. 3.15. The non-linear correction forces of droppers can be seen in Fig. 3.16. It can be observed that, after several blocks, the curves reach an agreement, and convergence is achieved. To ease convergence of the virtual HIL test, during the first 20 s of the simulation, the imposed displacement has been

multiplied by a factor that increases linearly from 0 to 1. This is reflected in the increasing values in the first blocks of the results.

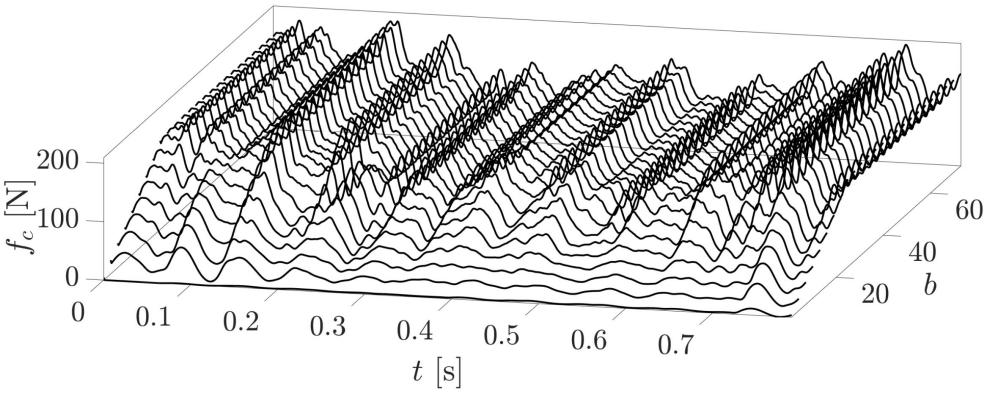

Figure 3.15: Contact force evolution.

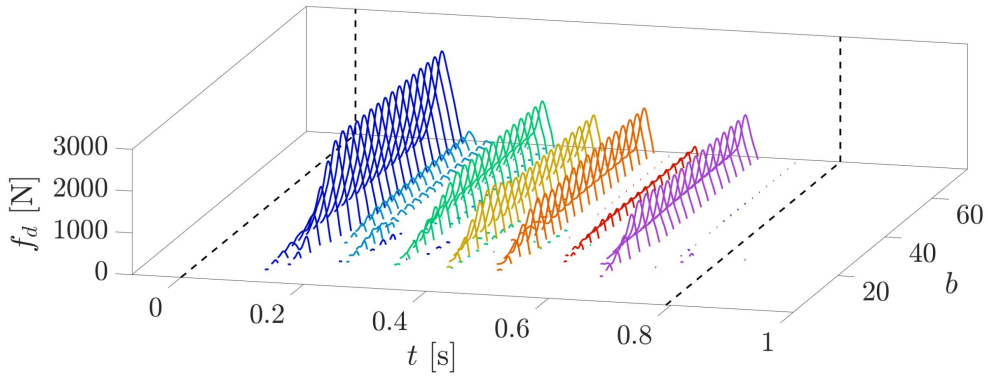

Figure 3.16: Dropper correction forces evolution.

To validate the results, the converged contact force obtained from the catenary PFEM is compared in Fig. 3.17 with the contact force of three consecutive central blocks computed with a conventional FEM simulation. We have used two catenary models with different lengths, namely 15 and 30 spans, respectively. The FEM solutions show minor differences with the contact force obtained from the PFEM. These differences are even smaller with the 30-span FE catenary model because a more stationary response is achieved on these central spans. The converged dropper correction forces obtained from the catenary

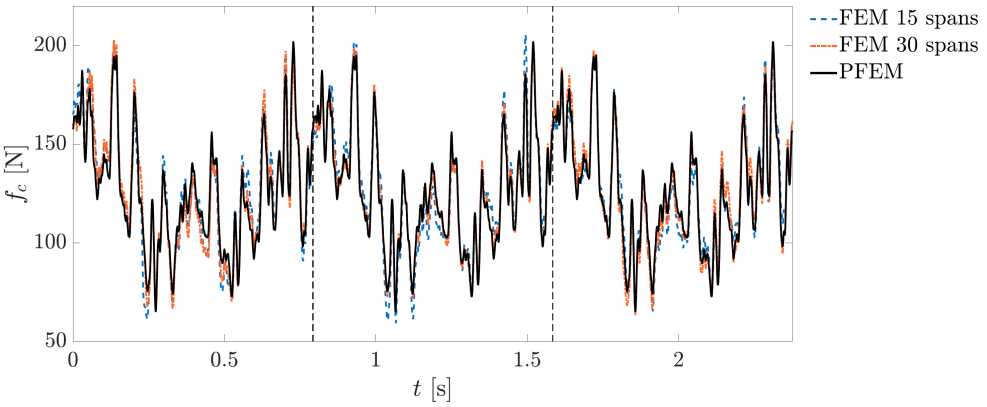

Figure 3.17: Comparison of contact force of catenary PFEM (solid line) with those obtained in three central spans of the section of a FE catenary model with 15 spans (dashed line) and 30 spans (dash-dotted line).

PFEM are also compared with those obtained from the longer FE catenary model in Fig. 3.18. As seen in both figures, the results provided by the proposed catenary PFEM are validated due to their great similarities with those obtained from a FEM simulation with a large enough catenary model.

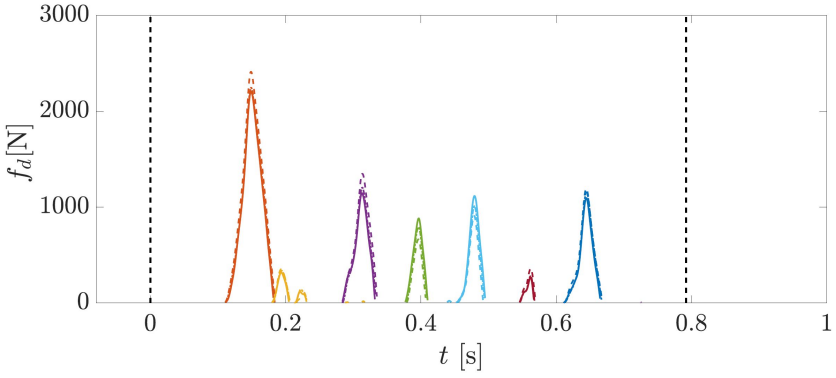

Figure 3.18: Comparison of dropper correction forces from catenary PFEM (solid lines) with those obtained in a central span of a FE catenary model with 30 spans (dashed lines).

3.4 Paper D

This paper adopts the periodic finite element model of the catenary proposed in Paper C. The model provides high accuracy results as demonstrated in Section 3.3, accounts for dropper slackening and presents some advantages for its practical implementation. Due to the periodic formulation, the steady-state solution provided by the PFEM is not influenced by boundary-layer effects. Furthermore, this model is suitable for a delay compensation technique, demonstrating good performance in virtual tests in Section 3.3.

3.4.1 Iterative algorithm to perform HIL pantograph tests

Here we provide details of the practical implementation of HIL, and additionally, a new variant of the iterative algorithm is proposed to tackle stability issues that could arise. Finally, the strategy to consider dropper non-linear behaviour is also introduced.

In Eq. (3.28) the moving load values are related to the contact point displacement. Both discrete variables can be arranged in vectors, $\mathbf{f}$ and $\mathbf{z}$, in which every position refers to a time instant. Due to the existing periodicity, the time domain includes just the instants that the load takes to travel a span of the catenary, and it is discretised into N steps which are indicated with n or $\hat{n} \in [1, ..., N]$. Where n is intended for evaluating the displacement and $\hat{n}$ for applying the force. Given a complete set of contact force $f(\hat{n})$ arranged in vector $\mathbf{f}$, the contact wire height vector $\mathbf{z}$, which includes the contact points $z(n)$, can be directly obtained as:

$$\mathbf{z} = \mathbf{z}_0 + \mathbf{I}_{\mathrm{cc}}\mathbf{f} \tag{3.32}$$

being $\mathbf{z_0}$ the initial configuration contact point height (initial geometric shape of the catenary).

With this scheme, the vertical displacement of the contact point $z(n)$ for all the time steps within the span can be calculated employing the product of the contact force $\mathbf{f}$ and matrix $\mathbf{I}_{\mathrm{cc}}$ which contains the contribution of every load value (column index $\hat{n}$) over every displacement value (row index n).

HIL tests are performed following a discrete time scheme. In each global time step, denoted with index k, every contact point displacement is imposed, and the contact force is measured. This global time is also organised in blocks of N samples, corresponding to the length of a period of the problem. Within every

block b, the time is denoted with index $\overline{n}$ starting from 1 at the beginning of the block. We denote the measured contact force in a given time step as $\overline{f}(k)$ and the vertical position of the actuator in this time step as $\overline{z}(k)$, which depends on the contact force of the previous time steps as will be explained bellow. When convergence in the test is reached, displacements and forces are repeated in every block, and they must satisfy Eq. (3.32). The measured contact force can be also labelled as $\overline{f}^b(\overline{n})$ and the position sent to the actuator as $\overline{z}^b(\overline{n})$ since every global time step k corresponds to a block b and a local time step within the block $\overline{n}$.

In this work, we discuss two alternatives for the iterative protocol of the HIL test: step-by-step and span-by-span updating. In the former, in every time step in which the force is measured, we need to compute the displacement of the next step. On the contrary, in the span-by-span updating strategy, the position of the actuator along the whole span b is already defined at the beginning of it, as a function of the previous spans.

The method used to perform step-by-step HIL tests with the periodic catenary model is schematically represented in Fig. 3.19. Note that the global time of the test is represented with the markers on the horizontal line. The different points of the figure are:

- Point 1: Let us say that the test is at the k global time step (or time step $\overline{n}$ within the block b, as represented by the pantograph illustration) and the pantograph has reached the displacement which was sent in the previous time step $k-1$.
- Point 2: Simultaneously to point 1, the force $\overline{f}^b(\overline{n})$ is measured.
- Point 3: The measured force is placed in vector $\mathbf{f}^k$ (which changes every time step k as denoted by the superscript) in the proper position $\overline{n}$ while the other elements of this vector remain unaltered.
- Point 4: Eq. (3.32) is applied to compute the response of the periodic model with $\mathbf{f}^k$, producing a $\mathbf{z}^k$ vector which replaces the one of the previous step $k-1$. In this case, all the components of vector $\mathbf{z}^k$ change.
- Point 5: The vertical position of the next step $\overline{n}+1$ is taken from $\mathbf{z}^k$ since this is the position that would be reached in the next step $k+1$. At this point, a more advanced position than $\overline{n}+1$ can be extracted from $\mathbf{z}^k$ to compensate any possible delay, as detailed below. This compensation is crucial for the feasibility of HIL tests.

- Point 6: The displacement is sent to the actuator.
- Point 7: It is time to move to the next step, and the timeline depicted at the bottom of the figure moves a position to the left so that the pantograph can reach the position sent in point 6. Additionally, the indexes of points 3 and 5 drop down a position to be ready to receive and give the right values in the next step $k+1$.

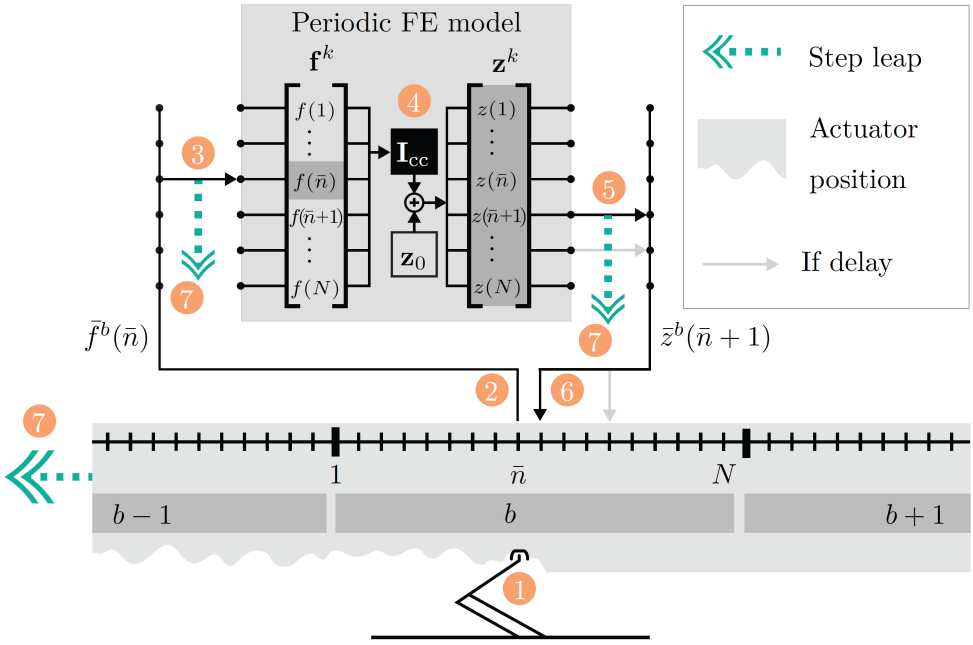

Figure 3.19: Graphical description of the step-by-step HIL test architecture with a PFEM of the catenary.

A different updating strategy is proposed in Paper D to avoid some convergence issues. This new strategy follows the four first points of Fig. 3.19 but the differences arise in point 5. Whereas in the step-by-step strategy, a single value of vector $\mathbf{z}^k$ was extracted and it would continue to point 6, in the span-by-span updating strategy, there is a rack of memory between points 5 and 6. Only at the time step $\overline{n} = N$ (at the end of each block) the whole vector $\mathbf{z}^k$ is extracted, and its N values are stored in the memory. The stored vector is called $\mathbf{z}^b$ and it fulfils $\mathbf{z}^b = \mathbf{z}^k$ if $k = bN$. According to the proposed scheme, the displacement $\overline{z}^b(\overline{n})$ that is sent to the actuator in point 6 is computed from

the stored vectors $\mathbf{z}^b$ of the two previous blocks, combining both with linear shape functions to avoid lack of continuity at the beginning of a new block. That is:

$$\overline{z}^b(\overline{n}) = N_1(\overline{n}) z^{b-2}(\overline{n}) + N_2(\overline{n}) z^{b-1}(\overline{n}) \; ; \quad \overline{n} \in [1, N] \tag{3.33}$$

in which N_1 and N_2 are linear shape functions which go from 1 to 0 and from 0 to 1, respectively. This method can perform better in terms of stability, as discussed in Paper D.

Unavoidably, there is a consumed time in the test loop that delays the response of the catenary. Let us consider that D time steps exist from the moment the contact force is measured in point 2 (Fig. 3.19) until the pantograph reaches the position computed in point 5. In Fig. 3.19, the representation corresponds to the unavoidable delay of one step $D = 1$. An extra delay is considered in point 6 of the figure with a grey arrow. If the position sent to the actuator takes the path defined by the grey arrow, it will be placed in a later position on the timeline because it will take more time steps to be reached by the pantograph.

To compensate a given delay, the position value extracted in point 5 of Fig. 3.19 is the $n = \overline{n} + D$ as indicated with a grey arrow. This procedure allows eliminating the error produced by the delay in the dynamic response since at the end of the test, when convergence is achieved, $\mathbf{f}^k$ and $\mathbf{z}^k$ do not change and the value at time step $n = \overline{n} + D$ will be a perfect prediction.

Another important aspect to consider is that we can limit the frequency content of the actuator displacement. As the vector $\mathbf{z}$ is periodic, it can be shifted to the frequency domain by the Discrete Fourier Transform (DFT) and then, the higher frequencies can be removed before being brought back to the time domain by the Inverse Discrete Fourier Transform (IDFT).

In this frequency reduction, a number of N_h frequencies are considered, being f_{max} the higher frequency included. This number plays an important role in the stability of the HIL test because if f_{max} is higher than the biggest frequency the gear can control, it will lead to bad performance. The whole process can be done directly by applying matrix operations to $\mathbf{z}$ as explained in Paper D.

Another difference between the numerical algorithm proposed in Section 3.3.3 and this one lies on the use of a relaxation coefficient μ_c to reduce the sharp change between the response of successive blocks during the iterative procedure. In point 3 of Fig. 3.19, the measured force replaces the element $\overline{n}$ of $\mathbf{f}^k$ in which the measure of the previous block was previously allocated. If the

relaxation is applied, the current measurement will be relaxed with the old one. Additionally, to avoid a sudden jump at the beginning of the HIL test, the height sent to the actuator is scaled by a factor that varies linearly from 0 to 1 step by step, defining an initial ramp.

3.4.2 Dropper slackening

In point 4 of the loop (see Fig. 3.19), Eq. (3.32) is used to compute the response of the catenary given a contact force, although additional external actions can also be applied to include the non-linear behaviour of dropper. If matrix $\mathbf{I}_{\mathrm{c}d}$ includes the stationary response of the contact point produced by a compressive force acting on both ends of dropper d, then Eq. (3.32) can be extended to:

$$\mathbf{z} = \mathbf{z}_0 + \mathbf{I}_{\mathrm{cc}}\mathbf{f} + \sum_{d=1}^{N_{\mathrm{d}}} \mathbf{I}_{\mathrm{c}d}\mathbf{f}_d \tag{3.34}$$

in which $\mathbf{f}_d$ is the correction force vector of dropper d and N_{d} is the total number of droppers.

The elongation of droppers needs to be computed to calculate the non-linear actions to be added. Let us define matrices $\mathbf{I}_{d\mathrm{c}}$ and $\mathbf{I}_{dd}$, which account for the elongation of droppers produced by the contact force and by the other droppers correction forces, respectively. The total elongation of dropper d can be therefore computed as:

$$\mathbf{\Delta L}_d = \mathbf{I}_{d\mathrm{c}}\mathbf{f} + \sum_{d=1}^{N_{\mathrm{d}}} \mathbf{I}_{dd}\mathbf{f}_d \tag{3.35}$$

Similarly to $\mathbf{z}$, it is important to limit the frequency content of $\mathbf{\Delta L}_d$ to facilitate the method convergence. In this case a different number of harmonics N_{hd} is considered in the variable $\mathbf{\Delta L}_d$.

3.4.3 Results of HIL tests

The data of the catenary models and parameters used in this test can be found in Paper D. The contact force results are filtered to 25 Hz, exceeding the 20 Hz that, according to the standard [4], must be considered for validation and comparison purposes in this kind of simulations. The same validation strategy as in Subsection 3.2.3 is performed with a mass model to measure the validity

of the tests. In this occasion, a force value of 160 N is added to the force measured by the load cells to simulate the situation in which the pantograph is pushing against the catenary. This is necessary to validate the non-linear behaviour of the catenary. The validation is shown in Fig. 3.20, where the contact force measured matches the obtained from the completely simulated HIL and the slackened droppers correction forces are in very good agreement.

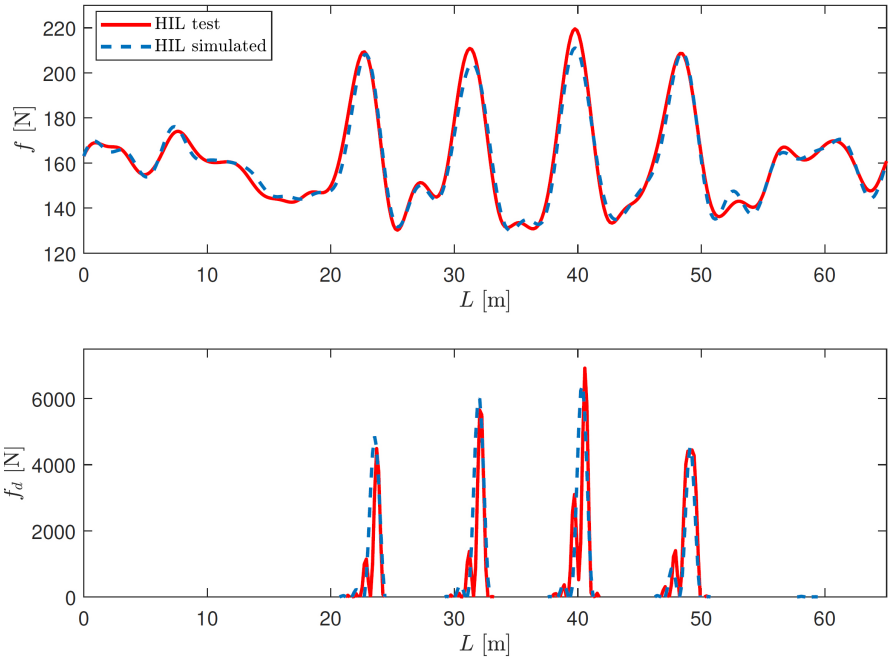

Figure 3.20: Comparison between contact forces (top figure) and slackened dropper correction forces (bottom figure) obtained from experimental HIL tests (solid line) and virtual HIL simulations (dashed line) with the mass travelling at 300 km/h and a mean pushing force of 160 N.

Once the test system has been validated, the pantograph DSA 380 is placed to simulate the interaction with the catenary. In Paper D the results with different catenaries and velocities are displayed. In this overview, just two tests with a simple and a stitched catenaries at 300 km/h are shown in Fig. 3.21. The experimental results are compared in this case with the contact force obtained from a standard simulation of the pantograph-catenary dynamic interaction. To perform these simulations, we use the software PACDIN [59] with a linear lumped mass model.

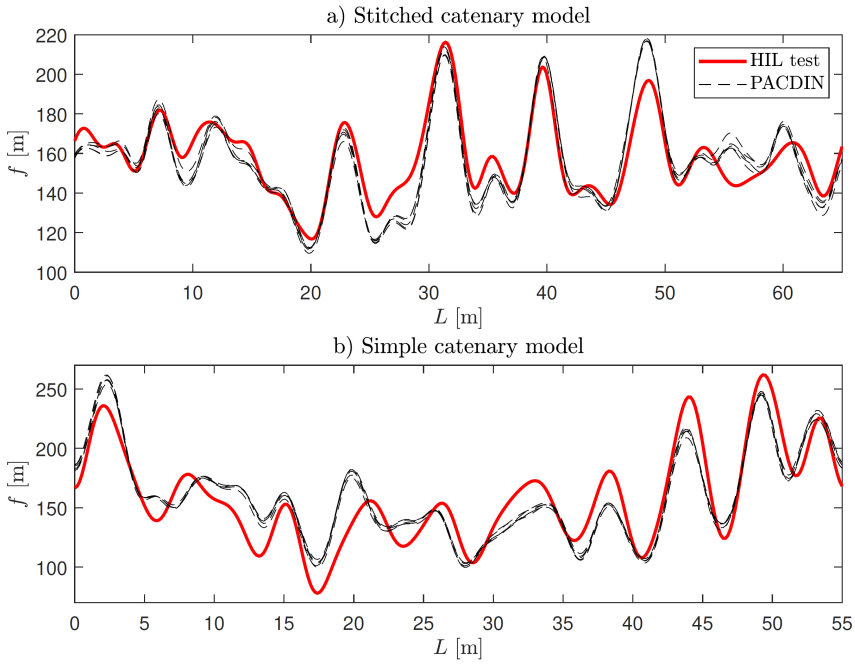

Figure 3.21: Comparison between contact forces obtained from experimental HIL tests (solid line) and conventional simulation of the pantograph-catenary dynamic interaction (dashed line) with the pantograph running at 300 km/h and interacting with a) the stitched catenary model and b) the simple catenary model.

In Fig. 3.21, the contact force curves of five consecutive spans of the PACDIN simulation are overlapped. The agreement of the five curves indicates that the steady-state regime was achieved. Therefore, this solution is suitable for comparing the PFEM HIL tests. The other important conclusion is drawn by the comparison between the HIL tests and the standard simulation. As the HIL set-up was adequately validated, the discrepancies observed in Fig. 3.21 are mainly due to the inability of the pantograph model used in PACDIN to accurately reproduce the dynamic behaviour of the real pantograph device because non-linear features are not considered in the model.

Chapter 4

Closure

This chapter emphasises some key points that account for the Thesis relevance. Additionally, there is a Section for proposing the steps on the subject that can be worth considering in future research.

4.1 Conclusions

The ultimate aim of this work is to implement Hardware-In-the-Loop tests of the pantograph-catenary system. This experimental technique has proved to be challenging, but clear improvements have been accomplished. The attainment of the experimental test has been realised by a new approach, consisting of a Periodic Finite Element Model (PFEM) of the catenary and an iterative algorithm. During the research process, different steps have been taken that have meant an advance towards the final goal:

- The first contribution of this work was the development of an analytical model of the catenary based on a string of periodic geometric profile. This model was a proposal to reduce the complexity of the catenary but still keeping the main features involved in the dynamic. We have compared the model with a high-fidelity reference model built by FEM to evaluate the differences and study the origin of those. The model is found to be a good tool for revealing the elemental behaviour of the catenary. And it

has proven useful in explaining a complex phenomenon: the interference between two pantographs.

- The analytical model was thought to be suitable for HIL due to its low computational cost. This model is particularly periodic, which means that it accounts for the steady state regime of the system. Thus, incorporating the analytical model in Hardware in the loop requires a mathematical adaptation by an iterative algorithm. This need has been solved, and the HIL test has been accomplished thanks to the algorithm ability to compensate implicit delays in HIL. The accuracy of the HIL facility has been assessed by looking at the agreement between tests and computational simulations. The agreement would be arduous if the validation tests were realised with the pantograph, due to the difficulty in getting an accurate model of the pantograph for the simulations. In order to avoid the uncertainty of the pantograph dynamics, the validation tests are carried out with a weight or mass model in the place of the pantograph. Minor differences are found between the computational simulation and the tests, implying the validation of the tests. Even though the analytical catenary model is not good enough to characterise the pantograph-catenary interaction, these tests have demonstrated the ability to simulate periodic models, compensate the delay and achieve good accuracy. This is a crucial point of the Thesis for the posterior application of HIL tests with PFEM models.

- The HIL tests with the analytic model have motivated the development of a more realistic periodic model, specifically, a Periodic Finite Element Model (PFEM). The FEM is chosen for the geometric discretisation of the catenary to avoid further topological and structural simplifications. The combination of the periodicity condition and discrete frequency analysis has served to create the formulation that governs the steady-state regime of periodic structures subjected to a moving load. The solution has been precalculated to get real-time computation capacity required by experimental tests. Additionally, the model non-linearities have been considered and incorporated into the formulation. The solution achieved has been compared with conventional FEM simulations, and a good agreement is found when comparing with the solution of equal-span catenary at the central zone of a section. This is due to the fact that the only additional simplification of the periodic catenary is the steady state assumption.

- Finally, HIL tests with PFEM catenaries are carried out thanks to an algorithm based on the one used for HIL tests with the analytical model. The previously stated strategy with a mass model has been used to val-

idate the test, achieving outstanding precision. These tests simulate the interaction of real pantographs with virtual periodic catenary models that include non-linear and accurate dynamics. This is the most significant achievement of this Thesis due to the sophistication of the model, the accuracy of the tests and the effectiveness in cancelling the delay.

4.2 Open research lines

After the finalisation of this work, there is still work to be done for the future HIL tests of the pantograph-catenary interaction. Some of the open lines are defined as follows:

- As it has been said, the HIL tests developed here have the limitation of the periodicity assumption. The implementation of HIL tests with complete FEM models is the current challenge. Even though there are full FEM models that can be computed in real-time [12], the existing delay makes its application unattainable. It is necessary to work on control techniques and compensation strategies to achieve conventional FEM-HIL tests without compromising accuracy.

- The success of HIL also relies on the electronic and technical capabilities of the test rig. Using the latest technology and improving the communication system will lead to a faster and more precise response. Working in this aspect will increment the feasibility of HIL tests with conventional FEM models. Additionally, it will allow increasing the frequency range of the tests, that in this work is up to 25 Hz.

- One imprecision of HIL is the absence of wind. Pantograph aerodynamics is often tested in wind tunnels, and these two techniques can be applied together in order to couple mechanical dynamics with aerodynamics.

- Other aspects can also be included in HIL tests to increase verisimilitude. The movement of the pantograph due to the rail bank angle and train vibrations are good candidates to consider. In our installations, including lateral movement to simulate the stagger of catenaries is the next mechanical improvement.

Bibliography

[1] BP, "Statistical review of world energy."

[2] AIReF, "La airef constata el fuerte esfuerzo inversor en la alta velocidad frente a una inversión insuficiente en cercanías y propone poner el foco en los criterios de movilidad."

[3] EN 50367:2016, "Railway applications. Current collection systems. Technical criteria for the interaction between pantograph and overhead line," *European Committee for Electrotechnical Standardization*, 2016.

[4] EN 50318:2018, "Railway applications. Current collection systems. Validation of simulation of the dynamic interaction between pantograph and overhead contact line," *European Union Agency for Railways*, 2018.

[5] EN 50317:2012, "Railway applications. Current collection systems. Requirements for and validation of measurements of the dynamic interaction between pantograph and overhead contact line," *European Union Agency for Railways*, 2012.

[6] EN 50119:2021, "Railway applications. Fixed installations. Electric traction overhead contact lines," *European Committee for Electrotechnical Standardization*, 2021.

[7] S. Bruni, J. Ambrosio, A. Carnicero, Y. H. Cho, L. Finner, M. Ikeda, S. Y. Kwon, J. P. Massat, S. Stichel, and M. Tur, "The results of the pantograph-catenary interaction benchmark," *Vehicle System Dynamics*, vol. 53, no. 3, pp. 412–435, 2015.

[8] S. Bruni, G. Bucca, M. Carnevale, A. Collina, and A. Facchinetti, "Pantograph–catenary interaction: recent achievements and future research challenges," *International Journal of Rail Transportation*, vol. 6, no. 2, pp. 57–82, 2018.

[9] M. Tur, E. García, L. Baeza, and F. Fuenmayor, "A 3D absolute nodal coordinate finite element model to compute the initial configuration of a railway catenary," *Engineering Structures*, vol. 71, pp. 234–243, 2014.

[10] S. Gregori, M. Tur, E. Nadal, J. Aguado, F. Fuenmayor, and F. Chinesta, "Fast simulation of the pantograph–catenary dynamic interaction," *Finite Elements in Analysis and Design*, vol. 129, pp. 1 – 13, 2017.

[11] M. Berzeri and A. Shabana, "Development of simple models for the elastic forces in the absolute nodal co-ordinate formulation," *Journal of Sound and Vibration*, vol. 235, no. 4, pp. 539–565, 2000.

[12] S. Gregori, M. Tur, A. Pedrosa, J. Tarancón, and F. Fuenmayor, "A modal coordinate catenary model for the real-time simulation of the pantograph-catenary dynamic interaction," *Finite Elem. Anal. Des.*, vol. 162, pp. 1–12, 2019.

[13] Y. Song, P. Antunes, J. Pombo, and Z. Liu, "A methodology to study high-speed pantograph-catenary interaction with realistic contact wire irregularities," *Mechanism and Machine Theory*, vol. 152, p. 103940, 2020.

[14] S. Gregori, M. Tur, J. E. Tarancón, and F. J. Fuenmayor, "Stochastic monte carlo simulations of the pantograph–catenary dynamic interaction to allow for uncertainties introduced during catenary installation," *Vehicle System Dynamics*, vol. 57, no. 4, pp. 471–492, 2019.

[15] T. Koyama, K. Nagao, and M. Ikeda, "Three-dimensional simulation of catenary/pantograph dynamic interaction," *Quarterly Report of RTRI*, vol. 62, pp. 104–109, 05 2021.

[16] W. Chu, Y. Song, and Z. Liu, "A comparative study on the wind deflection of railway overhead contact line based on empirical formula and finite element approach," *Shock and Vibration*, vol. 2021, pp. 1–9, 07 2021.

[17] Z. Dai, T. Li, N. Zhou, J. Zhang, and W. Zhang, "Numerical simulation and optimization of aerodynamic uplift force of a high-speed pantograph," *Railway Engineering Science*, vol. 30, pp. 1–12, 10 2021.

[18] Y. Song, Z. Wang, Z. Liu, and R. Wang, "A spatial coupling model to study dynamic performance of pantograph-catenary with vehicle-track excitation," *Mechanical Systems and Signal Processing*, vol. 151, p. 107336, 2021.

[19] Y. Yao, D. Zou, N. Zhou, G. Mei, J. Wang, and W. Zhang, "A study on the mechanism of vehicle body vibration affecting the dynamic interaction in the pantograph–catenary system," *Vehicle System Dynamics*, vol. 59, no. 9, pp. 1335–1354, 2021.

[20] A. Wilk, L. Gelman, S. Judek, K. Karwowski, M. Mizan, T. Maciołek, M. Lewandowski, A. Jakubowski, and K. Klimowska, "Novel method of estimation of inertial and dissipative parameters of a railway pantograph model," *Vehicle System Dynamics*, vol. 60, no. 7, pp. 2413–2435, 2022.

[21] M. Zhu, S. Y. Zhang, J. Z. Jiang, J. Macdonald, S. Neild, P. Antunes, J. Pombo, S. Cullingford, M. Askill, and S. Fielder, "Enhancing pantograph-catenary dynamic performance using an inertance-integrated damping system," *Vehicle System Dynamics*, vol. 60, no. 6, pp. 1909–1932, 2022.

[22] T. Wu and M. Brennan, "Basic analytical study of pantograph-catenary system dynamics," *Vehicle System Dynamics*, vol. 30, no. 6, pp. 443–456, 1998.

[23] A. D. S. Roy, G. Chakraborty, "Coupled dynamics of a viscoelastically supported infinite string and a number of discrete mechanical systems moving with uniform speed," *Journal of Sound and Vibration*, vol. 415, pp. 184–209, 2018.

[24] D. J. Mead, "Vibration response and wave propagation in periodic structures," *J. Eng. Ind.*, vol. 93, no. 3, pp. 783–792, 1971.

[25] C. Cai, Y. Cheung, and H. Chan, "Dynamic response of infinite continuous beams subjected to a moving force – An exact method," *J. Sound Vib.*, vol. 123, no. 3, pp. 461 – 472, 1988.

[26] P. Belotserkovskiy, "On the oscillations of infinite periodic beams subjected to a moving concentrated force," *J. Sound Vib.*, vol. 193, no. 3, pp. 705 – 712, 1996.

[27] A. Metrikine and A. Bosch, "Dynamic response of a two-level catenary to a moving load," *Journal of Sound and Vibration*, vol. 292, no. 3, pp. 676 – 693, 2006.

[28] Y. Song, Z. Liu, F. Duan, Z. Xu, and X. Lu, "Wave propagation analysis in high-speed railway catenary system subjected to a moving pantograph," *Applied Mathematical Modelling*, vol. 59, pp. 20 – 38, 2018.

[29] H. Ouyang, "Moving-load dynamic problems: A tutorial (with a brief overview)," *Mechanical Systems and Signal Processing*, vol. 25, no. 6, pp. 2039–2060, 2011. Interdisciplinary Aspects of Vehicle Dynamics.

[30] X. Sheng, C. Jones, and D. Thompson, "Responses of infinite periodic structures to moving or stationary harmonic loads," *J. Sound Vib.*, vol. 282, pp. 125–149, 04 2005.

[31] X. Sheng, C. Jones, and D. Thompson, "Using the fourier-series approach to study interactions between moving wheels and a periodically supported rail," *J. Sound Vib.*, vol. 303, pp. 873–894, 06 2007.

[32] J.-M. Mencik, "On the low- and mid-frequency forced response of elastic structures using wave finite elements with one-dimensional propagation," *Comput. Struct.*, vol. 88, no. 11, pp. 674 – 689, 2010.

[33] B. Claudet, T. Hoang, D. Duhamel, G. Foret, J.-L. Pochet, and F. Sabatier, "Wave finite element method for computing the dynamic response of railway transition zones subjected to moving loads," in *COMPDYN 2019*, (Crete, Greece), pp. 4538–4547, 01 2019.

[34] T. Hoang, D. Duhamel, G. Forêt, J.-L. L. Pochet, and F. Sabatier, "Wave finite element method and moving loads for the dynamic analysis of railway tracks," in *WCCM XIII*, (New York, United States), 2018.

[35] W. Song, C.-M. Chang, and V. K. Dertimanis, "Editorial: Recent advances and applications of hybrid simulation," *Frontiers in Built Environment*, vol. 6, 2020.

[36] W. Zhang, G. Mei, X. Wu, and Z. Shen, "Hybrid simulation of dynamics for the pantograph-catenary system," *Vehicle System Dynamics*, vol. 38, no. 6, pp. 393–414, 2002.

[37] W. Zhang, G. Mei, X. Wu, and L. Chen, "A study on dynamic behaviour of pantographs by using hybrid simulation method," *Proceedings of the Institution of Mechanical Engineers, Part F: Journal of Rail and Rapid Transit*, vol. 219, no. 3, pp. 189–199, 2005.

[38] A. Collina, A. Facchinetti, F. Fossati, and F. Resta, "Hardware in the loop test-rig for identification and control application on high speed pantographs," *Shock and Vibration*, vol. 11, pp. 445–456, 01 2004.

[39] F. Resta, A. Facchinetti, A. Collina, and G. Bucca, "On the use of a hardware in the loop set-up for pantograph dynamics evaluation," *Vehicle System Dynamics*, vol. 46, no. S1, pp. 1039–1052, 2008.

[40] A. Facchinetti and M. Mauri, "Hardware-in-the-loop overhead line emulator for active pantograph testing," *IEEE Transactions on Industrial Electronics*, vol. 56, no. 10, pp. 4071–4078, 2009.

[41] A. Facchinetti and S. Bruni, "Hardware-in-the-loop hybrid simulation of pantograph–catenary interaction," *Journal of Sound and Vibration*, vol. 331, no. 12, pp. 2783–2797, 2012.

[42] H. Zhou, B. Zhang, X. Shao, Y. Tian, C. Zeng, W. Guo, and T. Wang, "Recursive predictive optimal control algorithm for real-time hybrid simulation of vehicle–bridge coupling system," *International Journal of Structural Stability and Dynamics*, vol. 22, 03 2022.

[43] T. Horiuchi, M. Inoue, T. Konno, and Y. Namita, "Real-time hybrid experimental system with actuator delay compensation and its application to a piping system with energy absorber," *Earthquake Engineering & Structural Dynamics*, vol. 28, no. 10, pp. 1121–1141, 1999.

[44] C. Chen and J. M. Ricles, "Analysis of actuator delay compensation methods for real-time testing," *Engineering Structures*, vol. 31, no. 11, pp. 2643–2655, 2009.

[45] R.-Y. Jung, P. Benson Shing, E. Stauffer, and B. Thoen, "Performance of a real-time pseudodynamic test system considering nonlinear structural response," *Earthquake Engineering & Structural Dynamics*, vol. 36, no. 12, pp. 1785–1809, 2007.

[46] D. P. Stoten, T. Yamaguchi, and Y. Yamashita, "Dynamically substructured system testing for railway vehicle pantographs," *Journal of Physics: Conference Series*, vol. 744, p. 012204, sep 2016.

[47] S. Kobayashi, D. P. Stoten, Y. Yamashita, and T. Usuda, "Dynamically substructured testing of railway pantograph/catenary systems," *Proceedings of the Institution of Mechanical Engineers, Part F: Journal of Rail and Rapid Transit*, vol. 233, no. 5, pp. 516–525, 2019.

[48] S. Kobayashi, Y. Yamashita, T. Usuda, and D. Stoten, "Hybrid simulation testing of a pantograph-catenary system using a dynamically substructured system framework and a mdof catenary model," *Quarterly Report of RTRI*, vol. 61, pp. 127–132, 05 2020.

[49] A. Schirrer, G. Aschauer, E. Talic, M. Kozek, and S. Jakubek, "Catenary emulation for hardware-in-the-loop pantograph testing with a model predictive energy-conserving control algorithm," *Mechatronics*, vol. 41, pp. 17 – 28, 2017.

[50] M. Aboshi and M. Tsunemoto, "Installation guidelines for shinkansen high speed overhead contact lines," *Quarterly Report of Railway Technical Research Institute*, vol. 52, pp. 230–236, 11 2011.

[51] O. V. Van, J.-P. Massat, C. Laurent, and E. Balmes, "Introduction of variability into pantograph–catenary dynamic simulations," *Vehicle System Dynamics*, vol. 52, no. 10, pp. 1254–1269, 2014.

[52] S. Gregori, M. Tur, E. Nadal, and F. J. Fuenmayor, "An approach to geometric optimisation of railway catenaries," *Vehicle System Dynamics*, vol. 56, no. 8, pp. 1162–1186, 2018.

[53] Z. Liu, P.-A. Jönsson, S. Stichel, and A. Rønnquist, "On the implementation of an auxiliary pantograph for speed increase on existing lines," *Vehicle System Dynamics*, vol. 54, no. 8, pp. 1077–1097, 2016.

[54] O. V. Van, J.-P. Massat, and E. Balmes, "Waves, modes and properties with a major impact on dynamic pantograph-catenary interaction," *Journal of Sound and Vibration*, vol. 402, pp. 51 – 69, 2017.

[55] W. Zhang, N. Zhou, R. Li, G. Mei, and D. Song, "Pantograph and catenary system with double pantographs for high-speed trains at 350 km/h or higher," *Journal of Modern Transportation*, vol. 19, pp. 7–11, Mar 2011.

[56] O. Lopez-Garcia, A. Carnicero, and V. Torres, "Computation of the initial equilibrium of railway overheads based on the catenary equation," *Engineering Structures*, vol. 28, no. 10, pp. 1387 – 1394, 2006.

[57] M. Tur, L. Baeza, F. Fuenmayor, and E. García, "Pacdin statement of methods," *Vehicle System Dynamics*, vol. 53, no. 3, pp. 402–411, 2015.

[58] H. M. Hilber, T. J. Hughes, and R. L. Taylor, "Improved numerical dissipation for time integration algorithms in structural dynamics," *Earthq. Eng. Struct. Dyn.*, vol. 5, no. 3, pp. 283–292, 1977.

[59] M. Tur, L. Baeza, F. Fuenmayor, and E. García, "PACDIN statement of methods," *Vehicle System Dynamics*, vol. 53, no. 3, pp. 402–411, 2015.

Part II

Articles

PAPER A

Analytical Model of the Pantograph Catenary Dynamic Interaction and Comparison with Numerical Simulations

J. Gil, S. Gregori, M. Tur and F. J. Fuenmayor

Vehicle System Dynamics
Volume 60:1, Pages 132-155, 2022
DOI: 10.1080/00423114.2020.1802493

Abstract

Catenaries are large cable structures which transmit electric current to trains through sliding contact with a pantograph. The Finite Element Method is widely used to model this dynamic interaction problem and obtain the contact force between the pantograph and the catenary. As an alternative, analytical models can also be used to study catenary dynamics, although they require certain simplifications of the features considered in numerical models. In this paper, an analytical model composed of an infinite string and a visco-elastic support is introduced and enhanced by considering a Kelvin-Voigt damping model and the initial height of the contact wire. Considering the Finite Element (FE) model as a reference, the analytical model parameters are properly adjusted through static and wave propagation analyses to achieve similar behaviour in both the analytical and the FE models. To check the performance of the proposed model, the steady-state response of the pantograph-catenary coupled system is calculated and compared with the results of the FE model. Finally, the analytical model is used to analyse the interference phenomenon produced during two-pantograph operation.

Keywords

Analytical Catenary model, Pantograph dynamic interaction, Finite element, Infinite string, Pantograph interference

Contents

1 Introduction

Overhead contact lines, commonly known as railway catenaries, are currently the most widely used systems to supply high-speed trains with power through sliding contact with a moving pantograph. The dynamic behaviour of the pantograph-catenary interaction is of great interest in the system design as it can affect the reliability of vehicle operation. For this reason, many catenary models have been developed [1] and used to analyse the influence of design parameters in the current collection quality. These simulations are regulated and must be validated according to specific standards [2].

Finite Element (FE) models are the most frequently used technique to simulate the problem, as shown in the recent benchmark exercise [3]. For example, in previous studies [4, 5, 6], FE-based models have been used to analyse the influence of certain design parameters in the current collection quality, which is usually quantified by the standard deviation of the interaction contact force (CF). These studies concluded that higher CF variation is obtained when the operational velocity is close to the contact wire wave velocity, when there is higher stiffness variation along the span or when the pantograph collector head has greater mass.

As an alternative to FE models, analytical catenary models are also found to be a useful tool in providing a better understanding of the role played by the design variables in exchange for adopting certain simplifications. For example, in [7], the catenary is modelled as a single and two-degrees-of-freedom system with periodically time-varying mass and stiffness and the relations between the system parameters and the upper limit of the train speed are stated. In [8] an analytical model was used to analyse the interference between pantographs when two pantographs run simultaneously in a vehicle. An optimum distance between the pantographs is theoretically calculated, based on the phase opposition of the vertical displacement of the contact wire produced by the trailing pantograph and the displacement induced by the leading pantograph.

An infinite string with visco-elastic support is used in [9] to obtain the stationary response of lumped-parameters moving models coupled to the string. More complex infinite string models include periodic discrete elements, such as in [10] or in [11], in which a two-level infinite catenary model, composed of an upper and lower string (governed by the one-dimensional wave equation) joined by periodic supports and dampers, is simulated with a pantograph modelled by a harmonic point-load. Other similar models can be also found in the literature, such as that in [12] which is composed of several finite strings and is used to study the wave propagation and reflection phenomena in the catenary.

The objective of this paper is to propose a new analytical pantograph-catenary coupled model to obtain in a closed-form expression the pantograph interaction contact force. The proposed model is based on a previous model presented in [9]. In this work, the governing equation is modified to include a Kelvin-Voigt damping model in order to get a dissipative behaviour similar than that incorporated into the FE model. This modification implies to raise the order of the equation and the new solution is presented throughout the paper. Furthermore, the geometry of the contact wire under gravity is considered in the proposed model. The initial contact wire height profile is one of the main causes of CF variation as some studies shown [13]. Also, in [14, 15], the authors conclude that the geometric irregularities of the contact wire have a stronger influence on CF than other sources of irregularity, especially at high operating velocities as shown in [16]. This influence is also studied in [17, 18], which conclude that the optimal initial geometry significantly reduces CF variation. The analytical string models of the catenary found in the literature do not include the initial contact wire height profile and therefore, its important effect is not reflected in their results.

The interaction contact force obtained with the analytical model is compared with a verified FE model solution [19, 20]. With the aim to obtain a response as similar as possible to that of FE models, the stiffness and mass parameters of the analytical model are properly tuned by following a proposed methodology based on static and wave propagation considerations. Finally, as an example of application of the proposed model, a new approach is raised for understanding the multiple pantograph interference, by proposing a simplified analytical expression to evaluate the optimal distances between pantographs. This problem was also studied in [21], which obtained smaller CF variation in the trailing pantograph by using an auxiliary pantograph, or in [16], which showed reduced performance when the elapsed time between the pantographs passage matches the natural catenary frequencies.

The contents of this paper are organised as follows. After this introduction, the formulation of the reference FE model is described in Section 2. The proposed analytical model is developed in Section 3 and a procedure to obtain the required parameter's values is presented in Section 4. The results obtained by the proposed model and their validation are given in Section 5, before the concluding remarks in Section 6.

2 Reference models

The Finite Element Method (FEM) is the technique most frequently used to model railway catenaries [3]. These structures are composed of different wires and bars as can be seen in Fig. 1. In this paper, the catenary FE model [19, 20] validated according to EN-50318:2018 [2] is taken as the reference for the analytical model. The material properties and the geometric parameters of the model used are defined in 6.

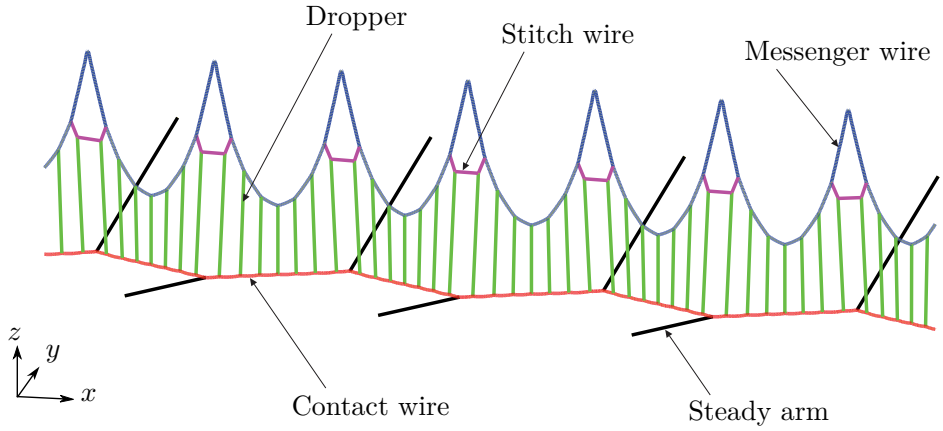

Figure 1: *FE model of the catenary.*

The pantograph is an articulated device on the locomotive roof that keeps in contact with the catenary. Although there are different options for modelling pantographs, in this work a lumped parameter model is used for its wide use and simplicity. The model consists of three masses that move vertically, which are connected by springs and dampers as shown in Fig. 2 (a). The pantograph lifting mechanism is replaced by a force applied on the bottom mass. For the pantograph-catenary interaction, the *penalty* method is used, which considers a high stiffness element ($k_\mathrm{h} = 50000$ N/m [2]) placed between the contact wire and the upper mass of the pantograph as depicted in Fig. 2 (b). This element applies a contact force f_c between both models as depicted in Fig. 2 (c).

To obtain the initial geometry of the catenary model, the static equilibrium equation and certain design constraint equations must be solved simultaneously. The reader is referred to [19], where this problem is described in detail. Once the initial configuration of the catenary has been solved, the pantograph-catenary

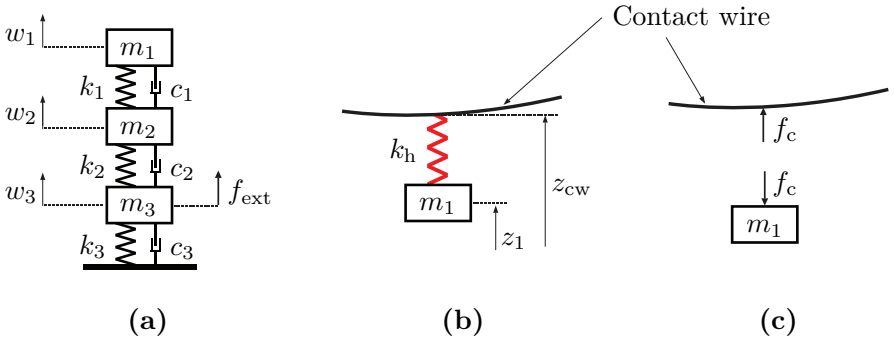

Figure 2: *(a) Pantograph model, (b) penalty model and (c) contact force* $f_{\text{c}} > 0$.

dynamic interaction problem is solved by following the procedure described in [20]. This problem can be stated assuming small displacements with respect to the static equilibrium position, which means it is governed by the linear equation:

$$\mathbf{M}\ddot{\mathbf{u}} + \mathbf{C}\dot{\mathbf{u}} + \mathbf{K}\mathbf{u} = \mathbf{F} \tag{1}$$

where $\mathbf{u}$, $\dot{\mathbf{u}}$ and $\ddot{\mathbf{u}}$ are the nodal displacements, velocities and accelerations respectively. $\mathbf{K}$ and $\mathbf{M}$ are the stiffness and mass matrices and a Rayleigh damping model is used to define the damping matrix $\mathbf{C} = \alpha\mathbf{M} + \beta\mathbf{K}$ with $\alpha = 0.0125$ s^{-1} and $\beta = 10^4$ s [3]. $\mathbf{F}$ is the vector of external forces applied to the pantograph. Despite the linear appearance, this is in fact a non-linear problem, since dropper slackening and contact loss are considered in the model. The Newmark or HHT [22] schemes can be used for the numeric integration of Eq. (1) combined with an iterative method to deal with the aforementioned non-linearities.

3 Analytical model of the catenary

Here we propose an analytical catenary model taking as a starting point the infinite string presented in [9]. The model is enhanced with the introduction of a Kelvin-Voigt damping model and the consideration of the initial geometry of the contact wire. The final model proposed is used to obtain the CF produced in the pantograph-catenary dynamic interaction problem.

3.1 Initial model

For the sake of clarity, we here summarise the model presented in [9] composed of an axially loaded infinite string prestressed with a force T and supported by a continuous visco-elastic layer, as shown in Fig. 3, with $\bar{k}$ and $\bar{c}$ being the stiffness and damping coefficients per unit of length, respectively. The linear density μ can also include the influence of the mass of the support.

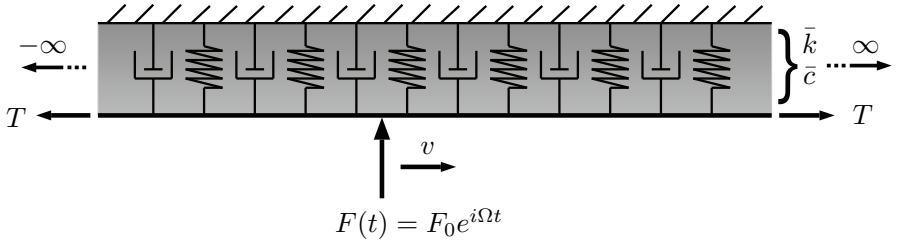

Figure 3: *Initial analytical string model (ASM1) with visco-elastic support under a harmonic moving load.*

The initial analytical string model (ASM1) subjected to a distributed load $p(x,t)$ is governed by the equation:

$$\mu \frac{\partial^2 w}{\partial t^2} - T \frac{\partial^2 w}{\partial x^2} + \bar{c} \frac{\partial w}{\partial t} + \bar{k} w = p(x,t) \tag{2}$$

where $w = w(x,t)$ is the vertical displacement of the contact wire.

The steady solution of Eq. (2) when the contact wire is loaded by a concentrated harmonic moving force $F(t) = F_0 e^{i\Omega t}$ (see Fig. 3) with frequency Ω, and velocity v, is given in [9]. In this case, the right-hand side term can be expressed as:

$$p(x,t) = F_0 e^{i\Omega t}\ \delta(x - vt) \tag{3}$$

where δ is the *Dirac* function. The solution of this problem is different for v greater or smaller than the critical velocity $v_c = \sqrt{T/\mu}$. However, as the standard EN50318 [2] limits the train velocity to $v < 0.7 v_c$, the solution used in this work is that in which $v < v_c$ or equivalently $\lambda > 0$, with $\lambda = T - \mu v^2$. In this case, the expression for the string vertical displacement is:

$$w(x,t) = \begin{cases} \dfrac{iF_0 e^{-i\left[k_1^{\Omega}(x-vt)-\Omega t\right]}}{\lambda\left(k_2^{\Omega}-k_1^{\Omega}\right)} & if \quad x-vt>0 \\ \dfrac{iF_0 e^{-i\left[k_2^{\Omega}(x-vt)-\Omega t\right]}}{\lambda\left(k_2^{\Omega}-k_1^{\Omega}\right)} & if \quad x-vt\leq 0 \end{cases} \tag{4}$$

where k_1^{Ω} and k_2^{Ω} are the poles of the system:

$$\begin{aligned} k_1^{\Omega} &= \left[\frac{2\mu v\Omega + p_{\mathrm{s}}}{2\lambda}\right] - i\left[\frac{\bar{c}v + q_{\mathrm{s}}}{2\lambda}\right] \\ k_2^{\Omega} &= \left[\frac{2\mu v\Omega - p_{\mathrm{s}}}{2\lambda}\right] - i\left[\frac{\bar{c}v - q_{\mathrm{s}}}{2\lambda}\right] \end{aligned} \tag{5}$$

being:

$$\begin{aligned} p_{\mathrm{s}} &= \left[\frac{1}{2}\left(\sqrt{A^2+B^2}+A\right)\right]^{\frac{1}{2}} \\ q_{\mathrm{s}} &= \left[\frac{1}{2}\left(\sqrt{A^2+B^2}-A\right)\right]^{\frac{1}{2}} \\ A &= 4T\mu\Omega^2 - \bar{c}^2v^2 - 4\lambda\bar{k} \\ B &= 4T\Omega\bar{c} \end{aligned} \tag{6}$$

The first expression in Eq. (4) applies to the points behind the excitation point $x - vt > 0$, while the second part is defined for the points ahead the excitation point $x - vt \leq 0$.

3.2 Simplifying assumptions in the analytical model

Important simplifications are adopted in ASM1 if compared to the more complex FE models. These simplifications are also applied to the proposed analytical string model (ASM2).

- Continuous support. In the FE model, the catenary can be divided into two parts, namely, the contact wire and its support system composed of droppers, steady arms and the messenger wire. In the analytical model these two parts can also be identified, but the latter is simplified by a continuous visco-elastic support which does not strictly describe the complex dynamics of the droppers and the messenger wire.

- Constant stiffness. Another feature accounted for in the FE model is the uneven stiffness and mass distribution of the support which holds the contact wire by discrete points (dropper connections), leading to additional irregularities and wave reflection.
- No propagation in the support system. In the FE model any two different points of the support are coupled, which allows the perturbations to propagate along the support. In the analytical model the wave propagation only takes place in the contact wire.
- Linear. FEM models include non-linearities due to contact loss and dropper slackening which are not considered in the analytical model.
- The contact wire in the ASM1 is modelled as a string which neglects its bending stiffness.
- Steady state response. As the catenary is assumed to be a long enough periodic structure, only the steady-state response is considered by ASM1.

Despite these simplifications, the analytical model includes the basic features of the catenary and leads to analytical expressions which provide explicit information on how the design parameters influence the solution and can reveal mechanisms that are not obvious in the response of FEM.

3.3 Consideration of a Kelvin-Voigt damping model

In the catenary FE model, a proportional Rayleigh damping model is used in which the damping matrix is a linear combination of the mass and stiffness matrices ($\mathbf{C} = \alpha\mathbf{M} + \beta\mathbf{K}$). In this section, an extension of the previous analytical model is proposed with a damping model similar to that of the FE model. Following the procedure presented in [23], a Kelvin-Voigt damping model is included in the differential equation Eq. (2) by writing the damping coefficients as a linear combination of the inertial and elastic terms:

$$\mu\frac{\partial^2 w}{\partial t^2} - T\frac{\partial^2 w}{\partial x^2} + \left(\alpha\mu + \beta\bar{k}\right)\frac{\partial w}{\partial t} - \beta T\frac{\partial}{\partial t}\left(\frac{\partial^2 w}{\partial x^2}\right) + \bar{k}w = p(x,t) \tag{7}$$

Note that in ASM1 the term $T\partial^2 w/\partial x^2$ is lacking its corresponding proportional damping term in the differential equation, which means the damping model in ASM1 is not comparable to the one in the FEM model.

This proposed analytical string model (hereinafter called ASM2) has an additional term and has become a third order equation. In the case of a moving

external force of frequency Ω, the improper integral used to compute $w(x,t)$ has a third order polynomial denominator instead of the second order polynomial in the ASM1 [9]:

$$w(x,t) = \frac{1}{2\pi}\int_{-\infty}^{\infty} \frac{F_0\ e^{-i(k(x-vt)-\Omega t)}}{\lambda k^3 + \eta k^2 + \tau k + \sigma}\mathrm{d}k \tag{8}$$

where:

$$\begin{aligned}
\lambda &= i\beta T v \\
\eta &= T - \mu v^2 + i\beta T\Omega \\
\tau &= i\left(\alpha\mu + \beta\bar{k}\right)v - 2\mu v\Omega \\
\sigma &= \bar{k} + i\left(\alpha\mu + \beta\bar{k}\right)\Omega - \mu\Omega^2
\end{aligned} \tag{9}$$

In this case the system has three poles k_1^Ω, k_2^Ω and k_3^Ω whose analytical expressions are:

$$\begin{aligned}
k_1^\Omega &= -\frac{\eta}{3\lambda} - \frac{\sqrt[3]{2}Q}{3\lambda S} + \frac{S}{3\sqrt[3]{2}\lambda} \\
k_2^\Omega &= -\frac{\eta}{3\lambda} - \left(-\frac{1}{2} + \frac{i\sqrt{3}}{2}\right)\frac{\sqrt[3]{2}Q}{3\lambda S} + \left(-\frac{1}{2} - \frac{i\sqrt{3}}{2}\right)\frac{S}{3\sqrt[3]{2}\lambda} \\
k_3^\Omega &= -\frac{\eta}{3\lambda} - \left(-\frac{1}{2} - \frac{i\sqrt{3}}{2}\right)\frac{\sqrt[3]{2}Q}{3\lambda S} + \left(-\frac{1}{2} + \frac{i\sqrt{3}}{2}\right)\frac{S}{3\sqrt[3]{2}\lambda}
\end{aligned} \tag{10}$$

where:

$$\begin{aligned}
S &= \sqrt[3]{R + \sqrt{4Q^3 + R^2}} \\
Q &= 3\lambda\tau - \eta^2 \\
R &= -2\eta^3 + 9\eta\lambda\tau - 27\lambda^2\sigma
\end{aligned} \tag{11}$$

Applying the residue theorem to Eq. (8), the string vertical displacement is:

$$w(x,t) = \begin{cases}
iF_0 \displaystyle\sum_p \frac{e^{-i\left(k_p^\Omega(x-vt)-\Omega t\right)}}{\lambda \displaystyle\prod_{r\neq p}\left(k_p^\Omega - k_r^\Omega\right)}; & x - vt \leq 0 \\
-iF_0 \displaystyle\sum_q \frac{e^{-i\left(k_q^\Omega(x-vt)-\Omega t\right)}}{\lambda \displaystyle\prod_{r\neq q}\left(k_q^\Omega - k_r^\Omega\right)}; & x - vt > 0
\end{cases} \tag{12}$$

where k_p^Ω are the poles with a positive imaginary part and k_q^Ω are the poles with a negative imaginary part. As in the ASM1, the solution is divided into two expressions which correspond to the displacements of the string section behind and ahead of the load application point, respectively. Each part of the solution consists of a sum of exponential terms which represent damped waves. In ASM2 there are three terms (or waves) included in the solution corresponding to the three poles. The poles with a positive imaginary part are contained in the first part of the solution, where $x - vt \leq 0$, while the poles with a negative imaginary part are used in the expression valid for $x - vt > 0$.

In the simpler ASM1 model, the sign of the imaginary part of the two poles depends on the velocity v. If $v < v_c$, there is one pole with a negative imaginary part and one pole with a positive imaginary part, which corresponds to a backward and a forward wave, respectively. On the other hand, if $v > v_c$, both poles have positive imaginary parts and the two waves propagate backwards, the section ahead of the applied force remaining unaltered. In the ASM2 it is difficult to find a mathematical criterion to define the sign of the imaginary part of the poles. However, numerical tests reveal that the imaginary parts of the poles do not vary their signs in the range of interest of Ω and v, if the values of the parameters T, $\bar{k}$ and μ are those obtained in Section 4. Specifically, only one pole k_1^Ω has a negative imaginary part, while the other two poles k_2^Ω and k_3^Ω remain with a positive imaginary part.

To highlight this feature, in Fig. 4 the imaginary part of the poles of ASM2 is plotted versus the velocity v for the excitation frequency $\Omega = 10$ Hz. It is important to note that this behaviour is analogous for all the frequencies studied and although the imaginary part of the poles is very close to zero for some values of v, it does not actually reach that value in any case. In ASM2 there is no critical speed at which the signs of the poles change, however, the solution is similar to that of ASM1. For speeds below v_c of ASM1 ($\sim$146 m/s with the parameter used in this paper) the imaginary part of k_3^Ω is very large and its associated wave is strongly damped. Thus, the only noticeable waves are those related to the poles k_1^Ω and k_2^Ω, as in ASM1. The same explanation is applicable for speeds greater than v_c, in which the absolute value of the imaginary part of k_1^Ω is large enough and for that reason has a negligible influence. In this case, k_2^Ω, k_3^Ω are the dominant poles and there are two noticeable backward waves, as in ASM1. Despite these similarities, the damping is different in the two analytical models and the influence of the additional pole in ASM2 is considerable for velocities close to v_c and also for points close to the load point.

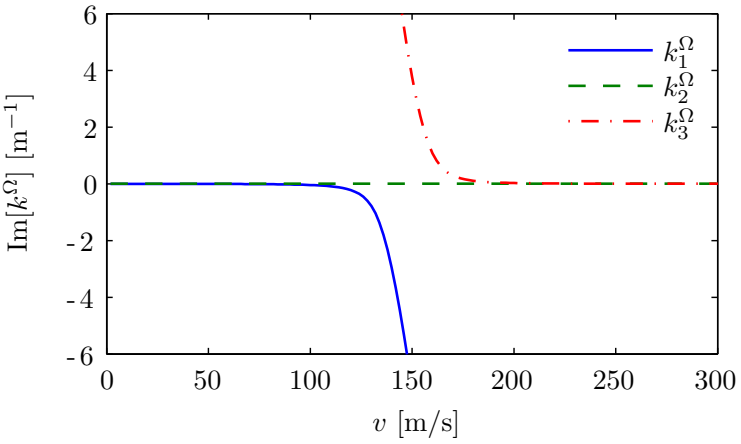

Figure 4: *Imaginary part of the poles of the ASM2 respect to v for $\Omega = 10$ Hz.*

3.4 Model with contact wire initial geometry and pantograph coupling

The force of gravity produces an uneven initial height of the contact wire, which is properly considered in the FE model. In this section, a realistic contact wire initial height profile is included in ASM2. For this, the total string height can be written as:

$$z(x,t) = z_0(x) + w(x,t) \tag{13}$$

where $z_0(x)$ is the initial height, which depends on the position x and, $w(x,t)$ satisfies Eq. (7) thanks to the linearity of the problem.

As catenaries can generally be assumed as periodic structures composed of a succession of equal spans, the height of the contact wire is a periodic function that can be broken down into a sum of harmonic functions by means of the Fourier transform. Due to the linearity of the system, the problem can be solved first by considering a harmonic height $z_0(x)$, after which the superposition principle can be applied to get the solution with a general contact wire height in a further step.

The main objective is to solve the dynamic interaction of two pantographs coupled to ASM2, which now incorporates an initial harmonic height $z_0(x)$. The pantographs move at the same speed v and are separated by a distance L, as seen in Fig. 5.

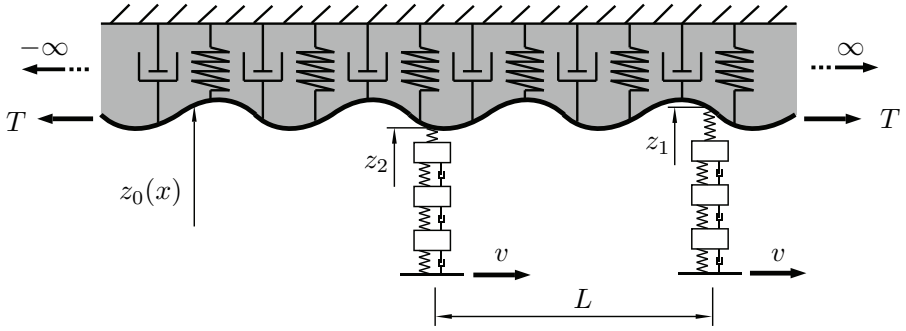

Figure 5: *Two pantographs coupled to the ASM2 with initial height $z_0(x)$.*

The methodology followed in [9] consists of using the dynamic stiffness matrices to solve the coupled interaction between the string and the pantograph models. In this paper the same methodology is considered to solve the problem, but nevertheless, the receptance functions are used and only one degree of freedom is included per pantograph, which corresponds to the vertical displacement of the point in contact with the string. The problem is thus reduced in size without affecting the accuracy of the results. Furthermore, this simplification allows to obtain an analytical expression of the solution.

In order to apply the described procedure, it is first necessary to obtain the Frequency Response Function (FRF). Given two points 1 and 2 on the string, located at a distance L and both moving at the same speed v (see Fig. 6), the FRF of the string H_{12} is defined as the ratio between the vertical displacement of 1 and the harmonic force applied at 2:

$$H_{12}(\Omega) = \frac{w(vt + L, t)}{F_0 e^{i\Omega t}} \tag{14}$$

Replacing the expression (12) in Eq. (14) and considering the signs of the imaginary parts of the poles discussed previously (Sec. 3.3), the FRF is:

$$H_{12}(\Omega) = \frac{-ie^{-ik_1^\Omega L}}{\lambda \left(k_1^\Omega - k_2^\Omega\right)\left(k_1^\Omega - k_3^\Omega\right)} \tag{15}$$

Similarly, H_{21} can be defined as the ratio between the displacement produced in 2 and the excitation applied at 1:

$$H_{21}(\Omega) = \frac{ie^{ik_2^\Omega L}}{\lambda \left(k_2^\Omega - k_1^\Omega\right)\left(k_2^\Omega - k_3^\Omega\right)} + \frac{ie^{ik_3^\Omega L}}{\lambda \left(k_3^\Omega - k_1^\Omega\right)\left(k_3^\Omega - k_2^\Omega\right)} \tag{16}$$

When the displacement is measured at the force application point, the direct FRF is:

$$H_{11}(\Omega) = H_{22}(\Omega) = \frac{-i}{\lambda\left(k_1^{\Omega} - k_2^{\Omega}\right)\left(k_1^{\Omega} - k_3^{\Omega}\right)} \tag{17}$$

It is also necessary to calculate the FRF of the pantograph model, which includes a penalty stiffness k_{h} on the upper mass (see Fig. 2). The pantograph FRF is thus defined as the ratio between the displacement of the upper point ($1'$ or $2'$ in Fig. 6) and the harmonic force applied at the same point:

$$H_{\mathrm{p}}(\Omega) = \frac{1}{k_{\mathrm{h}}} + \left[-\Omega^2\mathbf{M}_{\mathrm{p}} + i\Omega\mathbf{C}_{\mathrm{p}} + \mathbf{K}_{\mathrm{p}}\right]^{-1}_{(1,1)} \tag{18}$$

where $\mathbf{M}_{\mathrm{p}}$, $\mathbf{C}_{\mathrm{p}}$ y $\mathbf{K}_{\mathrm{p}}$ are the mass, damping and stiffness matrices of the pantograph respectively, and the operator $[\ ]_{(1,1)}$ extracts the first row and first column element of the matrix which refers to the upper mass degree of freedom.

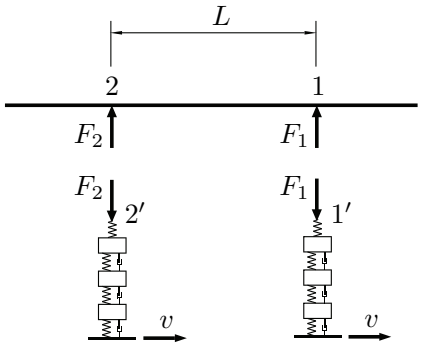

Figure 6: *Contact forces in the coupled string model with two pantographs.*

The contact forces F_1 and F_2 between each pantograph and the string, represented in Fig. 6, are the unknowns of the problem. The linearity of Eq. (7) allows writing the vertical displacement of the points 1 and 2 as the superposition of the displacement produced by each force acting separately. The height of points 1 and 2 are thus the sum of the initial height of the contact wire and the displacement produced by the contact forces according to the scheme in Fig. 6. This is:

$$\begin{aligned} z_1(t) &= z_{01}(t) + H_{11}(\Omega)F_1(t) + H_{12}(\Omega)F_2(t) \\ z_2(t) &= z_{02}(t) + H_{21}(\Omega)F_1(t) + H_{22}(\Omega)F_2(t) \end{aligned} \tag{19}$$

where $z_{01}(t) = z_0(vt + L)$ and $z_{02}(t) = z_0(vt)$. In turn, the height of the points $1'$ y $2'$ which belong to the pantograph model are:

$$\begin{aligned} z_{1'}(t) &= -H_{\mathrm{p}}(\Omega) F_1(t) \\ z_{2'}(t) &= -H_{\mathrm{p}}(\Omega) F_2(t) \end{aligned} \tag{20}$$

Since the initial height is considered a harmonic function of frequency Ω, it is possible to write them as:

$$\begin{aligned} z_{01}(t) &= \tilde{z}_{01} e^{i\Omega t} \\ z_{02}(t) &= \tilde{z}_{02} e^{i\Omega t} \end{aligned} \tag{21}$$

in which, there is a phase shift between the phasors $\tilde{z}_{01}$ and $\tilde{z}_{02}$

$$\tilde{z}_{01} = \tilde{z}_{02} e^{i\frac{\Omega L}{v}} \tag{22}$$

due to the distance between the points. This phasor notation can also be used for the CFs:

$$\begin{aligned} F_1(t) &= \tilde{F}_1 e^{i\Omega t} \\ F_2(t) &= \tilde{F}_2 e^{i\Omega t} \end{aligned} \tag{23}$$

Since the points 1 and 2 match with the points $1'$ and $2'$, the left hand side terms of Eqs. (19) and (20) can be equated to obtain the following system of equations:

$$\begin{bmatrix} -H_{\mathrm{p}}(\Omega) - H_{11}(\Omega) & -H_{12}(\Omega) \\ -H_{21}(\Omega) & -H_{\mathrm{p}}(\Omega) - H_{22}(\Omega) \end{bmatrix} \begin{Bmatrix} \tilde{F}_1 \\ \tilde{F}_2 \end{Bmatrix} = \begin{Bmatrix} \tilde{z}_{01} \\ \tilde{z}_{02} \end{Bmatrix} \tag{24}$$

which can be arranged in matrix notation:

$$\mathbf{H}(\Omega)\ \tilde{\mathbf{F}} = \tilde{\mathbf{z}}_0 \tag{25}$$

As stated above, in the static equilibrium configuration, the catenary contact wire adopts a periodic height $z_0(x)$ whose period is equal to the span length L_{v}. The periodic function $z_0(x)$ can be represented by the Fourier series:

$$z_0(x) = Z_0 + \sum_{n=1}^{\infty} Z_n\ e^{ik_n x} \tag{26}$$

where Z_0 is the mean value of the function, Z_n are the complex Fourier coefficients and the wavenumber is:

$$k_n = \frac{2\pi n}{L_{\mathrm{v}}} \qquad \text{for} \qquad n \in \mathbb{N} \tag{27}$$

By solving Eq. 25, the contact force of two pantographs coupled to ASM2 are obtained for the case of an initial harmonic height. Since that system is linear, the more general case in which $z_0(x)$ is a periodic function can also be solved by

applying Eq. (26) and the superposition principle:

$$\mathbf{F}(t) = \mathbf{F}_{\mathrm{m}} + \sum_{n=1}^{\infty} \mathbf{H}^{-1}(\Omega_n)\ \tilde{\mathbf{z}}_{0,n}\ e^{i\Omega_n t} \tag{28}$$

where $\mathbf{F}_{\mathrm{m}}$ is the vector with the mean CF of every pantograph, the excitation frequency is:

$$\Omega_n = k_n v \tag{29}$$

and $\tilde{\mathbf{z}}_{0,n}$ groups the complex Fourier coefficients of the contact wire initial height, which considers the phase shift between the pantographs:

$$\tilde{\mathbf{z}}_{0,n} = \left\{ \begin{array}{c} Z_n e^{i\frac{\Omega_n L}{v}} \\ Z_n \end{array} \right\} \tag{30}$$

4 Parameter setting

This section is devoted to determining the ASM2 parameters required to achieve similar behaviour to the reference FE model. These include string tension T, support stiffness $\bar{k}$ and linear density μ. The α and β damping parameters are the same as those considered in the FE model just like the tension T which can be taken directly from the FE model. This mechanical tension is given by the value of the axial pretension of the contact wire, which is 31500 N in this work.

4.1 Setting visco-elastic support stiffness

The value of $\bar{k}$ is tuned by comparing the static equilibrium response in both the ASM2 and FE models. Given a vertical force applied at a certain point on the contact wire, the vertical stiffness k_{z} is defined as the ratio between the applied force and the vertical displacement at the application point. This parameter is constant at any point in ASM2. However, as the FE model is not homogeneous and k_{z} varies according to the position in the span, as shown in Fig. 7, its mean value $k_{\mathrm{z,FEM}} = 2538.7$ N/m is adopted as a representative value.

Vertical stiffness k_{z} can be calculated in ASM2 by using the direct FRF defined in Eq. (17), assuming $v = 0$ and $\Omega = 0$:

$$k_{\mathrm{z}} = H_{11}^{-1}\Big|_{\substack{\Omega=0 \\ v=0}} = 2\sqrt{\bar{k}\ T} \tag{31}$$

Thus, if k_z is enforced to match $k_{z,FEM}$:

$$\bar{k} = \frac{k_{z,FEM}^2}{4\ T} \tag{32}$$

which leads to a visco-elastic support stiffness $\bar{k} = 51.15\ \mathrm{N/m^2}$.

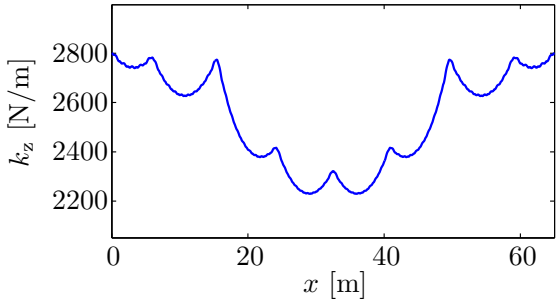

Figure 7: *Vertical stiffness k_z of the contact wire of the FE model in a span.*

In order to check the static solution with the adjusted $\bar{k}$, the FE model and ASM2 are compared in Fig. 8, in which the vertical displacement of the contact wire is adimensionalised with respect to its value at the load application point. Two curves are shown for the FE model, in which the load is applied in the middle of the span and in the steady arm. There is clearly good agreement between the response of both models, especially when the force is applied on the steady arm.

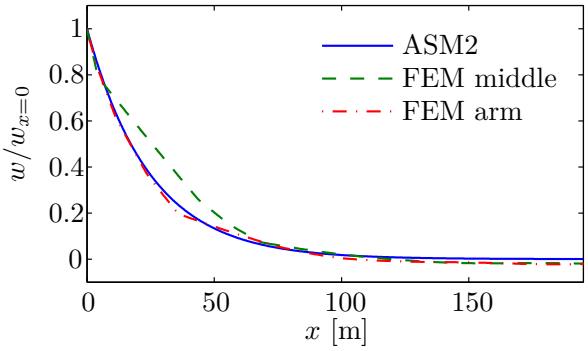

Figure 8: *Adimensionalised displacement of the contact wire in FE model and ASM2 produced by a static force.*

4.2 Setting string linear density

It is not enough to consider only the mass of the catenary contact wire to obtain the string linear density μ but, the mass of the other parts of the catenary must also be taken into account. A wave propagation analysis is performed to adjust the value of μ so that similar behaviour is found in both ASM2 and FE models.

To this end, the response of the contact wire is computed in both models for a harmonic force with $v = 0$. As the load has no forward velocity there are only two poles, k_1^Ω and k_2^Ω, in ASM2 and the displacement of the contact wire (backward side) is given by:

$$w(x,t) = \frac{ie^{-i\left(k_2^\Omega x - \Omega t\right)}}{\eta\left(k_2^\Omega - k_1^\Omega\right)} \tag{33}$$

where $\eta = T + i\beta T\Omega$ and the poles are:

$$\begin{aligned} k_1^\Omega &= \left[\frac{p_\mathrm{s}}{\sqrt{T+\beta^2 T\Omega^2}}\right] - i\left[\frac{q_\mathrm{s}}{\sqrt{T+\beta^2 T\Omega^2}}\right] \\ k_2^\Omega &= \left[\frac{-p_\mathrm{s}}{\sqrt{T+\beta^2 T\Omega^2}}\right] + i\left[\frac{q_\mathrm{s}}{\sqrt{T+\beta^2 T\Omega^2}}\right] \end{aligned} \tag{34}$$

in which, q_s and p_s are those defined in Eq. (6), but now the coefficients A and B result:

$$\begin{aligned} A &= -\bar{k} - \beta\left(\alpha\mu + \beta\bar{k}\right)\Omega^2 + \mu\Omega^2 \\ B &= \left(\alpha\mu + \beta\bar{k}\right)\Omega - \beta\bar{k}\Omega + \beta\mu\Omega^3 \end{aligned} \tag{35}$$

Eq. (33) represents a damped wave whose wavelength is:

$$\lambda_\Omega = -\frac{2\pi}{k_{2\mathrm{R}}^\Omega} \tag{36}$$

$k_{2\mathrm{R}}^\Omega$ being the real part of k_2^Ω. This wavelength λ_Ω is very sensitive to μ, as can be seen in Fig. 9, in which λ_Ω is plotted for different values of the excitation frequency and μ. λ_Ω is therefore a suitable magnitude to adjust linear density μ.

Regarding the reference FE model, the steady-state response is obtained when the contact wire is loaded by a fixed harmonic external force. The wavelength produced at the contact wire $\lambda_{\Omega_{\mathrm{FEM}}}$ can be computed by applying the Discrete Fourier Transform (DFT) in the spatial domain. As a pure harmonic wave cannot

be guaranteed due to the complexity of the FE model, the DFT is applied with a window of variable size in order to get the most dominant wavelength.

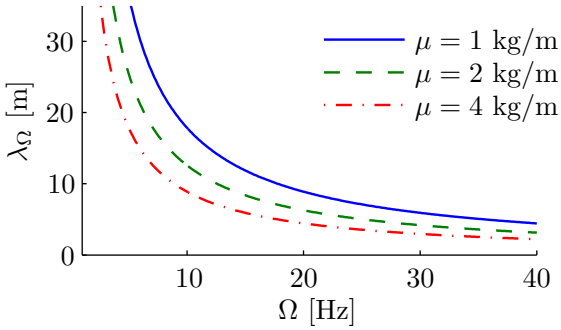

Figure 9: *Wavelength λ_Ω of ASM2 with $v = 0$.*

The values of $\lambda_{\Omega_{\text{FEM}}}$ are obtained for excitation frequencies ranging from 10 to 40 Hz. Lower frequencies lead to very a large wavelength and the upper limit is high enough, considering the low-pass cutoff frequency of 20 Hz defined in the standard [24] for the CF. Finally, the parameter μ is obtained by a least squares fitting of λ_Ω (Eq. (36)) to the results of the FE model $\lambda_{\Omega_{\text{FEM}}}$. This fitting gives a value of $\mu = 1.4735$ kg/m. The good agreement between the FE model ant the fitted ASM2 wavelengths can be seen in Fig. 10.

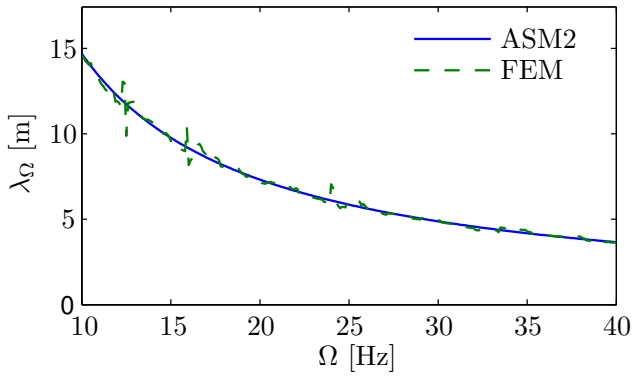

Figure 10: *Wavelength λ_Ω produced by a harmonic force in both ASM2 and the FE model.*

Two additional ranges of Ω are considered to ensure that the value of μ obtained does not depend on the choice of this range. The μ obtained after the fitting are compared in Table 1 for the three ranges of Ω. Given the small difference between the obtained values, the fitting can be considered valid.

Table 1: *Fitted values of μ for different ranges of Ω.*

Ω [Hz]	**5-20**	**10-20**	**10-40**
μ [kg/m]	1.4652	1.4790	1.4735

5 Numerical results

In this section, ASM2 and FE model are used to obtain and compare the contact force (CF) and its standard deviation (σ) produced in the pantograph-catenary dynamic interaction, considering one (single operation) and two pantographs (double operation). The FE catenary model is defined long enough to get a quasi-steady response in its central spans.

The mean value of the CF, F_{m}, is controlled by the external force applied to the pantograph mechanism. According to the standard [24], this magnitude must fulfil the following limitation:

$$F_{\mathrm{m}} \leq 0.0097v^2 + 70 \tag{37}$$

where v is the velocity of the pantograph expressed in km/h. In the ASM2 the CF is obtained as a sum of independent harmonic terms, so the mean value of the CF (F_{m}) does not influence either the harmonics $\tilde{F}(\Omega_n)$ or σ. On the other hand, in the FE model a higher value of F_{m} leads to a higher CF variation due to the uneven distribution of mass and stiffness along the contact wire. In the simulations carried out in the following examples, the maximum value of F_{m} according to Eq. (37) is used, since this is the case with the most CF variation. The CF is filtered by a 20 Hz low-pass filter, following the guidelines in [24].

5.1 Initial geometry of the catenary

The FE model of the catenary used in this paper is composed of periodic 65 m long spans with 7 droppers. The FEM static solution is used to determine the height of the contact wire under the force of gravity (shown in Fig. 11), which is used to calculate the CF in the analytical model. Fig. 12 represents the spatial frequency content of the contact wire height, which allows us to express $z_0(x)$ as a sum of harmonic functions. In this case, the 7^{th} and 8^{th} harmonics depicted in Fig. 12 are the most important and are directly related to the dropper-pass frequency. On the other hand, the frequency component related to the span-length (1^{st} harmonic) has low contribution because pre-sag, installation errors and irregularities produced by long-term service are not taken into account.

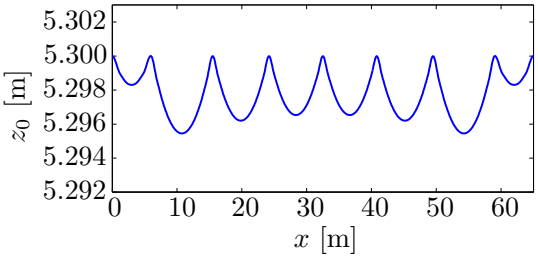

Figure 11: *Catenary contact wire height profile along a span.*

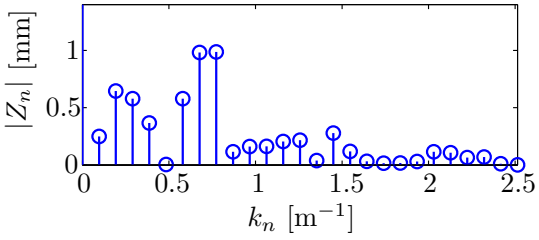

Figure 12: *Discrete Fourier Transform of the catenary contact wire height.*

5.2 Single pantograph operation

In this case, Eq. (24) can be particularised for only a single pantograph, assuming $\tilde{F}_2 = 0$:

$$-\left[H_{\mathrm{p}}(\Omega) + H_{11}(\Omega)\right]\tilde{F}_n = Z_n \tag{38}$$

whose solution is:

$$\tilde{F}_n = K_{\mathrm{D}}(\Omega) Z_n \tag{39}$$

In this expression, the dynamic stiffness $K_{\mathrm{D}}(\Omega)$ is defined as:

$$K_{\mathrm{D}}(\Omega) = \frac{\lambda(k_1^\Omega - k_2^\Omega)(k_1^\Omega - k_3^\Omega)}{i - H_{\mathrm{p}}\lambda(k_1^\Omega - k_2^\Omega)(k_1^\Omega - k_3^\Omega)} \tag{40}$$

and Z_n are the Fourier terms of the initial contact wire height represented in Fig. 12.

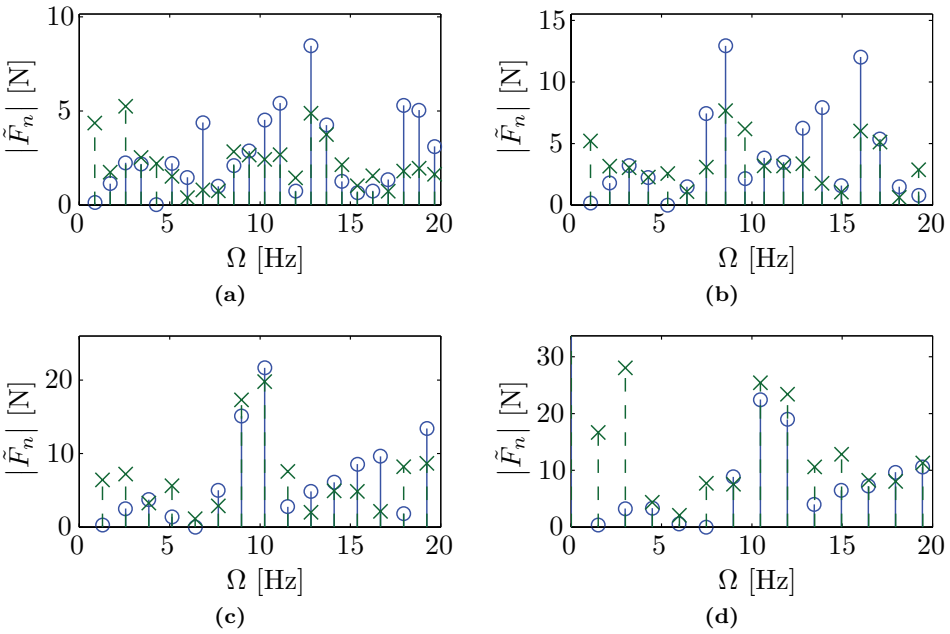

Figure 13: *CF in the frequency domain at (a) 200 km/h, (b) 250 km/h, (c) 300 km/h and (d) 350 km/h. ○ ASM2 × FEM.*

The frequency content of the CF $\left|\tilde{F}_n(\Omega)\right|$ obtained by ASM2 is compared in Fig. 13 with that computed by the FE model for excitation frequencies ranging from 0 to 20 Hz and the pantograph running at 200, 250, 300 and 350 km/h. The results of the FE model are obtained from a central span, where the solution is quasi-steady and thus, the contact force can be considered periodic. Note that the number of harmonics included in the considered frequency range is lower for high speeds due to the relation given in Eq. (29). There is a reasonable similarity between the results of both models since the magnitude of the analytical results is not too far from the FE results. However, great discrepancies are found at 350 km/h in the first two harmonics. They are caused probably by the high F_{m} imposed according to Eq. (37), since the higher the F_{m} the higher the influence of the stiffness variation in the FE model, which is dominated by the first harmonics.

The 20 Hz low-pass filtered CF is represented in the time domain in Fig. 14. Again, although the curves do not fit perfectly, a general similarity between ASM2 and the FEM curves can be appreciated. The discrepancies found at 350 km/h are also present in this temporal representation.

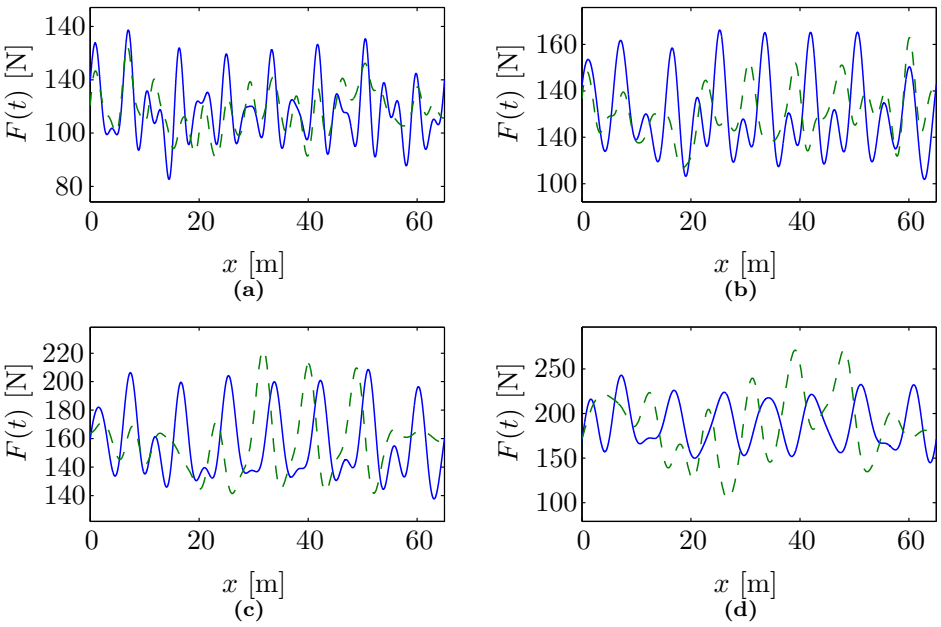

Figure 14: *CF in the time domain at (a) 200 km/h, (b) 250 km/h, (c) 300 km/h and (d) 350 km/h.* —*ASM2* - - *FEM.*

The CF standard deviation σ is the variable most often used to quantify current collection quality. σ can be computed from the CF defined in the frequency domain as:

$$\sigma = \sqrt{\frac{1}{2}\sum_{n=1}^{N_{20}} \left|\tilde{F}_n(\Omega_n)\right|^2} \tag{41}$$

where N_{20} is the number of harmonics whose frequency Ω_n is lower than 20 Hz. The standard deviation σ is plotted versus train velocity in Fig. 15. As σ depends on the mean CF in the FE model, FEM results are shown with a mean CF of 70, 80, 90 and 100% of the maximum mean CF allowed by Eq. (37). However, for the ASM2 the mean value of the CF (F_m) does not have any influence on σ and therefore, F_m is not indicated in the figure. Despite all the simplifications introduced in the analytical model, it is able to give a good approximation of σ with respect to the more accurate results obtained from the FE model. Especially, the similarity for the maximum mean contact force allowed by the standard is remarkable. Note that the mean CF effect is negligible for velocities smaller than 250 km/h for the studied pantograph-catenary system. In conclusion, the standard deviation calculated with the analytical model shows that the irregularities in contact wire height have a strong influence on the CF fluctuations.

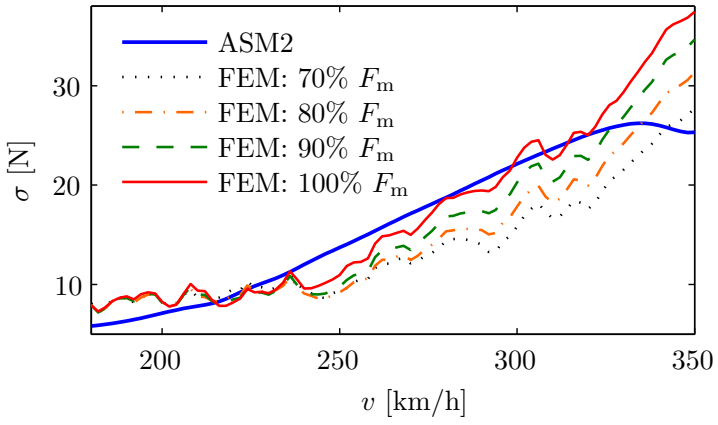

Figure 15: *Comparison of the standard deviation of the CF between the ASM2 and the FE model for different pantograph velocities and different values of the mean CF.*

5.3 Pantograph interference

In double pantograph operation, each pantograph affects the dynamic interaction of the other. However, the interference of the leading pantograph on the trailing pantograph is much greater than in the opposite case. In this section, the CF of the trailing pantograph is analysed with respect to the pantographs separation L. To simplify the analysis, the initial height of the contact wire $z_0(x)$ is considered as a pure harmonic function with frequency Ω.

The CF of both pantographs is obtained by solving Eq. (24). For certain L, the amplitude of the trailing pantograph CF is minimum when the displacement produced by the leading pantograph reaches the trailing pantograph in phase opposition to the given contact wire height. To explain this phenomenon, an approximate analytical solution is proposed to obtain the values of L which produce minimum oscillations in the trailing pantograph CF.

As the trailing pantograph has a negligible effect on the leading pantograph [8, 21], it is assumed here that $H_{12}(\Omega) = 0$, which implies that the CF of the leading pantograph is not modified with respect to the single operation scenario. With this assumption, the solution of Eq. (24) is:

$$\tilde{F}_2 = -\frac{\tilde{z}_0}{H_\mathrm{p} + H_{22}(\Omega)} \left(1 - C_\mathrm{a} e^{iL\left(\Omega/v + k_2^\Omega\right)} - C_\mathrm{b} e^{iL\left(\Omega/v + k_3^\Omega\right)}\right) \tag{42}$$

where:

$$\begin{aligned} C_\mathrm{a} &= \frac{i}{\left(H_\mathrm{p} + H_{11}\left(\Omega\right)\right) \lambda \left(k_2^\Omega - k_1^\Omega\right) \left(k_2^\Omega - k_3^\Omega\right)} \\ C_\mathrm{b} &= \frac{i}{\left(H_\mathrm{p} + H_{11}\left(\Omega\right)\right) \lambda \left(k_3^\Omega - k_1^\Omega\right) \left(k_3^\Omega - k_2^\Omega\right)} \end{aligned} \tag{43}$$

With these expressions is still complex to analytically find out the values of L in which the amplitude of $\tilde{F}_2$ is minimum. Thus, two additional simplifications are introduced:

- The exponential term which includes k_3^Ω can be neglected due to this wave is strongly damped for velocities lower than v_c (see Fig. 4).
- Due to the damping of the remaining exponential term which includes k_2^Ω is very small, a non-damped wave can be assumed so that $k_{2\mathrm{I}}^\Omega = 0$.

With these hypotheses, the minima of $\left|\tilde{F}_2\right|$ are found when:

$$\arg\left(C_\mathrm{a} e^{iL\left(\Omega/v + k_{2\mathrm{R}}^\Omega\right)}\right) = 2\pi n \ ; \qquad n = 0, 1, 2, ... \tag{44}$$

For every Ω there is a group of equidistant optimal values of L:

$$L_{\min} = \frac{2\pi n - arg(C_a)}{\Omega/v + k_{2R}^{\Omega}} \tag{45}$$

For ASM2, the exact value of $\left|\tilde{F}_2\right|$ (see Eq. (25)) and the approximation given in Eq. (42), which assumes negligible interference on the leading pantograph, are compared in Fig. 16 for $\Omega = 10$ Hz and $v = 300$ km/h. The similarity between the two curves is greater for higher L and for L close to $L_{\min}$, since the hypothesis assumed is more accurate (minor influence of the trailing on the leading pantograph), while the minima of both curves are close to the values given by Eq. (45).

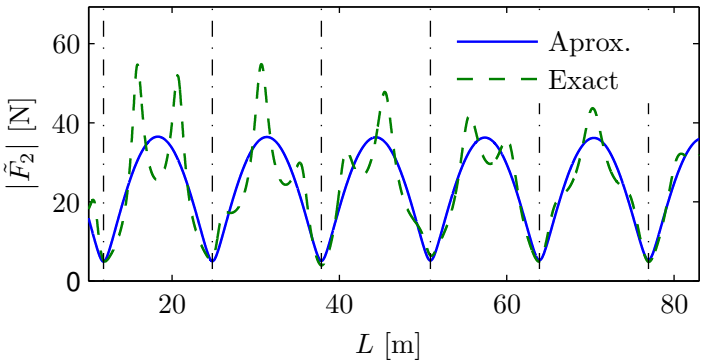

Figure 16: *Variation of approximate and exact analytical CF amplitude of the trailing pantograph with harmonic contact wire initial height of* $\Omega = 10$ *Hz, versus pantograph separation* L*, at* $v = 300$ *km/h. The* $L_{\min}$ *values given by Eq.* (45) *are represented by vertical dash-dotted lines.*

The optimal behaviour of the trailing pantograph is produced by its synchronisation with the wave generated by the leading pantograph. To explain this mechanism the CF phase of the leading pantograph in single operation $\tilde{F}_1$ is taken as a reference. This force generates a wave whose vertical displacement at point 1 (see Fig. 6), considering only the part due to k_2^{Ω} is:

$$\tilde{w}_1 = H_{11}^{k_2} \tilde{F}_1 \tag{46}$$

where:

$$H_{11}^{k_2} = \frac{i}{\lambda \left(k_2^{\Omega} - k_1^{\Omega}\right)\left(k_2^{\Omega} - k_3^{\Omega}\right)} \tag{47}$$

The phase of this displacement is $\varphi_{w_1} = \arg(H_{11}^{k_2})$. This wave has a phase of $\varphi_{w_1} = \arg(H_{11}^{k_2})$ and a wavelength $k_{2\mathrm{R}}^{\Omega}$. At point 2 it generates a displacement with phase $\varphi_{w_2} = \varphi_{w_1} + k_{2\mathrm{R}}^{\Omega} L$ due to the distance L between points 1 and 2. This displacement produces an interference force $\tilde{F}_{2\mathrm{i}}$ on the trailing pantograph whose phase is $\varphi_{F_{2\mathrm{i}}} = \varphi_{w_2} + \arg(K_{\mathrm{D}})$, according to Eq (39).

On the other hand, the CF of the trailing pantograph $\tilde{F}_2$, if considered in single operation, has a different phase with respect to the leading pantograph CF due to the delay between them, so that $\varphi_{F_2} = -\Omega L/v$. Thus, the CF of the trailing pantograph has minimum amplitude when its force in single operation is in phase opposition with the interference force, i.e. $\varphi_{F_{2\mathrm{i}}} - \varphi_{F_2} = \pi + 2\pi n$, which is equivalent to Eq. (44). After replacing terms it reads:

$$\arg(H_{11}^{k_2}) + \arg(K_{\mathrm{D}}) + k_{2\mathrm{R}}^{\Omega} L + \frac{\Omega L}{v} = \pi + 2\pi n \ ; \quad n = 0, 1, 2, ... \tag{48}$$

To conclude this analysis, all the phases of the magnitudes involved are summarised in Table 2.

Table 2: *Summary of the different phases of the magnitudes involved in the pantograph interference.*

	φ	
Pantograph/point	1	2
CF in single operation	0	$-\dfrac{\Omega L}{v}$
Wave produced by pant. 1	$\arg(H_{11}^{k_2})$	$\arg(H_{11}^{k_2}) + k_{2\mathrm{R}}^{\Omega} L$
Interference force	——	$\arg(H_{11}^{k_2}) + k_{2\mathrm{R}}^{\Omega} L + \arg(K_{\mathrm{D}})$

5.4 Double pantograph operation

To verify the accuracy of ASM2 in double pantograph operation, the standard deviation of the CF of the trailing pantograph σ_2 is compared with the FEM results in Fig. 17 for a wide range of L at the operating speeds of 200, 250, 300 and 350 km/h. In this case, since $z_0(x)$ contains several harmonics (see Fig. 12) the fluctuating σ_2 behaviour versus changes in L is produced by the contributions of all the CF harmonics, which fluctuate every $L_{\min}(\Omega)$. Considering all the differences between the models, the approximation obtained by the analytical model has reasonable accuracy, especially at 300 km/h. Note that σ_2 obtained from the FE model is higher than the analytical values when v increases, due probably to the effect of the greater mean CF imposed, according to Eq. (37). In

fact, a higher value of σ_2 at 350 km/h in the FEM model was already given in the analysis performed with single operation (Fig. 15).

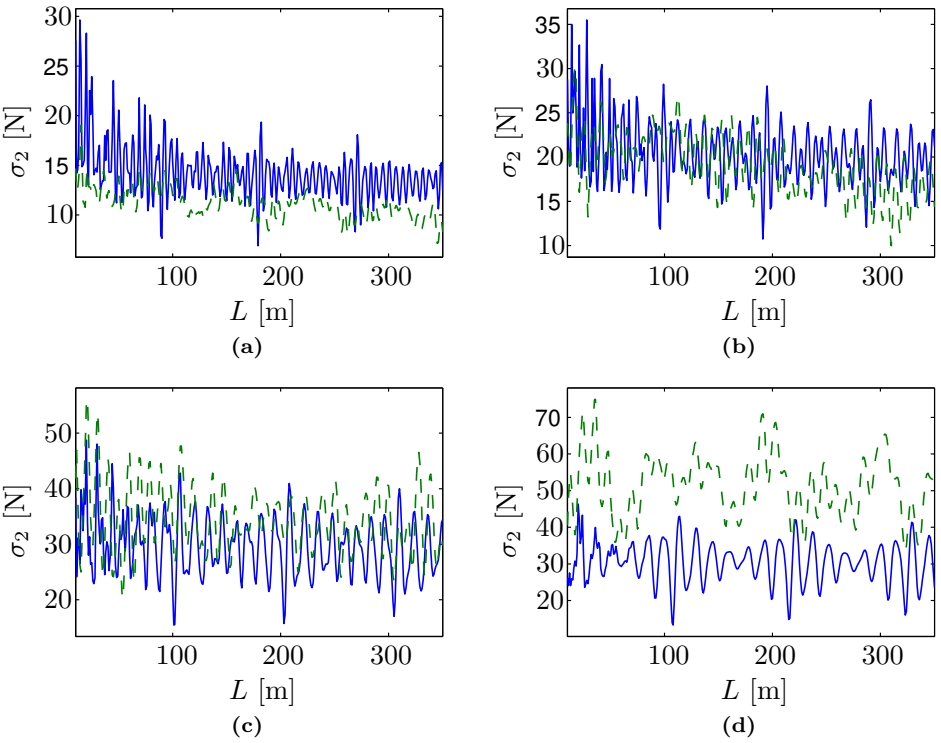

Figure 17: *SD of the trailing pantograph CF with respect to the distance between pantographs at (a) 200 km/h, (b) 250 km/h, (c) 300 km/h and (d) 350 km/h.* — *ASM2.* - - *FEM.*

6 Conclusions

The CF variation obtained in the FE simulations of the pantograph-catenary dynamic interaction is due to the combination of several sources of irregularities (geometric variation of the contact wire, uneven stiffness and mass distribution, etc.) with complex phenomena (wave propagation and reflection, complex dynamic response of the model, among others). This complexity makes these simulations computationally intensive and it is difficult to infer direct relations between the model input and output variables.

In this paper the enhanced analytical model ASM2 composed of an axially loaded infinite string with a visco-elastic support was based on that proposed in [9]. ASM2 includes a Kelvin-Voigt damping model, considers the initial height of the contact wire and uses the *penalty* method to model the contact between the pantograph and the contact wire. With this model, an analytic expression of the steady-state interaction force was obtained.

Different strategies were followed to fit the ASM2 parameters in order to obtain similar behaviour to the more complex FE model. The stiffness of the support was fitted by considering a static problem, while the proper linear density of the string was obtained by considering the wavelength generated in the contact wire by harmonic excitation.

The CF standard deviation σ was computed with the fitted ASM2 for a wide range of operational speeds (Fig. 15). The results obtained reveal that the initial contact wire height profile is one of the main factors that contribute to CF variation and therefore to the current collection quality. The uneven distribution of the vertical stiffness along the span is another important contribution to the CF variation, which becomes more important at high mean CF values. Since this feature is not considered in the analytical model, it can explain the greater σ obtained by the FE for the high velocities at which a greater mean CF is imposed.

A more complicated scenario arises when two pantographs interact simultaneously with the catenary, since the interference between them is a complex phenomenon which depends on wave propagation. Despite this complexity, with the proposed analytical model the string response can be separated into harmonic terms leading to obtain a simple formula for the optimal distance between the pantographs that gives the lowest trailing pantograph CF amplitude for every harmonic. Thus, the physical mechanism by which the interference occurs has been explained from ASM2. Furthermore, in a more realistic scenario, good approximations of the trailing pantograph σ are obtained by ASM2 for different distance between pantographs.

In order to improve the model and obtain a response closer to that from the FE model, future research could be focused on including a time-varying vertical stiffness which will lead to higher complexity in the differential equation and its solution. Furthermore, due to its simplicity and the low computational cost required to obtain the catenary response, the proposed analytical model could be used in future works to perform parametric analyses and even Hardware In the Loop (HIL) tests.

Acknowledgements

The authors would like to acknowledge the financial support received from the Regional Government of Valencia (PROMETEO/2016/007) and the Spanish Ministry of Economy, Industry and Competitiveness (TRA2017-84736-R), also the funds received jointly from the Regional Government of Valencia and the European Social Fund, under Grant APOSTD/2019/205.

Bibliography

[1] F. Kieling, R. Puschmann, A. Schmieder, and E. Schneider, *Contact lines for electrical railways: Planning, Design, Implementation, Maintenance*. Publicis Publishing, Erlangen, Germany, third ed., 2018.

[2] EN 50318:2018, "Railway applications. Current collection systems. Validation of simulation of the dynamic interaction between pantograph and overhead contact line," *European Union Agency for Railways*, 2018.

[3] S. Bruni, J. Ambrosio, A. Carnicero, Y. H. Cho, L. Finner, M. Ikeda, S. Y. Kwon, J. P. Massat, S. Stichel, and M. Tur, "The results of the pantograph-catenary interaction benchmark," *Vehicle System Dynamics*, vol. 53, no. 3, pp. 412–435, 2015.

[4] M. Aboshi and K. Manabe, "Analyses of contact force fluctuation between catenary and pantograph.," *Quarterly Report of Railway Technical Research Institute*, vol. 41, pp. 182–187, 2000.

[5] P. Nåvik, A. Rønnquist, and S. Stichel, "The use of dynamic response to evaluate and improve the optimization of existing soft railway catenary systems for higher speeds," *Proceedings of the Institution of Mechanical Engineers, Part F: Journal of Rail and Rapid Transit*, vol. 230, no. 4, pp. 1388–1396, 2016.

[6] J. Pombo and J. Ambrósio, "Influence of pantograph suspension characteristics on the contact quality with the catenary for high speed trains," *Computers & Structures*, vol. 110, pp. 32–42, 2012.

[7] T. Wu and M. Brennan, "Basic analytical study of pantograph-catenary system dynamics," *Vehicle System Dynamics*, vol. 30, no. 6, pp. 443–456, 1998.

[8] W. Zhang, N. Zhou, R. Li, G. Mei, and D. Song, "Pantograph and catenary system with double pantographs for high-speed trains at 350 km/h or higher," *Journal of Modern Transportation*, vol. 19, pp. 7–11, Mar 2011.

[9] S. Roy, G. Chakraborty, and A. DasGupta, "Coupled dynamics of a viscoelastically supported infinite string and a number of discrete mechanical systems moving with uniform speed," *Journal of Sound and Vibration*, vol. 415, pp. 184 – 209, 2018.

[10] P. Belotserkovskiy, "Forced oscillations and resonance of infinite periodic strings," *Journal of Sound and Vibration*, vol. 204, no. 1, pp. 41 – 57, 1997.

[11] A. Metrikine and A. Bosch, "Dynamic response of a two-level catenary to a moving load," *Journal of Sound and Vibration*, vol. 292, no. 3, pp. 676 – 693, 2006.

[12] Y. Song, Z. Liu, F. Duan, Z. Xu, and X. Lu, "Wave propagation analysis in high-speed railway catenary system subjected to a moving pantograph," *Applied Mathematical Modelling*, vol. 59, pp. 20 – 38, 2018.

[13] M. Aboshi and M. Tsunemoto, "Installation guidelines for shinkansen high speed overhead contact lines," *Quarterly Report of Railway Technical Research Institute*, vol. 52, pp. 230–236, 11 2011.

[14] O. V. Van, J.-P. Massat, C. Laurent, and E. Balmes, "Introduction of variability into pantograph–catenary dynamic simulations," *Vehicle System Dynamics*, vol. 52, no. 10, pp. 1254–1269, 2014.

[15] S. Gregori, M. Tur, J. E. Tarancón, and F. J. Fuenmayor, "Stochastic monte carlo simulations of the pantograph–catenary dynamic interaction to allow for uncertainties introduced during catenary installation," *Vehicle System Dynamics*, vol. 57, no. 4, pp. 471–492, 2019.

[16] O. V. Van, J.-P. Massat, and E. Balmes, "Waves, modes and properties with a major impact on dynamic pantograph-catenary interaction," *Journal of Sound and Vibration*, vol. 402, pp. 51 – 69, 2017.

[17] Y. H. Cho, K. Lee, Y. Park, B. Kang, and K. nam Kim, "Influence of contact wire pre-sag on the dynamics of pantograph–railway catenary," *International Journal of Mechanical Sciences*, vol. 52, no. 11, pp. 1471 – 1490, 2010.

[18] S. Gregori, M. Tur, E. Nadal, and F. J. Fuenmayor, "An approach to geometric optimisation of railway catenaries," *Vehicle System Dynamics*, vol. 56, no. 8, pp. 1162–1186, 2018.

[19] M. Tur, E. García, L. Baeza, and F. Fuenmayor, "A 3D absolute nodal coordinate finite element model to compute the initial configuration of a railway catenary," *Engineering Structures*, vol. 71, pp. 234–243, 2014.

[20] S. Gregori, M. Tur, E. Nadal, J. Aguado, F. Fuenmayor, and F. Chinesta, "Fast simulation of the pantograph–catenary dynamic interaction," *Finite Elements in Analysis and Design*, vol. 129, pp. 1 – 13, 2017.

[21] Z. Liu, P.-A. Jönsson, S. Stichel, and A. Rønnquist, "On the implementation of an auxiliary pantograph for speed increase on existing lines," *Vehicle System Dynamics*, vol. 54, no. 8, pp. 1077–1097, 2016.

[22] H. M. Hilber, T. J. R. Hughes, and R. L. Taylor, "Improved numerical dissipation for time integration algorithms in structural dynamics," *Earthquake Engineering & Structural Dynamics*, vol. 5, no. 3, pp. 283–292, 1977.

[23] D. Anastasio, A. Fasana, L. Garibaldi, and S. Marchesiello, "Analytical investigation of railway overhead contact wire dynamics and comparison with experimental results," *Mechanical Systems and Signal Processing*, vol. 116, pp. 277–292, Feb. 2019.

[24] EN 50367, "Railway applications. Current collection systems. Technical criteria for the interaction between pantograph and overhead line," *European Committee for Electrotechnical Standardization*, 2012.

Appendix A

Catenary and pantograph data

The values of the input parameters which define the catenary and pantograph models used in this paper are listed here. The catenary model is composed of 30 spans 65 m long. The spacing between the 7 droppers along the span is defined in Table A.1, where SA denotes the steady arm.

Table A.1: *Dropper spacing along the span.*

Droppers	SA-1	1-2	2-3	3-4	4-5	5-6	6-7	7-SA
d(m)	6	9.48	8.7	8.32	8.32	8.7	9.48	6

The mechanical and the geometric properties of the different wires of the catenary are given in Table A.2.

Table A.2: *Mechanical and geometric properties of the catenary elements.*

	ρ(kg/m^3)	E(MPa)	A(mm^2)	I(mm^4)	T (N)
Messenger wire	9114	$1.1{\cdot}10^{11}$	94.8	1237.2	15750
Contact wire	9160	$1.1{\cdot}10^{11}$	150	2170	31500
Droppers	9114	$1.1{\cdot}10^{11}$	10	0	3500 (“Y”)

The Rayleigh coefficients of the damping model are $\alpha = 0.0125$ s^{-1} and $\beta = 0.0001$ s and the constants of the HHT integration method are $\alpha_{\text{HHT}} = -0.05$, $\beta_{\text{HHT}} = 0.2756$, $\gamma = 0.55$ and $\Delta t = 0.001$ s.

The values of the lumped parameters of the pantograph model can be seen in Table A.3. The stiffness used in the *penalty* method is $k_{\text{h}} = 50000$ N/m.

Table A.3: *Parameters of the pantograph model.*

d.o.f.	m(kg)	c(Ns/m)	k(N/m)
1	6.6	0	7000
2	5.8	0	14100
3	5.8	70	80

PAPER B

Hardware in the loop pantograph tests using analytical catenary models

J. Gil, M. Tur, A. Correcher, S. Gregori, A. Pedrosa and F. J. Fuenmayor

Vehicle System Dynamics
Volume 60:10, Pages 3504-3518, 2022
DOI: 10.1080/00423114.2021.1962538

Abstract

Pantograph hardware-in-the-loop (HIL) testing is an experimental method in which a physical pantograph is excited by an actuator which reproduces the movement of a virtual catenary. This paper proposes a new method that uses analytical catenary models for HIL tests. The approach is based on an iterative scheme until achieving a steady-state regime. Some of the method's advantages include its ability to consider the delay in the control and communication system and its applicability to a wide range of analytical catenary models. The proposed algorithm was validated both numerically and experimentally. The experimental results obtained in the HIL pantograph tests were compared with those obtained from pure numerical simulations using a linear pantograph model and showed good accuracy with pantograph running at different speeds.

Keywords

Hardware-In-the-Loop, Analytical catenary model, Steady-state response, Pantograph

Contents

1 Introduction

High-speed locomotives collect current through the sliding contact between the pantograph and the railway catenary, which is composed of overlapping independent sections of about 1 km in length (see Fig. 1). Each section contains a messenger wire and droppers that hold the contact wire, which interacts with the collector strips on the pantograph, at the appropriate height. Messenger and contact wires are supported by brackets and posts at regular intervals, called spans.

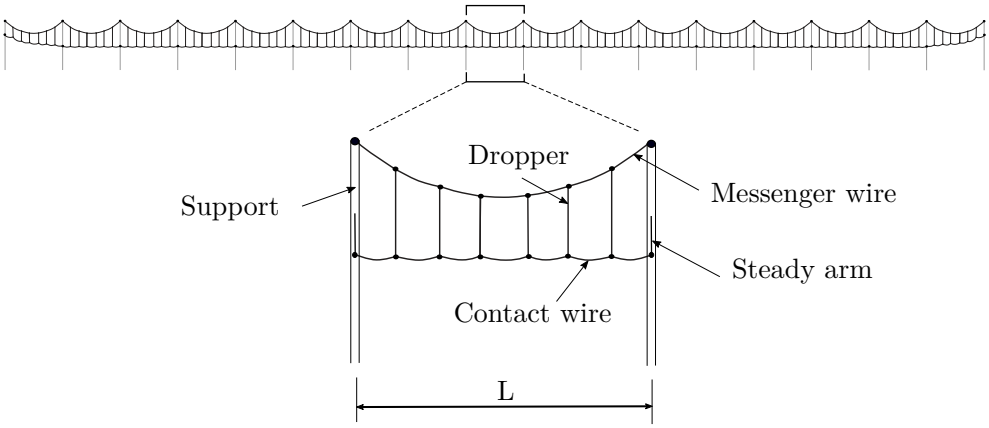

Figure 1: *Scheme of a catenary section and detail of a single span.*

The contact force produced in the pantograph-catenary dynamic interaction plays an important role in assessing the quality of the power supply. This contact force reaches a steady-state regime in the central spans of each catenary section, where the catenary can be assumed a periodic structure with repetitive spans. Both numerical and experimental methods are now widely used to assess the contact force. Several computer programs are able to simulate the pantograph-catenary dynamic interaction [1], which is especially useful in the early stages of the design process. In-line tests are also made with instrumented pantographs to measure experimentally the pantograph interaction force. These tests are required for the validation of a given pantograph-catenary couple; in Europe for example the requirements are provided by the EN 50317 standard [2].

To reduce the number of costly in-line tests, pantograph Hardware-In-the-Loop (HIL) lab tests have arisen as an appealing cheaper alternative, in which the catenary is replaced by an actuator that interacts with a real pantograph. The actuator movements simulate the position of the catenary contact point, which

depends on the catenary's dynamic behaviour and the measured interaction force. The catenary model should be as realistic as possible but at the same time must be solved in real-time, which is usually managed by the use of simplified catenary models instead of more complex finite element models with direct time integration.

The first works that proposed a pantograph HIL test rig were [3, 4] using a finite length catenary model based on a truncated modal approach to study the influence of different parameters on the pantograph-catenary dynamic interaction. Another HIL set-up for pantograph dynamics evaluation was proposed in [5], in which a hydraulic actuator reproduces the vertical movement of a very simple catenary model composed of three spans. This model was upgraded in [6] with the consideration of the non-linear dropper behaviour and in [7] by incorporating lateral movement in the test rig to simulate the catenary stagger. In [8], a linear model of the catenary with 3D Euler-Bernoulli beams is used in combination with a moving coordinates formulation and absorbing boundary layers at both ends of the catenary model. All the catenary models used in the above mentioned references are finite length models which need the use of specific boundary conditions to perform HIL tests.

In this work we propose a new method of performing pantograph HIL tests using analytical catenary models. In general terms, these analytical models provide the steady-state solution at the central spans of a catenary section with different degrees of approximation. One of the simplest models is found in [9], in which the catenary is modelled as a single and two-degrees-of-freedom system with periodically time-varying mass and stiffness. A more complex model was presented in [10], in which an infinite string with visco-elastic support is used to obtain the stationary response of lumped-parameter moving models coupled to the string. The even more complex infinite string models include periodic discrete elements, such as in [11] or [12], in which a two-level infinite catenary model, composed of an upper and lower string joined by periodic supports and dampers, is simulated along with a pantograph modelled by a harmonic point-load. Similar models can also be found in the literature, such as that proposed in [13], which is composed of several finite strings and is used to study the catenary wave propagation and reflection phenomena. Of the wide variety of analytical catenary models, we here use that proposed in [14], which considers the main catenary dynamic features and the initial contact wire height profile.

The paper is organised as follows. After this introduction, the analytical catenary model chosen for this work is briefly described in Section 2. The algorithm proposed to perform steady-state HIL tests is presented and validated in Section 3. Section 4 describes the test rig components and the control system. An

experimental validation of the setup and some HIL tests results are provided in Section 5, while the concluding remarks are given in Section 6.

2 Analytical catenary model

In this paper we present the results obtained with a particular analytical catenary model, but it should be noted that the proposed method can also be applied to other analytical models, as long as they provide the response of the catenary contact point under a harmonic load moving at a constant velocity.

2.1 Dynamic behaviour

The model chosen for this work is an improved version of the one proposed by Roy et al. [10], which is based on the response of a viscoelastically supported infinite string excited by a moving load with uniform speed. This model is schematically depicted in Fig. 2 and was analysed in [14], in which a good agreement was obtained with the steady-state results of Finite Element simulations. For the sake of completeness, here we summarise the main features of the model. It is composed of an axially loaded infinite string, with linear density μ and initial traction T, supported by a continuous visco-elastic layer of stiffness $\bar{k}$ per unit of length. A Kelvin-Voigt damping model of coefficients α and β considers the energy dissipation similarly to Finite Element models.

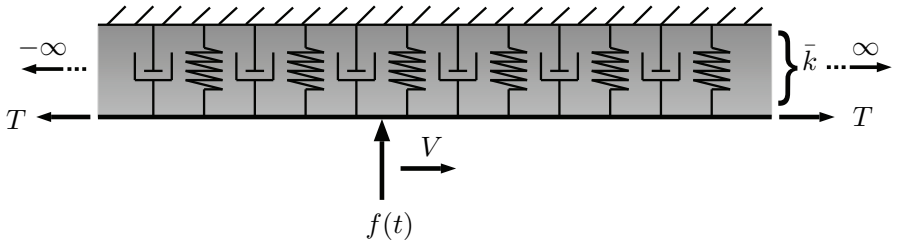

Figure 2: *Analytical string model with visco-elastic support under a moving load.*

The string model subjected to a general load $p(x,t)$ is governed by the following equation:

$$\mu\frac{\partial^2 u}{\partial t^2} - T\frac{\partial^2 u}{\partial x^2} + \left(\alpha\mu + \beta\bar{k}\right)\frac{\partial u}{\partial t} - \beta T\frac{\partial}{\partial t}\left(\frac{\partial^2 u}{\partial x^2}\right) + \bar{k}u = p(x,t) \tag{1}$$

where $u = u(x,t)$ is the vertical displacement of the string.

As depicted in Fig. 2, for a concentrated load moving at constant speed V, the right-hand side term of Eq. (1) can be expressed as:

$$p(x,t) = f(t)\ \delta(x - Vt) \tag{2}$$

where δ denotes the *Dirac* function.

If the load is a harmonic function of frequency ω, $f(t) = F_0 e^{i\omega t}$, the closed solution of Eq. (1) for any point x and time t, $u(x,t)$, is obtained using the method proposed in [10, 14]. The steady-state response of the contact point of an ideally infinite catenary under harmonic excitation can thus be written as:

$$u_c(t) = u(Vt,t) = \frac{-iF_0 e^{i\omega t}}{\lambda\left(k_1(\omega) - k_2(\omega)\right)\left(k_1(\omega) - k_3(\omega)\right)} \tag{3}$$

in which k_1, k_2, k_3 and λ depend on the excitation frequency (ω) and other model parameters (T, V, μ, $\bar{k}$, α, β) as defined in 6.

This response can be characterised by the Frequency Response Function (FRF) H_s, which is defined as the ratio between the vertical displacement and the harmonic force applied at the contact point:

$$H_s(\omega) = \frac{u_c(t)}{F_0 e^{i\omega t}} = \frac{-i}{\lambda\left(k_1(\omega) - k_2(\omega)\right)\left(k_1(\omega) - k_3(\omega)\right)} \tag{4}$$

2.2 Contact wire geometry

The contact wire height profile plays an important role in the dynamic behaviour of the pantograph-catenary system [15, 16, 17, 18]. The static configuration of the catenary that results from the stringing process can be obtained by different methods. For example, semi-analytical methods are used in [19] or a method based on a Finite Element (FE) model was proposed in [20]. Here we use a nonlinear FE model [21] to obtain the height of the contact wire $z_0(x)$ in a reference catenary span of length L (see Fig. 3 and Fig. 1).

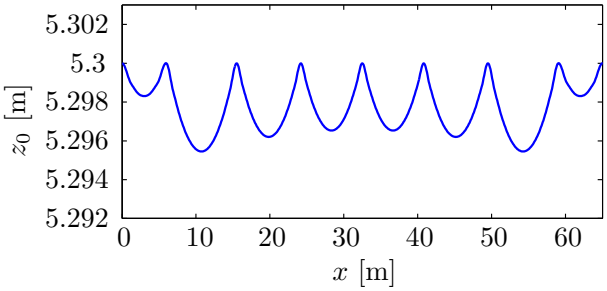

Figure 3: *Catenary contact wire height profile along a span.*

2.3 Contact point height calculation

Thanks to the linearity of the analytical model (Eq. (1)), we can obtain the contact wire height $z_c(t)$ that sees the pantograph moving at speed V as the sum of the static position and the displacement due to the moving interaction load:

$$z_c(t) = z_0(Vt) + u_c(t) \tag{5}$$

where $z_0(Vt)$ is computed in the moving contact point.

We assume that the same span is infinitely repeated, so that z_0 is considered L-periodic of period $T = L/V$. The contact force from the steady-state response of the pantograph-catenary interaction will therefore be repeated every span, i.e. $f(t)$ in Eq. (2) will be a time periodic function of period T, as will also the displacement of the contact wire $u_c(t)$. As a consequence, the steady position of the catenary $z_c(t)$ is also a periodic function.

In a HIL test the contact force is measured at a constant rate $f_s = 1/\Delta t$, Δt being the time increment. Let us assume that the stationary interaction force is known for a whole span, $f_c(t_n) = f_c(n\Delta t)$ for $n = 0, \ldots, N-1$, in which $N = L/(V\Delta t)$. This N-periodic discrete force can be shifted to the frequency domain by applying the Discrete Fourier Transform (DFT):

$$F_c(\omega_k) = \sum_{n=0}^{N-1} f_c(t_n)\, e^{-i\omega_k n\Delta t} \tag{6}$$

in which the discrete frequencies are:

$$\omega_k = k\frac{2\pi}{N\Delta t} \quad k = 0, \ldots, N-1 \tag{7}$$

The steady-state response of the catenary is directly obtained in the frequency domain with the FRF (Eq. (4)) as:

$$U_c(\omega_k) = H_s(\omega_k)F_c(\omega_k) \tag{8}$$

Applying Eq. (5) in the frequency domain, the total contact point height can be computed:

$$Z_c(\omega_k) = Z_0(\omega_k) + U_c(\omega_k) \tag{9}$$

in which

$$Z_0(\omega_k) = \sum_{n=0}^{N-1} z_0(Vn\Delta t)\, e^{-i\omega_k n\Delta t} \tag{10}$$

Finally, the Inverse Discrete Fourier Transform (IDFT) is used to return to the time domain. Given that $f_c(t_n)$ is a real sequence and $H_s(\omega)$ exhibits Hermitian symmetry, we can write:

$$z_c(t_n) = \frac{1}{N}\left(Z_c(\omega_0) + 2\sum_{k=1}^{\frac{N-1}{2}} \mathrm{Re}\left(Z_c(\omega_k)\, e^{i\omega_k n\Delta t}\right)\right) \tag{11}$$

3 Steady-state HIL test method

The previous section showed how to compute the steady-state height of the contact point in a whole span of the catenary if the stationary contact force is known in advance. Here we propose a method of achieving the steady state (force and displacement) if the virtual catenary model interacts with a physical pantograph and the contact force is measured every time step t_n.

Fig. 4 shows a scheme of the proposed HIL test strategy. The catenary contact point is replaced by a linear actuator that imposes the height of the contact wire $z_c(t_n)$ computed by the analytical catenary model in every time step (Eq. (11)). The aim of the test is to simulate the interaction of the pantograph travelling at constant velocity V with the virtual catenary model, which is composed of an infinite sequence of equal spans of length L.

The idea behind the proposed method is to obtain iteratively the response of the contact point in the current virtual span b using the force measured in the

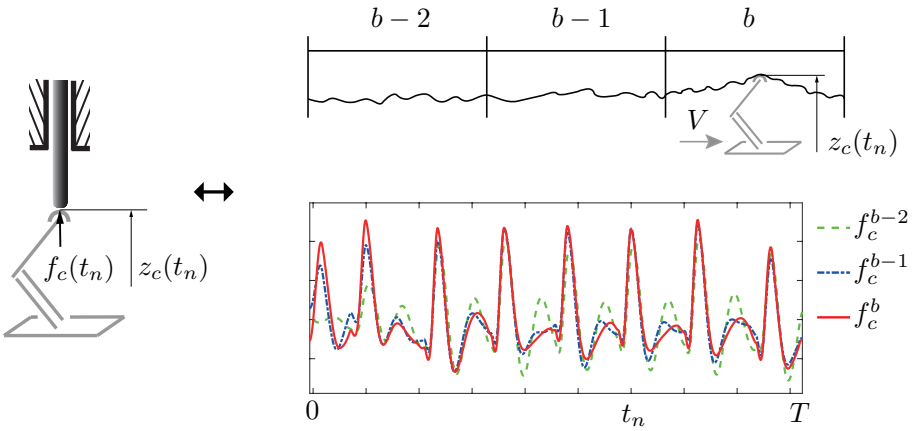

Figure 4: *Scheme of HIL test. From left to right, actuator with pantograph and the measured contact force in three successive virtual spans.*

previous one $b-1$ by means of the equations given in Section 2.3, in which the external force was assumed to be known. We define here the following variables:

- $f_c^b(t_n)$, $z_c^b(t_n)$: Contact force measured in the current virtual span at time $t_n = n\Delta t$, for $n = 0, \ldots, N-1$, and height of the contact point imposed.
- $f_c^{b-1}(t_n)$: Contact force measured in the previous virtual span, with t_n referring to the relative time in that span. Note that t_n is rebooted at the beginning of every virtual span.
- $F_c^{b-1}(\omega_k)$: DFT of the contact force in the previous virtual span.

3.1 Full virtual span iteration

We first define a more intuitive algorithm to better understand the final method proposed. The contact wire height of the current virtual span $z_c^b(t_n)$ is predicted by the measurements of the contact force in the previous one $f_c^{b-1}(t_n)$, following the method described in Section 2.3. The algorithm is initialised assuming null force $f_c^0(t_n)$ on the initial virtual span, so that the predicted height of the contact point $z_c^1(t_n)$ matches the static height of the contact wire $z_0(t_n)$ (Fig. 3). The linear actuator will prescribe this contact point height in the next virtual span and a new contact force will be measured. The test runs until the contact force measured is equal (with an admissible error) in two consecutive spans.

3.2 Single step iteration

The previous strategy can be implemented more efficiently if the measured contact force is updated every time step in the current virtual span instead of every whole span. As shown in Section 3.3, with this strategy the convergence is achieved very quickly after the pantograph interacts with a few virtual spans.

To obtain the contact wire height in a given time step t_n of the current virtual span, we make a calculation block of N contact force values composed of the force already measured in the current virtual span $f_c^b(t_m)$ for $m = 0, \ldots, n$, and the force measured in the previous virtual span $f_c^{b-1}(t_m)$ for time steps $m = n+1, \ldots, N-1$. The missing contact force values needed to complete the current virtual span are fulfilled with those of the previous one.

The DFT of the contact force $F_c^n(\omega_k)$ of the calculation block of time step t_n can be obtained from Eq. (6) as:

$$F_c^n(\omega_k) = \sum_{m=0}^{n} f_c^b(t_m) e^{-i\omega_k m\Delta t} + \sum_{m=n+1}^{N-1} f_c^{b-1}(t_m) e^{-i\omega_k m\Delta t} \tag{12}$$

Eq. (12) can be rewritten in incremental form as:

$$F_c^n(\omega_k) = F_c^{n-1}(\omega_k) + \Delta F_c^n(\omega_k) \qquad k = 0, \ldots, N-1 \tag{13}$$

in which F_c^{n-1} contains the frequency content of the contact force computed in the previous time step t_{n-1} and the increment term $\Delta F_c^n(\omega_k)$ is computed from:

$$\Delta F_c^n(\omega_k) = \alpha \left(f_c^b(t_n) - f_c^{b-1}(t_n) \right) e^{-i\omega_k n\Delta t} \qquad k = 0, \ldots, N-1 \tag{14}$$

The stabilisation parameter $\alpha \in [0, 1]$ is introduced here to ensure convergence in exchange for increasing the time in which the steady state is reached.

The displacement of the contact point $U_c^n(\omega_k)$ caused by the force obtained from Eq. (13) is obtained by applying Eq. (8). The frequency content of the contact point height $Z_c^n(\omega_k)$ is then directly computed by Eq. (9). Finally, the contact wire height at time t_n, which will be imposed by the linear actuator, is transformed to the time domain according to Eq. (11).

Remark. *The proposed method has the advantages of low computational cost and low memory requirements, which make it suitable for HIL tests. The formulation includes the entire frequency content (harmonics $k = 0, \ldots, N-1$). Given that pantograph-catenary dynamics can be computed using frequencies from 0 to ω_{max}, the computational cost of the method can be further reduced by computing the*

solution for the range of frequencies $k = 0, \ldots, N_{cut} - 1$*, in which* $N_{cut} < N$ *is the index associated with the maximum frequency:*

$$N_{cut} = \frac{N\Delta t}{2\pi}\omega_{max}$$

3.3 Numerical validation

Before moving to the real HIL tests, a computational reproduction of a HIL test was performed to demonstrate the the proposed method's theoretical validity, in which the measured force was replaced by the reaction force obtained from the time integration of a linear lumped-parameter pantograph model with the contact point height imposed on the pantograph collector. The parameters used to define the analytic catenary model shown in Table 1 were taken from [14], in which they were appropriately tuned according to a realistic FEM catenary model.

Table 1: *Parameters of the analytical catenary model.*

L (m)	T (N)	μ (kg/m)	$\bar{k}$ (N/m^2)	α (s^{-1})	β (s)
65	31500	1.4735	51.15	0.0125	10^{-4}

This computational test was first used to show the effect of the stabilisation parameter α on the solution. Fig. 5 shows the contact force obtained for three different values of α along seven virtual spans with a pantograph travelling speed of $V = 250$ km/h. It can be seen that the higher the α the faster the convergence to the steady state. However, as an excessively high value for this parameter could produce instabilities in a real HIL test, a balance must be experimentally achieved between convergence speed and stability.

Since the method was verified as converging, it was important to check whether it converged to the correct solution, for which the result of this computational HIL test was compared to that of the direct method briefly introduced in Section 2 and fully available in [14]. Fig. 6 shows the contact force in a full span. Note that the converged solution of the proposed algorithm perfectly matches that obtained from the direct method, which corroborates the validity of the proposed algorithm.

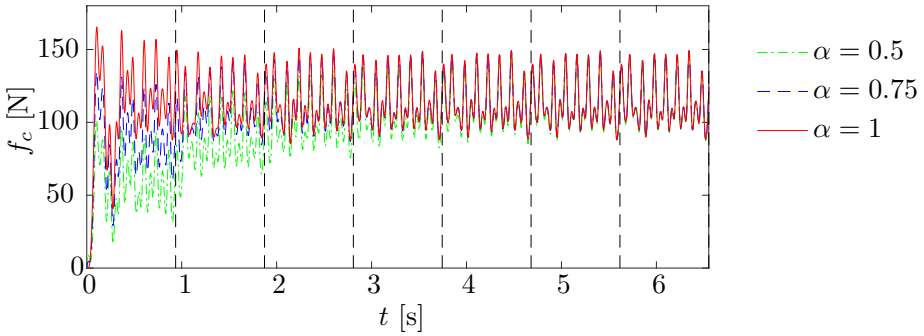

Figure 5: *Contact force in the computational HIL test with different values of the stabilisation parameter α along seven virtual spans at 250 km/h. Virtual spans are shown by vertical dashed lines.*

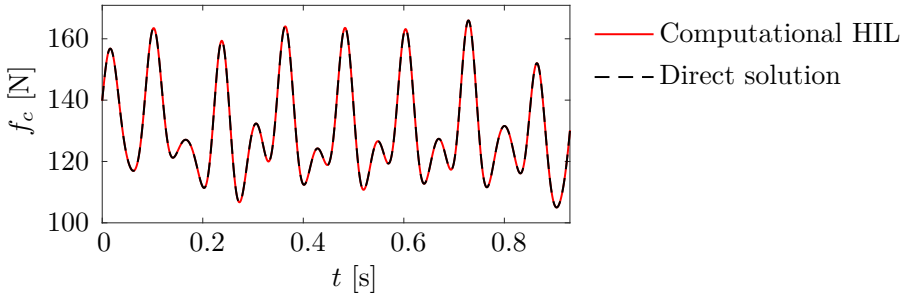

Figure 6: *Comparison of contact force obtained from the proposed algorithm and from the direct method presented in [14] for a pantograph running at 250 km/h.*

4 HIL test rig

The main components of the HIL test rig are depicted in Fig. 7. The contact force on each collector strip of the pantograph is measured by means of a load cell. This signal is filtered and conditioned and finally acquired by the National Instruments® cRio-9040 real-time controller in which the analytical catenary model runs to provide the contact point height that fulfils the linear actuator (LinMot® 70x400U) to simulate the catenary movement.

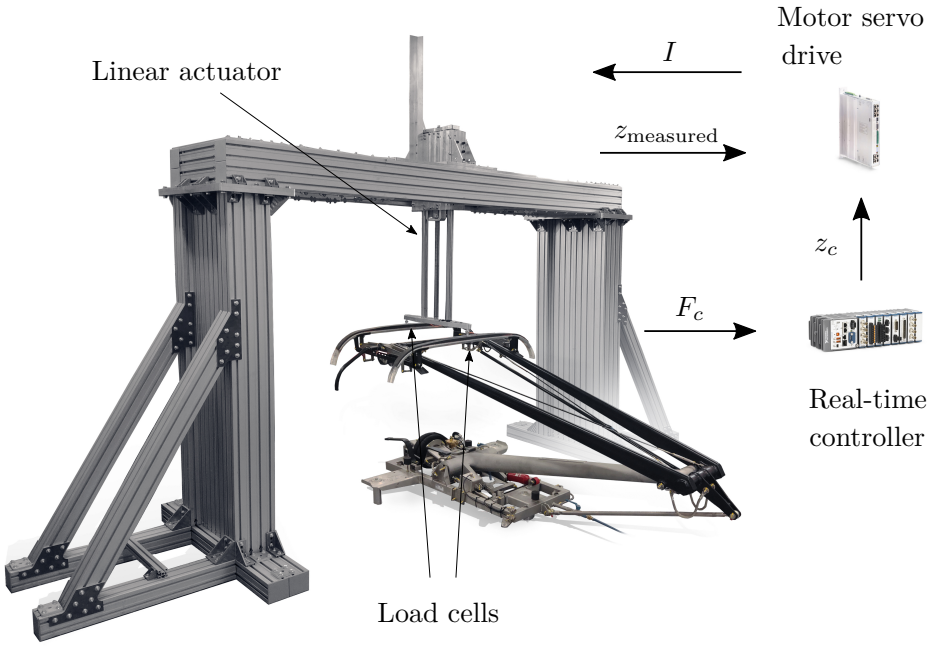

Figure 7: *HIL test rig.*

The contact point height is set as a reference for the servo drive LinMot® E1400, which drives the linear actuator, via Ethernet UDP communication. This servo includes a PID closed loop control of the motor position which is configured to reach the desired position using an acceleration and velocity-limited motion profile.

All these cycle tasks are shown schematically in Fig. 8. The contact force F_c between the linear actuator and the pantograph is measured, filtered and sampled to feed the catenary model which provides the contact point height z_c every $\Delta t = 1$ ms. However, communications between the real time controller and the motor servo drive cannot take place at this rate, so that one value of every N_{com} values of z_c is sent to LinMot servo drive. For the tests described here $N_{\text{com}} = 8$ was used to ensure communications without any data loss. The value received by LinMot z_{com} is set as the new reference and the controller tries to reach this reference by generating a set of intermediate reference points, at a rate of 0.3125 ms, linearly interpolated from z_{com} and the previous reference z_{old}. The LinMot servo drive uses a PID controller, which works at a higher rate, to fulfil these intermediate references.

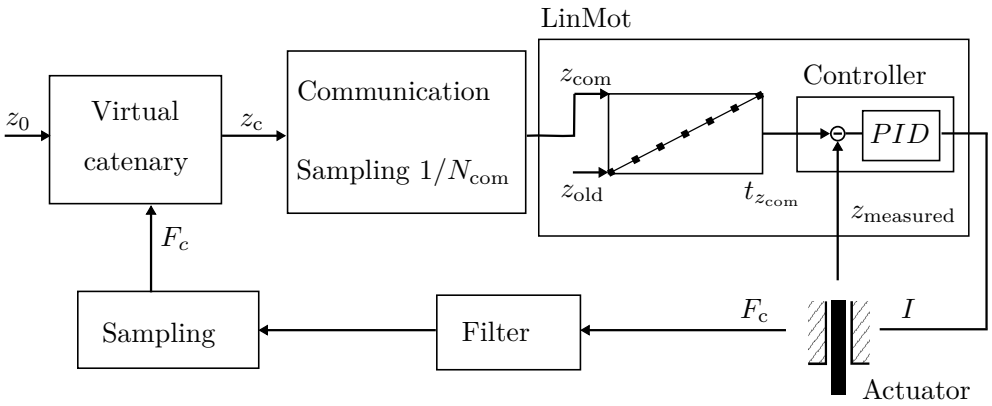

Figure 8: *Simulation cycle of tasks in HIL test.*

It is important to emphasise that the whole loop described in Fig. 8 requires a certain time to be accomplished. We can define the overall delay of the test rig, $\delta = N_\delta \Delta t$, as the time spent from when the force is measured until the computed contact point height is reached by the linear actuator. This value calculated both theoretically and experimentally gave a result of approximately 19 ms. Accounting for the test rig delay in the HIL tests is crucially important because omitting this step could modify the final response or even make it unstable.

One of the advantages of using analytical catenary models is the ease of dealing with the delay in the test rig. The height of the contact point can be obtained in any time step, so that if the test rig delay is known, the response of the catenary model can be obtained N_δ time steps in advance, meaning that the actuator reaches this position at the proper time.

For this end, the missing force values needed to complete the current virtual span b are assumed to be equal to the previous virtual span $b-1$. For example, if we have measured the contact force at time t_n and we want to obtain the contact point height at t_m for $m > n$, the force values between t_{n+1} and t_m, $f_c^b(t_{n+1}^m)$, are chosen as $f_c^{b-1}(t_{n+1}^m)$. As the test converges to the steady state, with this strategy the contact force will tend to be repetitive from one span to the next and the error of this assumption will thus tend to disappear.

The contact point height calculated from Eq. (11) only needs to be modified with the advanced time required:

$$\bar{z}_c(t_n) = \frac{1}{N}\left(Z_c(\omega_0) + 2\sum_{k=1}^{\frac{N-1}{2}} \mathrm{Re}\left(Z_c(\omega_k)e^{i\omega_k(n+N_\delta)\Delta t}\right)\right) \tag{15}$$

5 Experimental results

This section contains some experimental results obtained from the HIL test rig. The experimental validation of the control system and the overall performance of the test rig was first obtained by means of a benchmark test in which the pantograph was replaced by a mass. The results of the HIL tests with a real pantograph were then shown and compared with the analytical solution obtained from simulations with a linear pantograph model.

5.1 Experimental validation

In order to validate the control system and the proper operation of the HIL test rig, an experimental validation test was carried out in which the pantograph was replaced by a mass of 5.29 kg directly attached to the linear actuator, as shown in Fig. 9. This simple system can be modelled very accurately to obtain the analytical solution of its interaction with the catenary model.

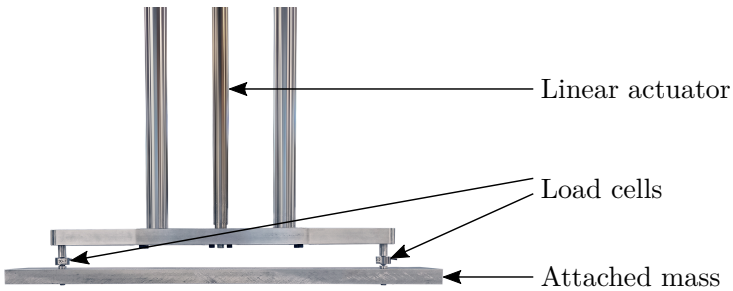

Figure 9: *Mass attached to the linear actuator for the validation test.*

This analytical solution is depicted in Fig. 10 when the mass is virtually moving at 300 km/h along with the contact force obtained from the HIL test rig. The experimental results include the contact force measured in the 10 last virtual spans to verify that the steady state has been achieved using the stabilisation

parameter $\alpha = 0.1$. The contact force measured is filtered at 30 Hz with an analogical low-pass filter and the catenary response is computed with the first 20 harmonics ($N_{cut} = 20$) including frequencies up to 25 Hz. Finally, the contact forces shown in Fig. 10 are low-pass filtered to 25 Hz with a digital filter.

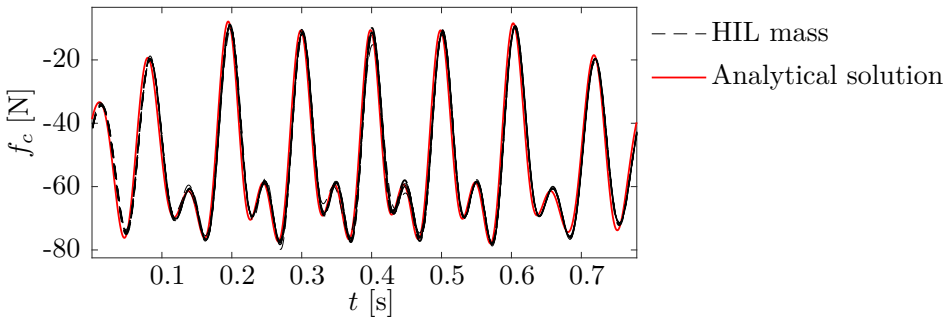

Figure 10: *Comparison of the contact force in the mass HIL test (10 spans overlapped) at 300 km/h with the analytical solution.*

As shown in Fig. 10, the experimental results are almost identical to the analytical solution, indicating a completely satisfactory experimental validation. Note that in this case the contact force has negative values because the attached mass pulls the load cells down, unlike the pantograph, which pushes them up.

5.2 Pantograph HIL tests

This section gives the results and an analysis of the pantograph HIL simulation with the same conditions to those used in the validation HIL test of Section 5.1. The contact force obtained for the last 10 virtual spans is shown in Fig. 11 with the pantograph running at 200, 225, 250, 275 and 300 km/h and with the stabilisation parameter α between 0.05 and 0.1. The number of harmonics N_{cut} included in the response varies from 30 (200 km/h) to 20 (300 km/h) to ensure that the frequency content of the response reaches up to 25 Hz.

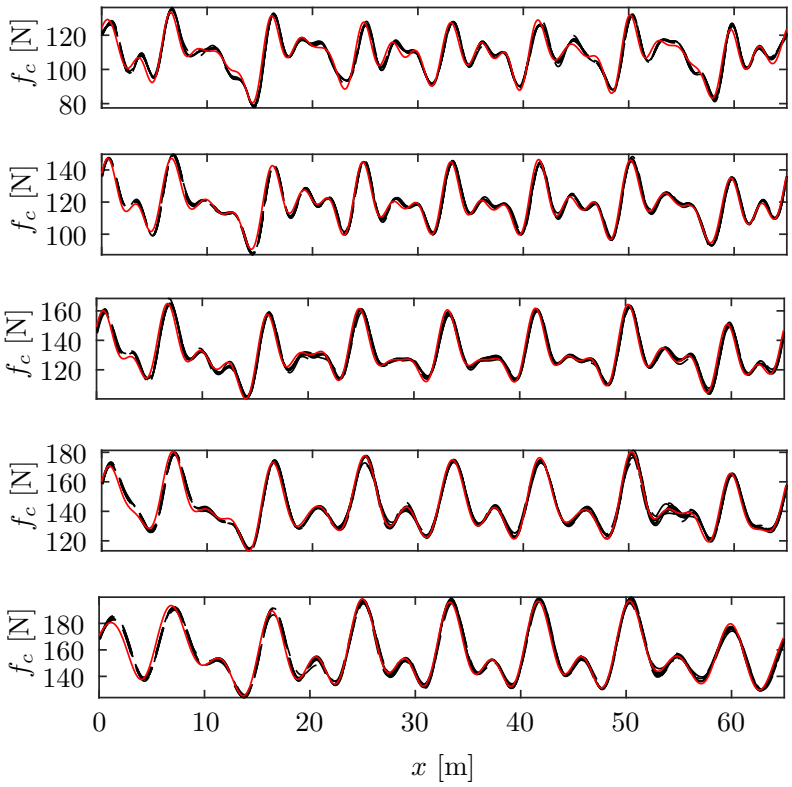

Figure 11: *Comparison of the contact force obtained from the pantograph HIL test (10 spans overlapped in black) and the analytical solution with a linear pantograph model (red curves). Tests performed at 200, 225, 250, 275 and 300 km/h from top to bottom.*

The repeatability of these 10 curves of every tests verifies that the tests have converged to the steady-state solution. This contact force is also compared in Fig. 11 with the analytical solution obtained when using a linear lumped-parameter pantograph model showing the great similarity between them.

Some additional tests have been executed at different pantograph velocities and the standard deviation σ of the contact force is plotted in Fig. 12. Again, the experimental tests show a good agreement with the analytical solution obtained by using a linear pantograph model.

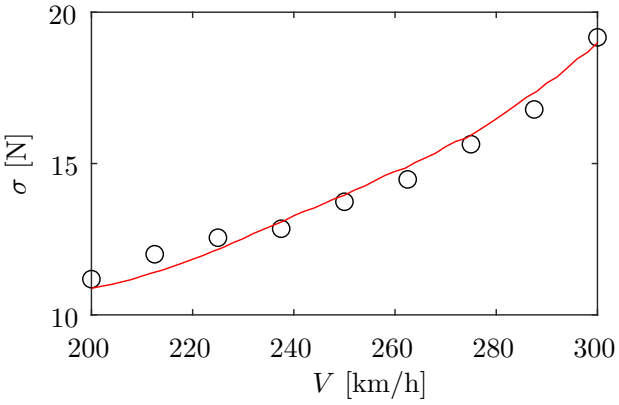

Figure 12: *Comparison of the standard deviation of the contact force obtained from pantograph HIL tests (black circles) and the analytical solution with a linear pantograph model (red curve).*

6 Conclusions

This paper defines a HIL test rig in which a physical pantograph interacts with a linear actuator that emulates the catenary dynamic behaviour, together with an algorithm to perform HIL pantograph tests with analytic catenary models to obtain the steady-state pantograph-catenary dynamic interaction. Although a very simple string catenary model was used in this work to illustrate the proposed method, it is important to note that this strategy is applicable to a wide range of analytical catenary models provided that the Frequency Response Function can be obtained under a harmonic load travelling at constant speed. With this type of analytical catenary models there is no need to avoid boundary effects and delays in measurement and signal transmission are easily dealt with.

Furthermore, the use of a simple analytical model in HIL pantograph tests can be a useful tool to check the validity of a given pantograph model or to compare the performance of different pantographs. In this work we proved the validity of a fitted linear model of the pantograph. However, if high fidelity is required, more realistic analytical models can be used with the proposed method.

A benchmark HIL test was performed in which the pantograph was replaced by a mass directly attached to the linear actuator to validate the whole performance of the test rig and the control system. The results obtained in this reference test

were then compared with the analytical response of the mass interacting with the analytical catenary model. The delay produced since the contact force is measured until the linear actuator achieves the specified height was considered in this experimental validation.

We also provide the results of the HIL tests on a physical pantograph, which show a good convergence to the steady-state solution. In general, there is good agreement between the contact force obtained from these tests and the analytical results when using a linear pantograph model.

Acknowledgements

The authors would like to acknowledge the financial support received from the Spanish Ministry of Economy, Industry and Competitiveness [TRA2017-84736-R].

Bibliography

[1] S. Bruni, J. Ambrosio, A. Carnicero, Y. H. Cho, L. Finner, M. Ikeda, S. Y. Kwon, J. P. Massat, S. Stichel, and M. Tur, "The results of the pantograph-catenary interaction benchmark," *Vehicle System Dynamics*, vol. 53, no. 3, pp. 412–435, 2015.

[2] EN 50317, "Railway applications. Current collection systems. Requirements for and validation of measurements of the dynamic interaction between pantograph and overhead contact line," *European Committee for Electrotechnical Standardization*, 2012.

[3] W. Zhang, G. Mei, X. Wu, and Z. Shen, "Hybrid simulation of dynamics for the pantograph-catenary system," *Vehicle System Dynamics*, vol. 38, no. 6, pp. 393–414, 2002.

[4] W. Zhang, G. Mei, X. Wu, and L. Chen, "A study on dynamic behaviour of pantographs by using hybrid simulation method," *Proceedings of the Institution of Mechanical Engineers, Part F: Journal of Rail and Rapid Transit*, vol. 219, no. 3, pp. 189–199, 2005.

[5] A. Collina, A. Facchinetti, F. Fossati, and F. Resta, "Hardware in the loop test-rig for identification and control application on high speed pantographs," *Shock and Vibration*, vol. 11, pp. 445–456, 01 2004.

[6] F. Resta, A. Facchinetti, A. Collina, and G. Bucca, "On the use of a hardware in the loop set-up for pantograph dynamics evaluation," *Vehicle System Dynamics*, vol. 46, no. S1, pp. 1039–1052, 2008.

[7] A. Facchinetti and M. Mauri, "Hardware-in-the-loop overhead line emulator for active pantograph testing," *IEEE Transactions on Industrial Electronics*, vol. 56, no. 10, pp. 4071–4078, 2009.

[8] A. Schirrer, G. Aschauer, E. Talic, M. Kozek, and S. Jakubek, "Catenary emulation for hardware-in-the-loop pantograph testing with a model predictive energy-conserving control algorithm," *Mechatronics*, vol. 41, pp. 17 – 28, 2017.

[9] T. Wu and M. Brennan, "Basic analytical study of pantograph-catenary system dynamics," *Vehicle System Dynamics*, vol. 30, no. 6, pp. 443–456, 1998.

[10] A. D. S. Roy, G. Chakraborty, "Coupled dynamics of a viscoelastically supported infinite string and a number of discrete mechanical systems moving with uniform speed," *Journal of Sound and Vibration*, vol. 415, pp. 184–209, 2018.

[11] P. Belotserkovskiy, "Forced oscillations and resonance of infinite periodic strings," *Journal of Sound and Vibration*, vol. 204, no. 1, pp. 41 – 57, 1997.

[12] A. Metrikine and A. Bosch, "Dynamic response of a two-level catenary to a moving load," *Journal of Sound and Vibration*, vol. 292, no. 3, pp. 676 – 693, 2006.

[13] Z. Liu, F. Duan, Z. Xu, and X. Lu, "Wave propagation analysis in high-speed railway catenary system subjected to a moving pantograph," *Applied mathematical modelling.*, vol. 59, pp. 20–38, 2018.

[14] J. Gil, S. Gregori, M. Tur, and F. Fuenmayor, "Analytical model of the pantograph–catenary dynamic interaction and comparison with numerical simulations," *Vehicle System Dynamics*, pp. 1–24, 2020.

[15] M. Aboshi and M. Tsunemoto, "Installation guidelines for shinkansen high speed overhead contact lines," *Quarterly Report of Railway Technical Research Institute*, vol. 52, pp. 230–236, 11 2011.

[16] O. V. Van, J.-P. Massat, C. Laurent, and E. Balmes, "Introduction of variability into pantograph–catenary dynamic simulations," *Vehicle System Dynamics*, vol. 52, no. 10, pp. 1254–1269, 2014.

[17] S. Gregori, M. Tur, J. E. Tarancón, and F. J. Fuenmayor, "Stochastic monte carlo simulations of the pantograph–catenary dynamic interaction to allow for uncertainties introduced during catenary installation," *Vehicle System Dynamics*, vol. 57, no. 4, pp. 471–492, 2019.

[18] S. Gregori, M. Tur, E. Nadal, and F. J. Fuenmayor, "An approach to geometric optimisation of railway catenaries," *Vehicle System Dynamics*, vol. 56, no. 8, pp. 1162–1186, 2018.

[19] O. Lopez-Garcia, A. Carnicero, and V. Torres, "Computation of the initial equilibrium of railway overheads based on the catenary equation," *Engineering Structures*, vol. 28, no. 10, pp. 1387 – 1394, 2006.

[20] M. Tur, E. García, L. Baeza, and F. Fuenmayor, "A 3D absolute nodal coordinate finite element model to compute the initial configuration of a railway catenary," *Engineering Structures*, vol. 71, pp. 234–243, 2014.

[21] M. Tur, L. Baeza, F. Fuenmayor, and E. García, "Pacdin statement of methods," *Vehicle System Dynamics*, vol. 53, no. 3, pp. 402–411, 2015.

Appendix A

String catenary model solution

The string catenary model used in this work was presented in [14]. This model is governed by Eq. (1) whose solution provides the following vertical displacement of the string:

$$u(x,t) = \begin{cases} iF_0 \sum\limits_p \dfrac{e^{-i(k_p(\omega)(x-Vt)-\omega t)}}{\lambda \prod\limits_{r\neq p} (k_p(\omega) - k_r(\omega))}; & x - Vt \leq 0 \\ -iF_0 \sum\limits_q \dfrac{e^{-i(k_q(\omega)(x-Vt)-\omega t)}}{\lambda \prod\limits_{r\neq q} (k_q(\omega) - k_r(\omega))}; & x - Vt > 0 \end{cases} \tag{A.1}$$

in which $k_p(\omega)$ are the poles with a positive imaginary part and $k_q(\omega)$ are the poles with a negative imaginary part. They are:

$$\begin{aligned} k_1(\omega) &= -\frac{\eta}{3\lambda} - \frac{\sqrt[3]{2}Q}{3\lambda S} + \frac{S}{3\sqrt[3]{2}\lambda} \\ k_2(\omega) &= -\frac{\eta}{3\lambda} - \left(-\frac{1}{2} + \frac{i\sqrt{3}}{2}\right)\frac{\sqrt[3]{2}Q}{3\lambda S} + \left(-\frac{1}{2} - \frac{i\sqrt{3}}{2}\right)\frac{S}{3\sqrt[3]{2}\lambda} \\ k_3(\omega) &= -\frac{\eta}{3\lambda} - \left(-\frac{1}{2} - \frac{i\sqrt{3}}{2}\right)\frac{\sqrt[3]{2}Q}{3\lambda S} + \left(-\frac{1}{2} + \frac{i\sqrt{3}}{2}\right)\frac{S}{3\sqrt[3]{2}\lambda} \end{aligned} \tag{A.2}$$

being

$$\begin{aligned} S &= \sqrt[3]{R + \sqrt{4Q^3 + R^2}} \\ Q &= 3\lambda\tau - \eta^2 \\ R &= -2\eta^3 + 9\eta\lambda\tau - 27\lambda^2\sigma \end{aligned} \tag{A.3}$$

and

$$\begin{aligned} \lambda &= i\beta TV \\ \eta &= T - \mu V^2 + i\beta T\omega \\ \tau &= i\left(\alpha\mu + \beta\bar{k}\right)V - 2\mu V\omega \\ \sigma &= \bar{k} + i\left(\alpha\mu + \beta\bar{k}\right)\omega - \mu\omega^2 \end{aligned} \tag{A.4}$$

PAPER C

Finite element periodic catenary model to perform HIL pantograph tests considering non-linear dropper behaviour

J. Gil, M. Tur, S. Gregori, A. Correcher and F. J. Fuenmayor

Finite Elements in Analysis and Design
Volume 210, Pages -, 2022
DOI:10.1016/j.finel.2022.103816

Abstract

In this paper, we propose a general approach to compute the dynamic response of periodic infinite structures subjected to a moving load. The method only considers one repetitive block of the structure which is modelled by the Finite Element Method. The problem is first shifted to the frequency domain where the periodicity condition is easily applied and then the temporal response is obtained. An infinite periodic catenary system has been chosen to illustrate the proposed formulation. The linear formulation is extended to include the non-linear behaviour of droppers. The efficiency and accuracy of the catenary model obtained make it very suitable for use in Hardware in the Loop (HIL) pantograph tests. We propose to combine this catenary model with an iterative strategy to achieve the steady-state response of the coupled system and its performance is analysed in a virtual HIL simulation.

Keywords

Non-linear periodic structures, Moving load, Pantograph-catenary interaction, Hardware-in-the-loop, Finite Element Method

Contents

1 Introduction

1.1 Background

In the last decades, the expansion of electric railway systems has brought an important increase in the number of investigations focused on pantograph-catenary dynamic interaction. The proper sliding contact between both systems is crucial to achieve higher velocities, reduce the wear of the sliding interfaces and ensure a stable and safe operation. The pantograph is a mechanism that is mounted on the roof of the locomotive, which keeps contact with the contact wire of the catenary by pushing it up. This interaction has been studied by means of different techniques as it is described in [1]. Essentially, the three main options are numerical simulations, hardware-in-the-loop (HIL) tests or hybrid simulations and in-line testing.

Numerical simulations are widely used being the Finite Element Method (FEM) the most chosen approach. A deep analysis of the results of a pantograph-catenary interaction benchmark can be found in [2] and the references therein, which included the participation of 10 international research groups. Hybrid simulations or HIL tests are in the midway between numerical simulations and in-line testing. They consist on splitting the whole system into two substructures, being one of them replaced by a numerical model while the other is physically present in the simulation. The interaction between both systems, namely the virtual and the physical, is carried out by an interface made up by sensors and actuators. An insightful review of hybrid simulations applied to different systems can be found in [3]. This approach has also been applied successfully to the pantograph-catenary system [4]. In this case, the pantograph is the physical substructure and the catenary is replaced by a numerical model playing the role of the virtual system.

1.2 Problem of interest

The implementation of HIL pantograph tests involves certain issues and challenges. The catenary model must be solved in real time while keeping a high accuracy and there is usually a control-loop delay between the contact force measurement time and the imposition to the pantograph collector of the displacement computed from the catenary model. In order to solve these issues, some authors proposed different degrees of simplification in the catenary model used that compromise the accuracy of the results obtained. This work is aimed at setting an

entire framework that allows HIL testing with a high accuracy in the catenary model.

As depicted in Fig. 1, a catenary section is composed of a succession of spans. In its central region they use to be equal, which leads to a repetitive structure that presents a steady-state response when interacting with the pantograph. We choose the FEM to model the catenary and we assume the hypothesis of periodicity that is representative of the most part of the catenary. Furthermore, to achieve realistic results, the non-linear behaviour of droppers must be considered, which is also a challenge dealt with in this work.

However, if we consider a steady-state response it can present some disadvantages such as the inability to consider uneven spans, realistic contact wire irregularities and overlaps between consecutive sections. The influence of these phenomena was studied in [5, 6], concluding that their effect is not the most significant on the overall catenary dynamic response.

The procedure to implement a HIL test with a periodic catenary model includes two clearly differentiated parts. The first stage consists on creating a periodic catenary FEM model which reproduces the steady-state regime subject to a constant velocity moving load. In the formulation proposed in this work, only one span is discretised by the FEM and periodic boundary conditions are applied on the ends of the model to avoid modelling the entire catenary. The second stage is focused on defining a methodology to use the proposed periodic model, which represents the steady-state response of the catenary, in a HIL pantograph test, which unavoidably presents control-loop delays and an initial transient regime.

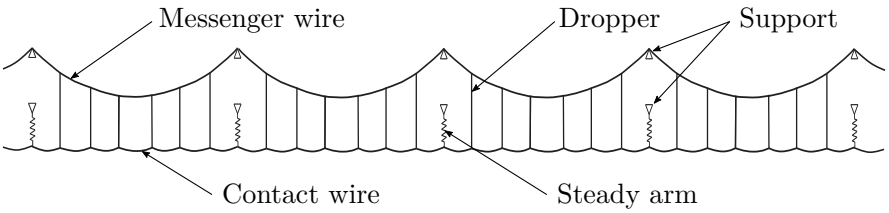

Figure 1: *Main components of a railway catenary.*

1.3 Literature review

In this subsection we present a literature review of the problem addressed in this work, distinguishing the works related to periodic models subjected to moving loads and the works that deal with HIL pantograph tests.

A broad overview of the dynamic response of structures under moving loads can be found in [7], in which the solution of different moving-load problems are discussed from an analytical point of view. The study of this type of problems has gained interest in the analysis of the steady-state response of systems such as rails, overhead contact lines or bridges. This problem has been traditionally addressed with analytic models based on a periodically supported infinite string/beam [8, 9, 10]. These approaches have in common the consideration of a periodic solution which allows considering only a repetitive block of the model between two consecutive supports. Specifically, an infinite periodic Euler-Bernoulli beam subjected to a uniform moving harmonic pressure field is used in [8] to simulate the dynamic behaviour of the rail. The differential equation is solved in the domain defined between two supports to which appropriate boundary periodicity conditions are applied. A similar model is proposed in [9], in which a modal representation results in a system of uncoupled differential equations. The limit of the solution of such a system when the number of blocks tends to infinity is computed for a moving constant load. The same problem is also solved in [10], applying the Fourier Transform to shift to the frequency domain where the periodicity condition is more easily formulated. The solution in the frequency domain is moved back to the time domain by the Inverse Fourier Transform.

The main limitation to the previous solutions is the simplicity of the model used, with which it is not possible to model more complex structures. To this end, some solutions are proposed in the literature. An extension of the approach given in [10] is presented in [11] to solve a catenary model that includes two interconnected strings. Two-and-a-half dimensional (2.5D) Finite Element models appear as an alternative to solve infinite periodic structures with constant cross section. This strategy is applied in [12], to model a rail. Fourier Transform with respect to space and time is performed to solve the problem which allows the application of the periodicity condition on the reactions of the supports in the frequency domain. The same authors presented an improved model in [13] where the dynamic interaction of multiple wheels with the periodic model is computed by means of Fourier series decomposition of the contact force.

A more general method is the so-called Wave Finite Element Method (WFEM) that is not only used to model infinite periodic structures, but also can be applied to finite periodic structures [14, 15]. WFEM is used in [16] to obtain the frequency

response function of a periodic infinite structure which is used to compute the response of the system excited by a moving load. WFEM also allows to consider structures with transition zones [15].

Regarding the HIL tests applied to the pantograph-catenary interaction, it can be found in the literature several solutions that include different degrees of simplification to carry out the tests. The first works that presented a pantograph HIL test rig were [17, 18]. They used a finite length linear catenary model based on a truncated modal approach. Another HIL set-up was proposed in [19] with a simple catenary model composed of three spans and a sliding window strategy. This model was upgraded in [20] with the consideration of dropper slackening and in [21], with the incorporation of lateral movement to the test rig to simulate the catenary stagger. A linear catenary model is used in [22] for HIL tests using 3D Euler-Bernoulli beams discretised with finite differences based on a moving coordinate formulation in combination with an absorbing boundary layer to attenuate outgoing waves. Other appealing catenary model intended to perform HIL pantograph tests was proposed in [23]. It is based on a modal truncation of a full FE model, which would allow to consider non-periodic features such as overlaps or installations errors. However, the practical use of this model in HIL tests is challenging due to the presence of control-loop delays that can make the test unstable.

1.4 Scope and contributions of this study

This paper is aimed at: i) solving the steady-state interaction of constant velocity moving loads with periodic structures modelled by the FEM and ii) proposing an strategy to use that solution to perform HIL tests. The global objective is to define a complete framework to perform high fidelity HIL pantograph tests dealing with the usual control-loop delay that appears in this type of tests.

The Periodic Finite Element Model (PFEM) of the catenary proposed accomplishes the first aim of this work and overcomes some of the limitations of other models found in the literature. The PFEM allows modelling more complex structures than the analytical models [8, 9, 10, 10], multi-strings models [10, 11] and 2.5D FEM models [12, 13]. Furthermore, it is a general method that can be applied to any periodic structure modelled by the FEM. WFEM [14, 15] can provide a similar solution by means of the method proposed in [16], however, when WFEM is applied to slender structures with long spatial period such as a railway catenary, some numerical problems arise making its solution not usable in practise. Additionally, control-loop delays can be easily handled with the catenary

PFEM unlike with full FE catenary models, in which the response of the catenary in future steps is not known in advance.

The final proposed model results very suitable for its application in HIL tests and provides more accurate results than other catenary models used for this purpose. In [17, 18], the accuracy of the model is limited due to either the severe modal truncation considered or the small length of the system modelled to fulfil both memory requirements and real-time performance. Sliding window methods [19, 20, 21] also focus on the steady-state response but the boundary conditions imposed lead to not negligible errors. Even in [22], in which boundary layers are used to avoid undesirable effects on the ends of the model, the fidelity of the results is compromised. The model proposed in this paper avoids these boundary effects by considering periodic boundary conditions that lead to the proper steady-state response. Additionally, it has the potential to compensate the control-loop delay that appears in HIL tests. Unlike most models found in the literature, other important contribution of this work relies on considering the non-linear behaviour of droppers, which are not able to hold compressive forces. This feature is essential to obtain high-fidelity results in HIL pantograph tests.

The second aim of this work is accomplished by adapting the iterative procedure proposed in [24] to the scenario of a periodic catenary model. This procedure allows both the virtual catenary and the physical pantograph to achieve the steady-state regime in a HIL test.

1.5 Organisation of the paper

The paper is structured as follows. The case of study of this work is described in Section 2. In Section 3, the impulse response of the catenary FE model with periodicity conditions is computed by solving the problem in the frequency domain. This impulse response is used in Section 4 combined with an iterative procedure to perform HIL pantograph tests. The model is enhanced in Section 5 to include the non-linear behaviour of droppers and some numerical results to verify the computational costs and the accuracy of the proposed model are presented in Section 6. A discussion and the main concluding remarks are given in Section 7. Finally, a demonstrative example that facilitates the reproduction of some numerical results is included in 7.

2 Description of the case study

The formulation developed in this paper is general in the sense that it can be applied to any periodic structure as long as it can be modelled by the FEM. However, as the final goal of this study is to perform HIL pantograph tests, the proposed formulation is applied to a railway catenary model along the paper.

As depicted in Fig. 1, a catenary is mainly composed of a contact wire, which interacts with the pantograph and is held by the messenger wire through vertical cables called droppers. The wiring is supported at regular intervals defining a span between two consecutive supports. The parameters that define the catenary and the pantograph models which are used to obtain the results presented in Section 6 can be found in [2]. Additionally, the pantograph-catenary dynamic interaction is solved according to the method proposed in [25] when full FE simulations are required for comparison and validation purposes.

To obtain the PFEM proposed in this work it is only necessary to obtain the FE model of the repeated block of the structure, in this case one span of the catenary, to apply the formulation described in the following sections. The resulting catenary PFEM is suitable to perform HIL pantograph tests in which the contact force applied to the pantograph collectors is measured and the displacement of the contact point obtained from the catenary PFEM is imposed by means of an actuator. In this work, all the HIL environment is treated by means of simulations, leaving for future work the application to real HIL tests. To this end, the physical substructure (i.e. the pantograph) is also simulated with a numerical model to evaluate the capabilities of the proposed method.

3 Impulse response of the catenary

In this section, we present a general method to obtain the impulse response of an infinite periodic structure subject to a periodic load moving at constant speed. To illustrate the method, a railway catenary has been chosen as shown in Fig. 2. As a periodic structure, the catenary is subdivided into consecutive blocks b of length L, which are repeated infinitely in the longitudinal direction $\mathbf{e}_1$. A 2D catenary is depicted in Fig. 2 in which each periodic block b is a single span. In the case of a 3D catenary, the repetitive block would consist of two spans, due to the stagger arrangement of the catenary wires. It is important to note that, as opposed to applying moving window strategies, the accuracy of the proposed method is not further improved by including more spans into the repetitive block.

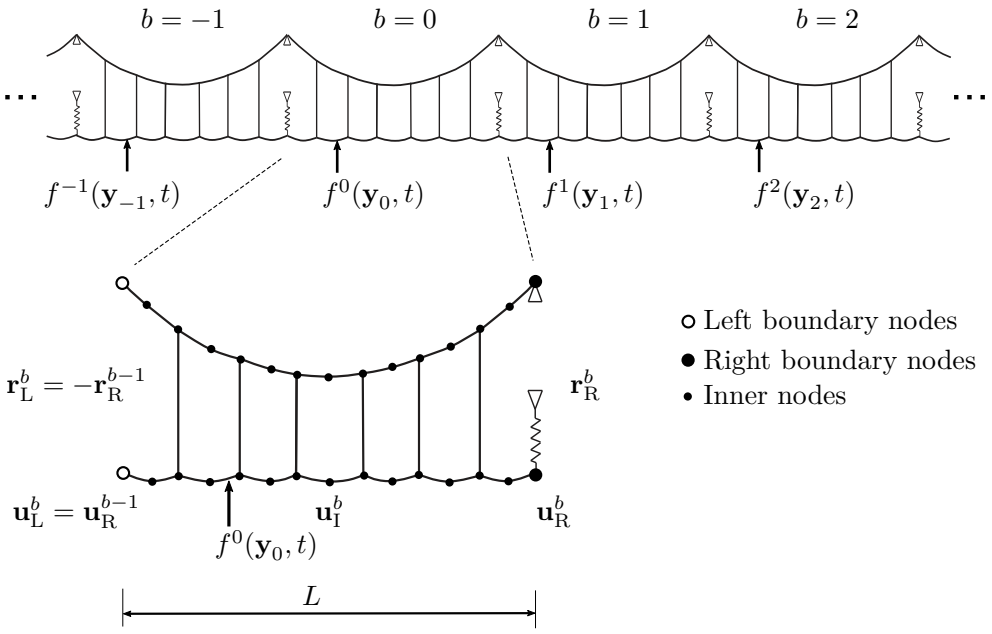

Figure 2: *Catenary as a periodic infinite structure and Finite Element discretization of block* $b=0$.

The pantograph moves at a constant speed V and the interaction with the catenary will be indefinitely repeated at every block if one considers that the stationary state is achieved. Therefore, the external contact force applied to the catenary is a periodic moving load of period $T=L/V$.

Under the hypothesis of periodic interaction, any force applied in a given block b is actually applied sequentially in every block $b\in[-\infty,\,\infty]$ at the same instant with respect to that in which the pantograph started to interact with each block. It is possible to calculate the impulse response produced by a sequence of unit impulses $f^{b}(\mathbf{y}_{b},t)$, which are periodically applied in each block b (only once per block) at points $\mathbf{y}_{b}$ and at time $t=bT$, as depicted in Fig. 2.

The sequence of unit impulses that defines the impulse response can be defined as:

$$f^{b}(\mathbf{y}_{b},t)=\delta(t-bT)\qquad b=-\infty,\ldots,\infty \tag{1}$$

in which δ is the Dirac function and they are applied to every block b at the global coordinate $\mathbf{y}_{b}=\mathbf{y}+bL\mathbf{e}_{1}$.

Given a point $\mathbf{y}$ in the reference block $b = 0$, the sequence of infinite unit impulses $f^b(\mathbf{y}, t)$ produces the catenary displacement $u(t, \mathbf{x}, \mathbf{y})$ at point $\mathbf{x}$. In this case, this is the unit impulse response $h(t, \mathbf{x}, \mathbf{y})$ under periodic conditions. Note that the coordinates of the excitation point are denoted by vector $\mathbf{y} = [y_1, y_2, y_3]^\top$ whereas, the coordinates of the point at which the response is measured are referred to as $\mathbf{x} = [x_1, x_2, x_3]^\top$. Both the impulse excitation f^b and catenary displacement u can be defined in an arbitrary direction, which are not explicitly indicated for simplification in the notation.

The stationary response of the catenary u, will be repeated in each block. Thus, for a given point $\mathbf{x}$, the periodicity condition reads as:

$$u(t, \mathbf{x}, \mathbf{y}) = u(t - bT, \mathbf{x} + bL\mathbf{e}_1, \mathbf{y}) \tag{2}$$

which allows the description of the response of the entire catenary with that of a single block, so that the response of the reference block $b = 0$ will be considered herein after. If this reference block is discretised by the Finite Element Method (FEM), the displacements of its N_{dof} nodal degrees of freedom are denoted by $\mathbf{u}^0(t, \mathbf{y})$ or $\mathbf{u}(t, \mathbf{y})$ in which superscript 0 is deleted for simplicity in the notation. The nodes of the FE mesh of the reference block can be divided into left (L) and right (R) boundary nodes and inner (I) nodes as shown in Fig. 2.

3.1 Frequency Response Function

The impulse response of the above described infinite periodic system will be obtained by considering only the reference block [8, 9, 10] and imposing the periodicity condition defined in Eq. (2). Some authors have solved this problem by applying the Floquet decomposition [26]. However, we followed the strategy proposed in [10, 11], which is based on the movement of the problem to the frequency domain in which the periodicity condition is more easily stated. Thus, we first need to find the Frequency Response Function (FRF) that relates the displacement of point $\mathbf{x}$ to a harmonic unit force of frequency ω applied at point $\mathbf{y}$.

Without loss of generality, in this work, the displacements of inner and right boundary nodes, $\mathbf{u}_\mathrm{I}(t)$ and $\mathbf{u}_\mathrm{R}(t)$ respectively, are chosen as the unknowns of the problem. Displacements of the left boundary nodes $\mathbf{u}_\mathrm{L}$ must fulfil Eq. (2), that is:

$$\mathbf{u}_\mathrm{L}(t) = \mathbf{u}_\mathrm{R}(t + T) \tag{3}$$

which after applying the Fourier Transform, it becomes:

$$\mathbf{U}_\mathrm{L}(\omega) = e^{i\omega T}\mathbf{U}_\mathrm{R}(\omega) \tag{4}$$

being $\mathbf{U}_{\mathrm{L,I,R}}(\omega)$ the Fourier Transform of $\mathbf{u}_{\mathrm{L,I,R}}(t)$, respectively.

The nodal equivalent external force vector $\mathbf{F}$ can be divided into left, inner and right nodal degrees of freedom, namely $\mathbf{F}_{\mathrm{L}}$, $\mathbf{F}_{\mathrm{I}}$ and $\mathbf{F}_{\mathrm{R}}$, respectively. If the degrees of freedom of left and right boundary nodes are properly defined (mesh compatibility), $\mathbf{F}_{\mathrm{L}}$ and $\mathbf{F}_{\mathrm{R}}$ are related through the following equation:

$$\mathbf{F}_{\mathrm{L}} = e^{i\omega T}\mathbf{F}_{\mathrm{R}} \tag{5}$$

The FRF of the system can be found by solving the following problem for every frequency:

$$\begin{aligned} \mathbf{D}(\omega)\,\mathbf{U} &= \mathbf{F} + \mathbf{R} \\ \mathbf{D}(\omega) &= \mathbf{K} + i\omega\mathbf{C} - \omega^2\mathbf{M} \end{aligned} \tag{6}$$

where $\mathbf{M}$ is the mass matrix, $\mathbf{K}$ the stiffness matrix and $\mathbf{C}$ the damping matrix of the substructure contained in a single block. The reaction force vector $\mathbf{R}$, applied to the left and right boundary nodes $\mathbf{R} = [\mathbf{R}_{\mathrm{L}},\ \mathbf{0},\ \mathbf{R}_{\mathrm{R}}]^{\top}$, is also unknown. Eq. (6) can be rearranged in left boundary, inner and right boundary degrees of freedom:

$$\begin{bmatrix} \mathbf{D}_{\mathrm{LL}} & \mathbf{D}_{\mathrm{LI}} & \mathbf{D}_{\mathrm{LR}} \\ \mathbf{D}_{\mathrm{IL}} & \mathbf{D}_{\mathrm{II}} & \mathbf{D}_{\mathrm{IR}} \\ \mathbf{D}_{\mathrm{RL}} & \mathbf{D}_{\mathrm{RI}} & \mathbf{D}_{\mathrm{RR}} \end{bmatrix} \begin{Bmatrix} \mathbf{U}_{\mathrm{L}} \\ \mathbf{U}_{\mathrm{I}} \\ \mathbf{U}_{\mathrm{R}} \end{Bmatrix} = \begin{Bmatrix} \mathbf{F}_{\mathrm{L}} \\ \mathbf{F}_{\mathrm{I}} \\ \mathbf{F}_{\mathrm{R}} \end{Bmatrix} + \begin{Bmatrix} \mathbf{R}_{\mathrm{L}} \\ \mathbf{0} \\ \mathbf{R}_{\mathrm{R}} \end{Bmatrix} \tag{7}$$

Considering again the periodicity condition and the action reaction principle, the reaction force vector in the left and right boundary $\mathbf{R}_{\mathrm{L}}$ and $\mathbf{R}_{\mathrm{R}}$ are related by:

$$\mathbf{R}_{\mathrm{L}} = -e^{i\omega T}\mathbf{R}_{\mathrm{R}} \tag{8}$$

Introducing Eqs. (4) and (5) to Eq. (7):

$$\begin{bmatrix} \mathbf{D}_{\mathrm{LI}} & \mathbf{D}_{\mathrm{LR}} + e^{i\omega T}\mathbf{D}_{\mathrm{LL}} \\ \mathbf{D}_{\mathrm{II}} & \mathbf{D}_{\mathrm{IR}} + e^{i\omega T}\mathbf{D}_{\mathrm{IL}} \\ \mathbf{D}_{\mathrm{RI}} & \mathbf{D}_{\mathrm{RR}} + e^{i\omega T}\mathbf{D}_{\mathrm{RL}} \end{bmatrix} \begin{Bmatrix} \mathbf{U}_{\mathrm{I}} \\ \mathbf{U}_{\mathrm{R}} \end{Bmatrix} = \begin{Bmatrix} e^{i\omega T}\mathbf{F}_{\mathrm{R}} \\ \mathbf{F}_{\mathrm{I}} \\ \mathbf{F}_{\mathrm{R}} \end{Bmatrix} + \begin{Bmatrix} \mathbf{R}_{\mathrm{L}} \\ \mathbf{0} \\ \mathbf{R}_{\mathrm{R}} \end{Bmatrix} \tag{9}$$

and then using Eq. (8), the unknowns can be rearranged to the left-hand side:

$$\begin{bmatrix} \mathbf{D}_{\mathrm{LI}} & \mathbf{D}_{\mathrm{LR}} + e^{i\omega T}\mathbf{D}_{\mathrm{LL}} & e^{i\omega T}\mathbf{I} \\ \mathbf{D}_{\mathrm{II}} & \mathbf{D}_{\mathrm{IR}} + e^{i\omega T}\mathbf{D}_{\mathrm{IL}} & \mathbf{0} \\ \mathbf{D}_{\mathrm{RI}} & \mathbf{D}_{\mathrm{RR}} + e^{i\omega T}\mathbf{D}_{\mathrm{RL}} & -\mathbf{I} \end{bmatrix} \begin{Bmatrix} \mathbf{U}_{\mathrm{I}} \\ \mathbf{U}_{\mathrm{R}} \\ \mathbf{R}_{\mathrm{R}} \end{Bmatrix} = \begin{bmatrix} \mathbf{0} & e^{i\omega T}\mathbf{I} \\ \mathbf{I} & \mathbf{0} \\ \mathbf{0} & \mathbf{I} \end{bmatrix} \begin{Bmatrix} \mathbf{F}_{\mathrm{I}} \\ \mathbf{F}_{\mathrm{R}} \end{Bmatrix} \tag{10}$$

in which $\mathbf{I}$ denotes for the identity matrix. Problem (10) can be solved as:

$$\left\{ \begin{array}{c} \mathbf{U}_{\mathrm{I}} \\ \mathbf{U}_{\mathrm{R}} \\ \mathbf{R}_{\mathrm{R}} \end{array} \right\} = \hat{\mathbf{H}}(\omega) \left\{ \begin{array}{c} \mathbf{F}_{\mathrm{I}} \\ \mathbf{F}_{\mathrm{R}} \end{array} \right\} \tag{11}$$

where:

$$\hat{\mathbf{H}}(\omega) = \left[\begin{array}{ccc} \mathbf{D}_{\mathrm{LI}} & \mathbf{D}_{\mathrm{LR}} + e^{i\omega T}\mathbf{D}_{\mathrm{LL}} & e^{i\omega T}\mathbf{I} \\ \mathbf{D}_{\mathrm{II}} & \mathbf{D}_{\mathrm{IR}} + e^{i\omega T}\mathbf{D}_{\mathrm{IL}} & \mathbf{0} \\ \mathbf{D}_{\mathrm{RI}} & \mathbf{D}_{\mathrm{RR}} + e^{i\omega T}\mathbf{D}_{\mathrm{RL}} & -\mathbf{I} \end{array} \right]^{-1} \left[\begin{array}{cc} \mathbf{0} & e^{i\omega T}\mathbf{I} \\ \mathbf{I} & \mathbf{0} \\ \mathbf{0} & \mathbf{I} \end{array} \right] \tag{12}$$

Eq. (11) can be rewritten in terms of the displacements of the block as:

$$\left\{ \begin{array}{c} \mathbf{U}_{\mathrm{L}} \\ \mathbf{U}_{\mathrm{I}} \\ \mathbf{U}_{\mathrm{R}} \end{array} \right\} = \mathbf{H}(\omega) \left\{ \begin{array}{c} \mathbf{F}_{\mathrm{I}} \\ \mathbf{F}_{\mathrm{R}} \end{array} \right\} \tag{13}$$

with

$$\mathbf{H}(\omega) = \left[\begin{array}{c} e^{i\omega T}\hat{\mathbf{H}}_{\mathrm{R}}(\omega) \\ \hat{\mathbf{H}}_{\mathrm{I}}(\omega) \\ \hat{\mathbf{H}}_{\mathrm{R}}(\omega) \end{array} \right] \tag{14}$$

in which $\hat{\mathbf{H}}_{\mathrm{I}}(\omega)$ and $\hat{\mathbf{H}}_{\mathrm{R}}(\omega)$ are the two first rows of $\hat{\mathbf{H}}(\omega)$.

3.2 Impulse response

Eq. (13) relates nodal displacements with nodal forces of the entire block by means of the FRF $\mathbf{H}(\omega)$. However, we are interested in the displacement of point $\mathbf{x}$ produced by a unit harmonic force F_u applied at point $\mathbf{y}$ in the reference block. The FEM operator $\mathbf{N}(\mathbf{x}) = [\mathbf{N}_{\mathrm{L}}(\mathbf{x}),\ \mathbf{N}_{\mathrm{I}}(\mathbf{x}),\ \mathbf{N}_{\mathrm{R}}(\mathbf{x})]$ is the $1 \times N_{\mathrm{dof}}$ matrix, composed of nodal shape functions that transforms nodal displacements into point displacements in a given direction and can also be used to transform point forces to nodal equivalent forces.

With this operator, the nodal equivalent forces relative to the unit force F_{u} can be written as:

$$\left\{ \begin{array}{c} \mathbf{F}_{\mathrm{I}} \\ \mathbf{F}_{\mathrm{R}} \end{array} \right\} = \left\{ \begin{array}{c} \mathbf{N}_{\mathrm{I}}(\mathbf{y})^{\top} \\ \mathbf{N}_{\mathrm{R}}(\mathbf{y})^{\top} + e^{-i\omega T}\mathbf{N}_{\mathrm{L}}(\mathbf{y})^{\top} \end{array} \right\} \tag{15}$$

in which the term $e^{-i\omega T}\mathbf{N}_{\mathrm{L}}(\mathbf{y})^{\top}$ considers the nodal forces at the right boundary of the reference block ($b = 0$) that would appear if the unit force was applied on

the next block ($b = 1$). Note that this contribution is only active if the unit force is applied on an element of the reference block that has some node on the left boundary.

With the use of the operator $\mathbf{N}(\mathbf{x})$ applied to the right-hand side of Eq. (13) and including Eq. (15), it is possible to compute the harmonic displacement of point $\mathbf{x}$ when a unit harmonic force acts at $\mathbf{y}$:

$$I(\omega, \mathbf{x}, \mathbf{y}) = \mathbf{N}(\mathbf{x})\ \mathbf{H}(\omega)\ \left\{ \begin{array}{c} \mathbf{N}_{\mathrm{I}}(\mathbf{y})^{\top} \\ \mathbf{N}_{\mathrm{R}}(\mathbf{y})^{\top} + e^{-i\omega T}\mathbf{N}_{\mathrm{L}}(\mathbf{y})^{\top} \end{array} \right\} \tag{16}$$

As the structure is modelled with FEM, Eq. (16) cannot be analytically defined but is computed for a discrete number of frequencies N_{f} with a frequency increment $\Delta\omega$:

$$\omega_k = k\Delta\omega \qquad k = 0, \ldots, N_{\mathrm{f}} - 1 \tag{17}$$

In addition, time t is also discretised with a time increment Δt:

$$t_n = n\Delta t \tag{18}$$

Thus, applying the Inverse Discrete Fourier Transform to Eq. (16), the impulse response at time step t_n is obtained as:

$$h(t_n, \mathbf{x}, \mathbf{y}) = \sum_{k=0}^{N_f - 1} a_k \mathrm{Re}\left(I(\omega_k, \mathbf{x}, \mathbf{y})\ e^{i\omega_k n\Delta t} \right) \Delta\omega \tag{19}$$

being $a_k = 2$ if $k \neq 0$ or $a_k = 1$ if $k = 0$.

It is important to remark that there is no relation between $\Delta\omega$ and the period T. In practise, $\Delta\omega$ has to be chosen little enough to obtain an accurate time response and N_{f} is limited by Δt to avoid aliasing effects.

4 Hardware In the Loop test methodology with a linear catenary model

The concept of Hardware In the Loop (HIL) tests applied to railway pantographs consists of hybrid simulations with a virtual catenary model and a physical pantograph (see Fig. 3). In these tests, the catenary is replaced by an actuator that interacts with a real pantograph and simulates the vertical movement of the catenary contact point. The contact force measured in the test rig is the input of the

virtual catenary model which must supply the contact point vertical position in real time.

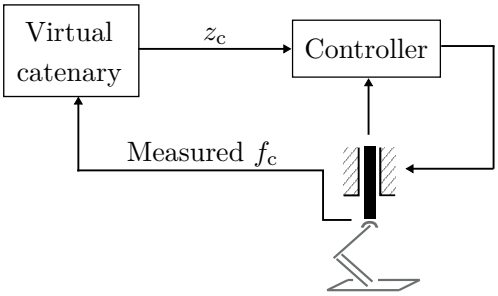

Figure 3: *Scheme of a HIL pantograph test.*

Eq. (19) condenses the linear behaviour of the periodic catenary under a moving periodic load, so that non-linear effects such as dropper slackening are not considered in this section. Thus, the general response can be obtained with the load applied at the contact wire of a single block.

The pantograph is virtually moving at a constant speed V and applies a vertical excitation over the contact wire of the catenary model. Δt is chosen so that the contact wire of a periodic block of length L is divided in N_c virtual contact points $\mathbf{y}_{cw}(t_n)$ with $n = 0, \ldots, N_c - 1$.

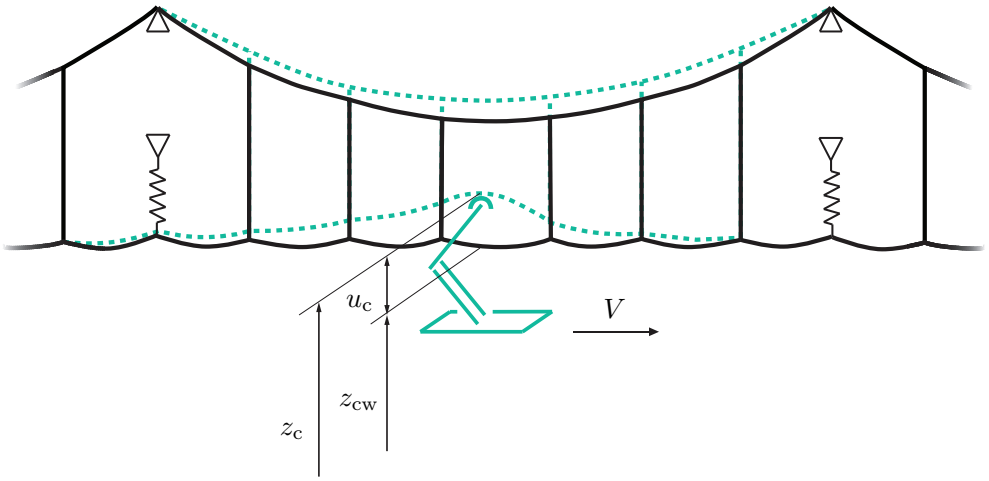

Figure 4: *Pantograph interaction with the periodic catenary.*

If the contact force $f_c(t_n)$ applied to a virtual contact point $\mathbf{y}_{cw}(t_n)$ is assumed to be known, Eq. (19) can be particularised to compute the vertical displacement $u(t_n, \mathbf{x})$ of a given point $\mathbf{x}$, by applying the superposition principle as the sum of the contribution of each force applied on the block:

$$u(t_n, \mathbf{x}) = \sum_{\hat{n}=0}^{N_c-1} h(t_n - t_{\hat{n}}, \mathbf{x}, \mathbf{y}_{cw}(t_{\hat{n}}))\ f_c(t_{\hat{n}})\Delta t \tag{20}$$

Note that $\hat{n}$ denotes the time instant at which the force is applied and n, the instant at which the displacement is evaluated. It should also be noted that the origin of time in the impulse response function (Eq. (19)) corresponds to the instant at which the impulse is applied. However, in Eq. (20), $t_n = 0$ which is the time step at which the force is applied at the beginning of the block. This is the reason why the impulse function is evaluated at $t_n - t_{\hat{n}}$.

For the pantograph interaction, we are interested in the displacement of the contact point $u_c(t_n) = u(t_n, \mathbf{x}_{cw}(t_n))$. Therefore, Eq. (20) can be evaluated at this point as:

$$u_c(t_n) = u(t_n, \mathbf{x}_{cw}(t_n)) = \sum_{\hat{n}=0}^{N_c-1} \mathbb{I}(n, \hat{n})\ f_c(t_{\hat{n}}) \tag{21}$$

in which:

$$\mathbb{I}(n, \hat{n}) = h(t_n - t_{\hat{n}}, \mathbf{x}_{cw}(t_n), \mathbf{y}_{cw}(t_{\hat{n}}))\Delta t \tag{22}$$

In addition to the displacement due to interaction with the pantograph, the vertical position of the contact wire depends on the static configuration of the catenary. If $z_{cw}(t_n)$ is the contact wire height at the initial catenary configuration, the global height of the contact point at time step n can be obtained, as shown in Fig. 4, from:

$$z_c(t_n) = z_{cw}(t_n) + u_c(t_n) \tag{23}$$

Eq. (21) condenses in a $N_c \times N_c$ matrix $\mathbb{I}(n, \hat{n})$ the steady-state vertical displacement of the contact point at time t_n as a function of the stationary force applied in all contact points of the block at time $t_{\hat{n}}$ for $\hat{n} = 0, ..., N_c - 1$. It is important to note that when the force is measured and applied at a given time step $\bar{n} \in \hat{n}$, the response for all the time steps n is affected.

Matrix $\mathbb{I}(n, \hat{n})$ can be precomputed making the proposed model very suitable for use in HIL testing because few operations are required to obtain the contact point

response. We propose to apply this model in combination with an algorithm in which the measured contact force is iteratively updated until the steady-state response is achieved.

Defining k as the global counter of each step or iteration of the HIL test, at the beginning of the test ($k = 0$), a set of N_c (the number of contact points in a block) null values of the contact force are considered, so that $z_\mathrm{c}(t_n) = z_\mathrm{cw}(t_n)$. At a given iteration k, the contact force is measured at time step $\bar{n}$ relative to the beginning of the current block b. In this step, only the contact force values measured from t_0 to $t_{\bar{n}}$ are available in the current block. To complete the set of N_c measures of contact force required to compute the response of the catenary model, the contact force values from $t_{\bar{n}+1}$ to $t_{N_\mathrm{c}-1}$ are taken from the previous block $b-1$. Thus, by combining Eqs. (23) and (21) the contact point height in iteration k is computed as:

$$z_\mathrm{c}^k(t_n) = z_\mathrm{cw}(t_n) + \sum_{\hat{n}=0}^{\bar{n}} \mathbb{I}(n,\hat{n})\; f_\mathrm{c}^b(t_{\hat{n}}) + \sum_{\hat{n}=\bar{n}+1}^{N_\mathrm{c}-1} \mathbb{I}(n,\hat{n})\; f_\mathrm{c}^{b-1}(t_{\hat{n}}) \tag{24}$$

Note that the response $z_\mathrm{c}(t_n)$, defined from t_0 to $t_{N_\mathrm{c}-1}$, must be updated for all t_n every iteration k.

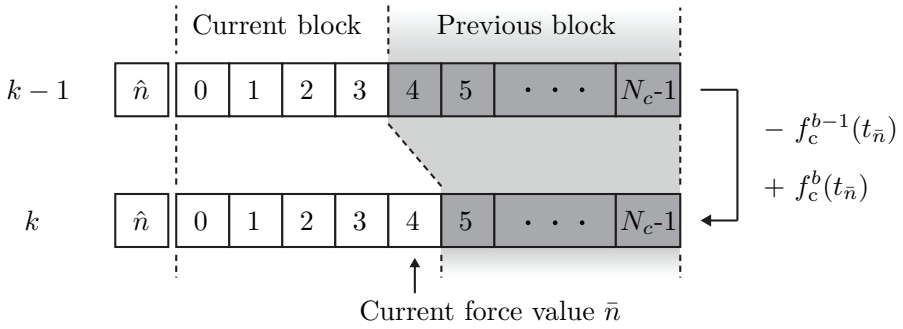

Figure 5: *Modification of the set of N_c force values by replacing $f_\mathrm{c}^{b-1}(t_{\bar{n}})$ by $f_\mathrm{c}^{b}(t_{\bar{n}})$ at two consecutive iterations.*

Eq. (24) can be rewritten based on the difference of the measured contact force of the current block and that of the same instant of the previous block. That is:

$$z_\mathrm{c}^k(t_n) = z_\mathrm{c}^{k-1}(t_n) + \mathbb{I}(n,\bar{n}) \left(f_\mathrm{c}^b(t_{\bar{n}}) - f_\mathrm{c}^{b-1}(t_{\bar{n}}) \right) \tag{25}$$

This strategy is schematically illustrated at Fig. 5.

Once the contact wire height is available, only the vertical position of the contact point for the next time step $z_c^k(t_{\bar{n}+1})$ is sent to the actuator. The method runs iteratively step by step until the measured contact force in two consecutive blocks matches with a given tolerance.

The methodology explained so far is exemplified in 7 by means of a very simple academic model that allows the numerical results to be better understood and reproduced.

5 Hardware in the loop method with nonlinear catenary model

The HIL procedure explained in Section 4 is now extended to include the non-linear behaviour of droppers. We use the same idea introduced in [25] but adapted to account for the periodic nature of the system. The proposed formulation is developed in two stages. In the first, the response is computed with assumption to the linear model described in Section 4. The second is devoted to apply correction forces to the slackened droppers.

5.1 Dropper correction forces

The static equilibrium problem in a catenary system is a non-linear problem governed by large displacements. However, the dynamic behaviour can be linearised around the static equilibrium position in which each dropper d has a tension value f_{d0} and a stiffness k_d in the dropper direction. Droppers are cables that cannot exert compression forces. However, these compression forces are considered in the linear catenary model in which the tension of dropper d is computed as $f = k_d \Delta L_d$ (dashed line in Fig. 6(a)). To satisfy the condition of no compression forces, the internal force of a dropper must be greater than -f_{d0} (continuous line in Fig. 6(a)). Thus, a correction force f_d must be applied to correct the linear behaviour as shown in Fig. 6(a). This consists of two compression forces applied at both ends of the dropper $\mathbf{y}_{d,\text{inf}}$ and $\mathbf{y}_{d,\text{sup}}$, as depicted in Fig. 6(b).

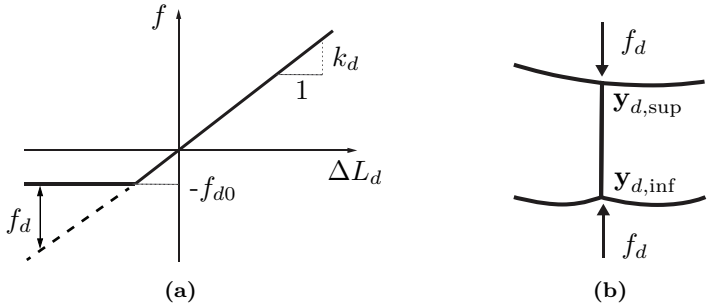

Figure 6: *(a) Non-linear behaviour of droppers. (b) Correction forces f_d applied on dropper d.*

5.2 Unitary operators

In this subsection, we attempt to explain the influence which a periodic sequence of unitary impulses applied on contact points and dropper ends has on the displacement of these points.

We first define the dropper elongation ΔL_d as:

$$\Delta L_d = u(\mathbf{x}_{d,\text{sup}}) - u(\mathbf{x}_{d,\text{inf}}) \tag{26}$$

$\mathbb{I}(n, \hat{n})$ in Eq. (21) can be redefined as $\mathbb{I}_{\text{c}}^{\text{c}}(n, \hat{n})$ in which the subscript c denotes that the excitation is produced by the contact force and the superscript c indicates that the response is evaluated at the contact point. With this notation, the displacement of the contact point produced by the contact force defined in Eq. (21) is now renamed:

$$u_{\text{c}}^{\text{l}}(t_n) = \sum_{\hat{n}=0}^{N_{\text{c}}-1} \mathbb{I}_{\text{c}}^{\text{c}}(n, \hat{n})\ f_{\text{c}}(t_{\hat{n}}) \tag{27}$$

Superscript l is used to point out the fact that this displacement is considered the linear part of the total response.

Dropper elongation due to the contact force is:

$$\Delta L_d^{\text{l}}(t_n) = \sum_{\hat{n}=0}^{N_{\text{c}}-1} \mathbb{I}_{\text{c}}^{d}(n, \hat{n})\ f_{\text{c}}(t_{\hat{n}}) \tag{28}$$

in which:

$$\mathbb{I}_{\mathrm{c}}^{d}(n,\hat{n}) = \left[h(t_n - t_{\hat{n}}, \mathbf{x}_{d,\mathrm{sup}}, \mathbf{y}_{\mathrm{cw}}(t_{\hat{n}})) - h(t_n - t_{\hat{n}}, \mathbf{x}_{d,\mathrm{inf}}, \mathbf{y}_{\mathrm{cw}}(t_{\hat{n}}))\right] \Delta t \tag{29}$$

To include the influence of dropper correction forces in the catenary response, we first assume that the dropper correction force $f_d(t_n)$ of dropper d at t_n is known. It is important to remark that the correction of the infinite droppers of the catenary model at all time steps should be considered because they affect the response on the contact point at time step $\bar{n}$. In practise however, dropper correction will not be considered in time instants at which the pantograph is far enough from the reference block because it is highly improbable that a dropper slackens and in such a case, its influence on the pantograph interaction has been proven to be negligible. Thus, dropper correction is active only at time instants from $t_{-n_{\mathrm{b}}}$ to $t_{n_{\mathrm{a}}}$.

The displacement produced on the contact point due to dropper correction forces is called the non-linear part of the response (denoted by superscript nl) and is defined as:

$$u_{\mathrm{c}}^{\mathrm{nl}}(t_n) = \sum_{d=1}^{N_{\mathrm{d}}} \sum_{\hat{n}=-n_{\mathrm{b}}}^{n_{\mathrm{a}}} \mathbb{I}_{d}^{\mathrm{c}}(n,\hat{n})\ f_d(t_{\hat{n}}) \tag{30}$$

in which N_{d} is the number of droppers of the reference block and

$$\mathbb{I}_{d}^{\mathrm{c}}(n,\hat{n}) = \left[h(t_n - t_{\hat{n}}, \mathbf{x}_{\mathrm{cw}}(t_n), \mathbf{y}_{d,\mathrm{inf}}) - h(t_n - t_{\hat{n}}, \mathbf{x}_{\mathrm{cw}}(t_n), \mathbf{y}_{d,\mathrm{sup}})\right] \Delta t \tag{31}$$

Dropper d elongation caused by the correction forces applied to dropper $\hat{d}$ are computed from:

$$\Delta L_{d}^{\mathrm{nl}}(t_n) = \sum_{\hat{d}=1}^{N_{\mathrm{d}}} \sum_{\hat{n}=-n_{\mathrm{b}}}^{n_{\mathrm{a}}} \mathbb{I}_{\hat{d}}^{d}(n,\hat{n})\ f_{\hat{d}}(t_{\hat{n}}) \tag{32}$$

being

$$\begin{aligned}\mathbb{I}_{\hat{d}}^{d}(n,\hat{n}) = &\left[h(t_n - t_{\hat{n}}, \mathbf{x}_{d,\mathrm{sup}}, \mathbf{y}_{\hat{d},\mathrm{inf}}) - h(t_n - t_{\hat{n}}, \mathbf{x}_{d,\mathrm{sup}}, \mathbf{y}_{\hat{d},\mathrm{sup}})\right] \Delta t \\ &- \left[h(t_n - t_{\hat{n}}, \mathbf{x}_{d,\mathrm{inf}}, \mathbf{y}_{\hat{d},\mathrm{inf}}) - h(t_n - t_{\hat{n}}, \mathbf{x}_{d,\mathrm{inf}}, \mathbf{y}_{\hat{d},\mathrm{sup}})\right] \Delta t\end{aligned} \tag{33}$$

The total response can be obtained by adding the linear (l) and non-linear (nl) contributions defined above.

5.3 HIL with dropper correction forces

The same procedure as that defined in Section 4 is used here but now, dropper correction forces are added to the system. It is important to highlight that dropper correction forces can be applied at instants before and after the time instants at which the pantograph stays within the domain of the block ($t_{\hat{n}}$ for $\hat{n} = 0, ..., N_\mathrm{c} - 1$).

At a given iteration k, the first step consists of updating the response due to the contact force measured at $t_{\bar{n}}$ as in Eq. (25):

$$u_\mathrm{c}^{\mathrm{l},k}(t_n) = u_\mathrm{c}^{k-1}(t_n) + \mathbb{I}_\mathrm{c}^\mathrm{c}(n,\bar{n}) \left(f_\mathrm{c}^b(t_{\bar{n}}) - f_\mathrm{c}^{b-1}(t_{\bar{n}}) \right) \tag{34}$$

In this case, it is also necessary to update the elongation of droppers due to this contact force:

$$\Delta L_d^{\mathrm{l},k}(t_n) = \Delta L_d^{k-1}(t_n) + \mathbb{I}_\mathrm{c}^d(n,\bar{n}) \left(f_\mathrm{c}^b(t_{\bar{n}}) - f_\mathrm{c}^{b-1}(t_{\bar{n}}) \right) \tag{35}$$

The second stage consists of modifying the response according to the effect of dropper correction forces. Note that the dropper corrections forces $f_d(t_{\hat{n}})$ are applied at time instants $t_{\hat{n}}$ for $\hat{n} = -n_\mathrm{b}, ..., n_\mathrm{a}$ (a bigger interval than $[0,\, N_\mathrm{c} - 1]$). Thus, at every iteration k, f_d must be calculated in several instants in order to include all the instants from $-n_\mathrm{b}$ to n_a. For example, if $-n_\mathrm{b} = -N_\mathrm{c}$ and $n_\mathrm{a} = 2N_\mathrm{c} - 1$, which means that dropper correction is active since the pantograph gets into the previous block ($b = -1$) until the pantograph gets off the next block ($b = 1$), f_d must be computed and applied at three instants of time, namely $t_{\bar{n}}$, $t_{\bar{n}-N_\mathrm{c}}$ and $t_{\bar{n}+N_\mathrm{c}}$.

The effect of dropper correction forces modifies the linear response defined in Eqs. (34) and (35) so that:

$$u_\mathrm{c}^k(t_n) = u_\mathrm{c}^{\mathrm{l},k}(t_n) + \sum_{d=1}^{N_\mathrm{d}} \sum_{\hat{n}=\bar{n}_d} \mathbb{I}_d^\mathrm{c}(n,\hat{n}) \left(f_d^b(t_{\hat{n}}) - f_d^{b-1}(t_{\hat{n}}) \right) \tag{36}$$

$$\Delta L_d^k(t_n) = \Delta L_d^{\mathrm{l},k}(t_n) + \sum_{\hat{d}=1}^{N_\mathrm{d}} \sum_{\hat{n}=\bar{n}_d} \mathbb{I}_{\hat{d}}^d(n,\hat{n}) \left(f_{\hat{d}}^b(t_{\hat{n}}) - f_{\hat{d}}^{b-1}(t_{\hat{n}}) \right) \tag{37}$$

in which $\bar{n}_\mathrm{d}$ considers all the instants included into $[-n_\mathrm{b},\, n_\mathrm{a}]$ that are spaced N_c steps from the current measuring time $\bar{n}$. For the choice of $-n_\mathrm{b}$ and n_a indicated above, $\bar{n}_\mathrm{d} = [\bar{n}, \bar{n} - N_\mathrm{c}, \bar{n} + N_\mathrm{c}]$. This is equivalent to applying this correction to the droppers of the previous and next blocks at the current instant $t_{\bar{n}}$.

At this point, the dropper correction forces $f_d^b(t_{\bar{n}_\mathrm{d}})$ are the only magnitudes left to calculate to know the response at iteration k. First, we must find out the droppers to which the correction must be applied. To this end, the dropper state $\mathbb{O}_d^k$ defines the slackening state of dropper d, being equal to 0 if the dropper is tensed and 1 if it is slackened. At time $\bar{n}_\mathrm{d}$, it reads:

$$\mathbb{O}_d^k(t_{\bar{n}_\mathrm{d}}) = \begin{cases} 0 & \text{if} \quad k_d\ \Delta L_d^{\mathrm{l},k}(t_{\bar{n}_\mathrm{d}}) \geq -f_{d0} \\ 1 & \text{if} \quad k_d\ \Delta L_d^{\mathrm{l},k}(t_{\bar{n}_\mathrm{d}}) < -f_{d0} \end{cases} \tag{38}$$

in which $\Delta L_d^{\mathrm{l},k}(t_{\bar{n}_\mathrm{d}})$ is obtained from Eq. (35).

As shown in Fig. 6(a), the dropper correction force can be written as:

$$f_d^b(t_{\bar{n}_\mathrm{d}}) = \mathbb{O}_d^k(t_{\bar{n}_\mathrm{d}}) \left(-f_{d0} - k_d \Delta L_d^k(t_{\bar{n}_\mathrm{d}})\right) \tag{39}$$

According to Eq. (37), the previous equation becomes:

$$f_d^b(t_{\bar{n}_\mathrm{d}}) = \mathbb{O}_d^k(t_{\bar{n}_\mathrm{d}}) \Bigg(- f_{d0} - k_d \Bigg(\Delta L_d^{\mathrm{l},k}(t_{\bar{n}_\mathrm{d}}) + \sum_{\hat{d}=1}^{N_\mathrm{d}} \sum_{\hat{n}=\bar{n}_\mathrm{d}} \mathbb{I}_{\hat{d}}^d(\bar{n}_\mathrm{d}, \hat{n}) \left(f_{\hat{d}}^b(t_{\hat{n}}) - f_{\hat{d}}^{b-1}(t_{\hat{n}}) \right) \Bigg) \Bigg) \tag{40}$$

This is a system of $N_\mathrm{d} \times N_{\bar{n}_\mathrm{d}}$ linear equations that allows to calculate the dropper correction forces $f_d^b(t_{\bar{n}_\mathrm{d}})$. Note that $N_{\bar{n}_\mathrm{d}}$ is the number of time steps included in $\bar{n}_\mathrm{d}$ and the system is in practice reduced since some of the equations become $f_d^b(t_{\bar{n}_\mathrm{d}}) = 0$ because dropper correction is not active in dropper d at some instants considered in $\bar{n}_\mathrm{d}$.

The final response at iteration k, including dropper correction, is calculated with Eqs. (36) and (37). Dropper state can change once the correction is applied but it is not necessary to recalculate it. If the convergence is achieved after several blocks, the difference between the response in two consecutive blocks tends to zero and the stationary dropper state is achieved.

6 Numerical results

In this section, the algorithm proposed is tested in a virtual HIL simulation in which a numerical pantograph model is used to replace the real pantograph used in a standard HIL test. The time integration of the pantograph model is carried out independently of the catenary model by means of the Hilber-Hughes-Taylor (HHT) integration method [27]. In this virtual test, the displacement of the

catenary contact point obtained from Eq. (36) is imposed on the pantograph model and the contact force in the next time step is computed. Unlike in a real HIL test in which this force would be measured by load cells, in the simulated test, a penalty stiffness is used [2].

To validate the method, the results obtained in the virtual HIL test are compared with a FEM conventional simulation. It is noteworthy to mention that the virtual HIL test assumes an infinite periodic catenary while the size of conventional FEM model is limited by the number of degrees of freedom. However, we have made a long enough catenary section so that the steady-state regime can be assumed on its central spans. In this way, transient effects are negligible due to the notable length of the FEM catenary model and it is expected to obtain the same solution in both the proposed periodic model (PFEM), and the finite length FEM model.

Specifically, in this example, we chose the catenary model used in the benchmark exercise [2] with spans (or blocks) of 55 m in length having 9 droppers and 55 mm of pre-sag in the contact wire each of them. A Rayleigh damping model is used with $\mathbf{C} = \beta\mathbf{K} + \gamma\mathbf{M}$, being $\beta = 10^{-4}$ s and $\gamma = 1.25 \cdot 10^{-2}$ s^{-1}. For the pantograph, a lumped mass model with 3 vertical degrees of freedom is used whose parameters are provided in Table 1. The penalty stiffness used in the contact model is $k_h = 50000$ N/m according to [2].

Table 1: *Parameters of the pantograph model.*

d.o.f.	m(kg)	c(Ns/m)	k(N/m)
1	6.6	0	7000
2	5.8	0	14100
3	5.8	70	80

In the PFEM, the catenary impulse responses have to be computed for a discrete number of frequencies (see Eq. (17)). We have found that $\Delta\omega = 0.025$ rad/s with a maximum frequency $\omega_{max} = 750$ rad/s are accurate enough values. Note that the frequency resolution $\Delta\omega$ must be small enough to guarantee a large period $2\pi/\Delta\omega$ of the functions to which the DFT is applied. In turn, the maximum frequency involved in the IDFT must be high enough to provide a fine time discretisation of the nodal forces. The time resolution is chosen to $\Delta t = 1$ ms, a value which is smaller than π/ω_{max} to avoid aliasing effects. This value is also used for time integration of the pantograph model, although in this case, a smaller value could be used.

In the numerical case analysed in this section, the velocity of the pantograph is set at 250 km/h and the virtual HIL simulation runs until there is not noticeable differences in the computed contact force of two consecutive blocks. To ease convergence of the virtual HIL test, during the first 20 s of the simulation, the displacement of the catenary contact point that is imposed on the pantograph model is scaled by a factor that increases linearly from 0 to 1. This is reflected in the increasing values in the first blocks of the results shown in this example (see Fig. 7 and Fig. 8).

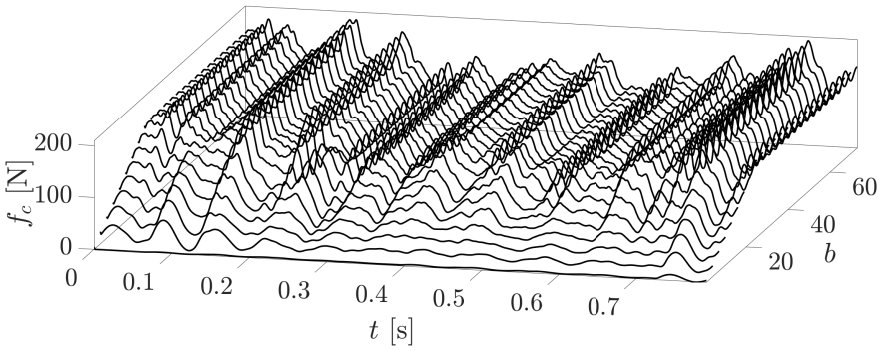

Figure 7: *Contact force evolution.*

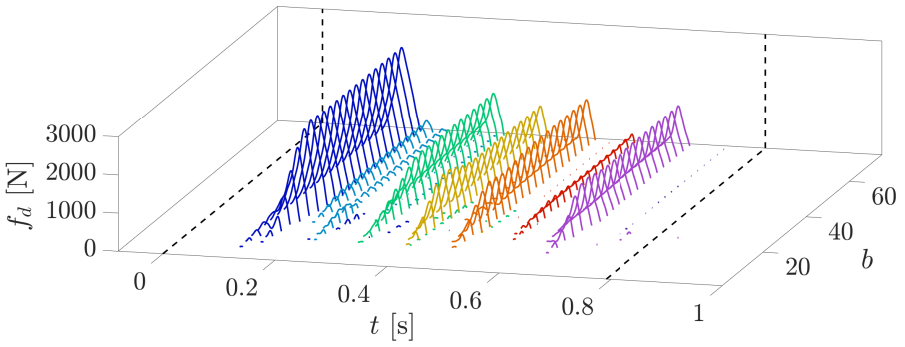

Figure 8: *Dropper correction forces evolution.*

The contact force obtained in successive blocks of the virtual test is depicted in Fig. 7 in which only one in three curves are shown for a better visualisation of

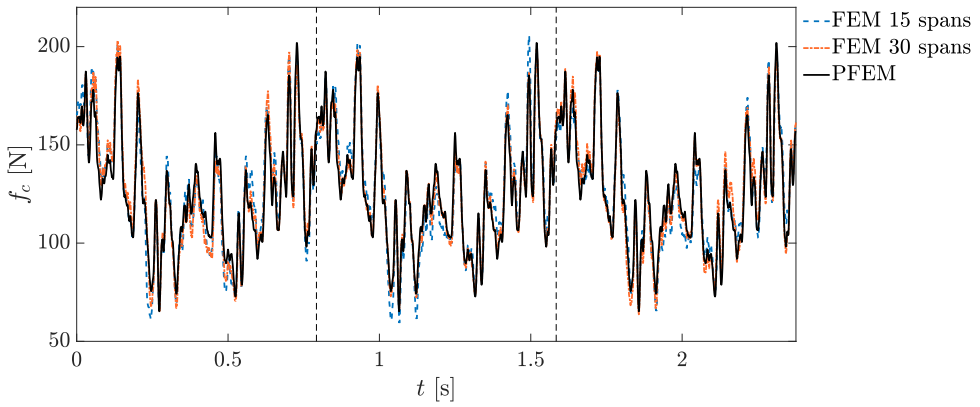

Figure 9: *Comparison of contact force of catenary PFEM (solid line) with those obtained in three central spans of the section of a FE catenary model with 15 spans (dashed line) and 30 spans (dash-dotted line).*

the figure. The non-linear correction forces of droppers 2 to 8 (Eq. (39)) can be seen in Fig. 8 from left to right and again one in three curves are displayed. Note that the first and last droppers do not present any correction force since they do not slacken due to their greater initial tensile force caused by the pre-sag of the contact wire. The two black dashed lines show the times in which the pantograph is placed inside the reference block from $t = 0$ to $t = 0.792$ s. However, dropper correction forces are also computed outside this period but they are null in this example. Specifically, the period in which dropper correction is active covers two blocks, from step $-n_b = 80$ to $n_a = 1504$.

As seen in both figures, convergence is properly achieved, although it is important to mention that some convergence issues can arise if the periodic structure is very low damped. Thus, a certain amount of damping is required to guarantee the convergence of the proposed approach.

In order to validate the results, the converged contact force obtained from the catenary PFEM is compared in Fig. 9 with the contact force of three consecutive central blocks computed with a conventional FEM simulation. We have used two catenary models with different length, namely 15 and 30 spans respectively. The FEM solutions show minor differences with the contact force obtained from the PFEM. These differences are even smaller with the 30-spans FE catenary model because a more stationary response is achieved on these central spans. The converged dropper correction forces obtained from the catenary PFEM are also compared with those obtained from the longest FE catenary model in Fig. 10. As

can be seen in both figures, the results provided by the proposed catenary PFEM are validated according to their great similarities with those obtained from a FEM simulation with a large enough catenary model.

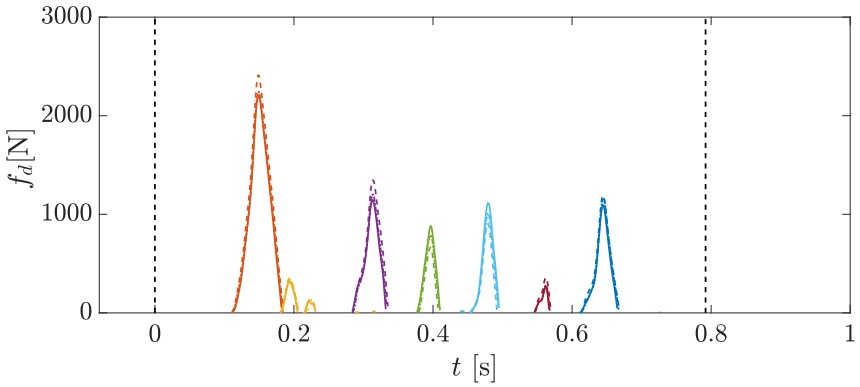

Figure 10: *Comparison of dropper correction forces from catenary PFEM (solid lines) with those obtained in a central span of a FE catenary model with 30 spans (dashed lines).*

Regarding the computational cost required to obtain the PFEM solution, a distinction must be made between the *off-line* and *on-line* stages. The former takes a relatively long computation time which mainly includes the FRF of the catenary periodic block and the unitary impulse response functions. Specifically, for the example previously analysed, it takes approximately 30 minutes in a conventional computer.

The *on-line* stage covers the computations that must fulfil real-time performance to perform HIL tests. For a given time-step t_n, the measured contact force is taken as input and the contact point height must be given before the next contact force is measured. The operations involved are described in Table 2.

For the numerical example previously analysed in which $\Delta t = 1$ ms, $N_c = 792$, $N_{\bar{n}_d} = 2$, $N_d = 9$ and N_{sd} ranges from 0 to N_d. With these values, that can be taken as usual, the operations involved in each time step need about 0.15 ms to be performed, which confirms the real-time capability of the proposed formulation and its potential use for HIL pantograph tests.

Table 2: *Operations performed in a given time step in the on-line stage.*

Equation	Description	Operations
Eq. (34)	Contact point displacement due to contact force.	$[\ ]_{N_c \times 1} + \Delta f_c \cdot [\ ]_{N_c \times 1}$
Eq. (35)	Droppers elongation due to contact force.	$[\ ]_{N_c \cdot N_{\bar{n}_d} \cdot N_d \times 1} + \Delta f_c \cdot [\ ]_{N_c \cdot N_{\bar{n}_d} \cdot N_d \times 1}$
Eq. (38)	Dropper state.	$k_d \cdot [\ ]_{N_c \cdot N_{\bar{n}_d} \cdot N_d \times 1} < -f_{d0} \quad d = 1, ..., N_d$
Eq. (40)	Slackened droppers correction force.	$[\ ]^{-1}_{N_{sd} \times N_{sd}} \cdot [\ ]_{N_{sd} \times 1}$
Eq. (36)	Contact point displacement due to slackened droppers correction force.	$[\ ]_{N_c \times 1} + [\ ]_{N_c \times N_{sd}} \cdot \Delta f_d$
Eq. (37)	Droppers elongation due to slackened droppers correction force.	$[\ ]_{N_c \cdot N_{\bar{n}_d} \cdot N_d \times 1} + [\ ]_{N_c \cdot N_{\bar{n}_d} \cdot N_d \times N_{sd}} \cdot \Delta f_d$

7 Conclusions

In this paper, we present a whole framework to perform HIL pantograph tests achieving the steady state of the pantograph-catenary dynamic interaction. The contribution of this paper is twofold: on the one hand we proposed the formulation to build an infinite periodic structure model, discretised by the FEM and subjected to a moving load travelling at constant velocity. The PFEM formulation is directly built from the common FE matrices that define the repetitive block of the system, so that it is valid for any generic periodic structure. The proposed formulation has been applied to compute the impulse response of a railway catenary PFEM to be subsequently used in HIL pantograph tests. On the other hand, an iterative strategy to achieve the steady state when the the catenary PFEM is used in HIL pantograph tests is proposed and numerically validated, even with the extension of the method in which the non-linear behaviour of droppers is also considered.

The main conclusions that can be drawn from this work are:

- From the FE model of a given infinite periodic structure repetitive block and applying periodic boundary conditions, it has been verified, by means of standard simulations with a very long FE catenary model, that the proposed catenary PFEM provides the precise steady-state response under a constant velocity moving load.
- The catenary PFEM requires very low computational cost which allows its implementation in HIL tests, in which real-time performance is mandatory. Even when the non-linear behaviour of droppers is included into the algorithm, it is still able to be solved in real time.
- Although it is unavoidable to manage a delay produced in the communication and execution of the control loop of the actuator, the proposed formulation has the advantage of being able of easily compensate this delay since the response for a later time is available at the current time step.
- The proposed framework to perform HIL tests with the catenary PFEM only focuses on the steady-state response and therefore, other particularities of the pantograph-catenary interaction such as contact wire irregularities, uneven spans or overlaps can not be addressed.

Future work will lead to the implementation of the proposed method in a HIL test rig, in which the stability of the method needs to be checked in the presence of experimental issues such as noise, delays, limited measuring accuracy, vibrations and so on. Additionally, the catenary PFEM can be extended to consider the interaction with two pantographs offering the opportunity of studying the interference phenomenon between pantographs.

Acknowledgements

The authors would like to acknowledge the financial support received from the State Research Agency of the Spanish Science and Innovation Ministry (PID2020-113458RB-I00) and from the Valencian Regional Government (PROMETEO/2021/046).

Bibliography

[1] S. Bruni, G. Bucca, M. Carnevale, A. Collina, and A. Facchinetti, "Pantograph–catenary interaction: recent achievements and future research challenges," *International Journal of Rail Transportation*, vol. 6, no. 2, pp. 57–82, 2018.

[2] S. Bruni, J. Ambrosio, A. Carnicero, Y. H. Cho, L. Finner, M. Ikeda, S. Y. Kwon, J. P. Massat, S. Stichel, and M. Tur, "The results of the pantograph-catenary interaction benchmark," *Veh Syst. Dyn.*, vol. 53, no. 3, pp. 412–435, 2015.

[3] W. Song, C.-M. Chang, and V. K. Dertimanis, "Editorial: Recent advances and applications of hybrid simulation," *Frontiers in Built Environment*, vol. 6, 2020.

[4] A. Facchinetti and S. Bruni, "Hardware-in-the-loop hybrid simulation of pantograph–catenary interaction," *Journal of Sound and Vibration*, vol. 331, no. 12, pp. 2783–2797, 2012.

[5] Y. Song, Z. Liu, A. Rønnquist, P. Nåvik, and Z. Liu, "Contact wire irregularity stochastics and effect on high-speed railway pantograph–catenary interactions," *IEEE Transactions on Instrumentation and Measurement*, vol. 69, no. 10, pp. 8196–8206, 2020.

[6] S. Gregori, J. Gil, M. Tur, J. Tarancón, and F. Fuenmayor, "Analysis of the overlap section in a high-speed railway catenary by means of numerical simulations," *Engineering Structures*, vol. 221, p. 110963, 2020.

[7] H. Ouyang, "Moving-load dynamic problems: A tutorial (with a brief overview)," *Mechanical Systems and Signal Processing*, vol. 25, no. 6, pp. 2039–2060, 2011. Interdisciplinary Aspects of Vehicle Dynamics.

[8] D. J. Mead, "Vibration response and wave propagation in periodic structures," *J. Eng. Ind.*, vol. 93, no. 3, pp. 783–792, 1971.

[9] C. Cai, Y. Cheung, and H. Chan, "Dynamic response of infinite continuous beams subjected to a moving force – An exact method," *J. Sound Vib.*, vol. 123, no. 3, pp. 461 – 472, 1988.

[10] P. Belotserkovskiy, "On the oscillations of infinite periodic beams subjected to a moving concentrated force," *J. Sound Vib.*, vol. 193, no. 3, pp. 705 – 712, 1996.

[11] A. Metrikine and A. Bosch, "Dynamic response of a two-level catenary to a moving load," *J. Sound Vib.*, vol. 292, no. 3, pp. 676 – 693, 2006.

[12] X. Sheng, C. Jones, and D. Thompson, "Responses of infinite periodic structures to moving or stationary harmonic loads," *J. Sound Vib.*, vol. 282, pp. 125–149, 04 2005.

[13] X. Sheng, C. Jones, and D. Thompson, "Using the fourier-series approach to study interactions between moving wheels and a periodically supported rail," *J. Sound Vib.*, vol. 303, pp. 873–894, 06 2007.

[14] J.-M. Mencik, "On the low- and mid-frequency forced response of elastic structures using wave finite elements with one-dimensional propagation," *Comput. Struct.*, vol. 88, no. 11, pp. 674 – 689, 2010.

[15] B. Claudet, T. Hoang, D. Duhamel, G. Foret, J.-L. Pochet, and F. Sabatier, "Wave finite element method for computing the dynamic response of railway transition zones subjected to moving loads," in *COMPDYN 2019*, (Crete, Greece), pp. 4538–4547, 01 2019.

[16] T. Hoang, D. Duhamel, G. Forêt, J.-L. L. Pochet, and F. Sabatier, "Wave finite element method and moving loads for the dynamic analysis of railway tracks," in *WCCM XIII*, (New York, United States), 2018.

[17] W. Zhang, G. Mei, X. Wu, and Z. Shen, "Hybrid simulation of dynamics for the pantograph-catenary system," *Veh. Syst. Dyn.*, vol. 38, no. 6, pp. 393–414, 2002.

[18] W. Zhang, G. Mei, X. Wu, and L. Chen, "A study on dynamic behaviour of pantographs by using hybrid simulation method," *Proc. Inst. Mech. Eng. F: J. Rail Rapid Transit*, vol. 219, no. 3, pp. 189–199, 2005.

[19] A. Collina, A. Facchinetti, F. Fossati, and F. Resta, "Hardware in the loop test-rig for identification and control application on high speed pantographs," *Shock Vib.*, vol. 11, pp. 445–456, 01 2004.

[20] F. Resta, A. Facchinetti, A. Collina, and G. Bucca, "On the use of a hardware in the loop set-up for pantograph dynamics evaluation," *Veh. Syst. Dyn,*, vol. 46, no. S1, pp. 1039–1052, 2008.

[21] A. Facchinetti and M. Mauri, "Hardware-in-the-loop overhead line emulator for active pantograph testing," *IEEE Trans. Ind. Electron.*, vol. 56, no. 10, pp. 4071–4078, 2009.

[22] A. Schirrer, G. Aschauer, E. Talic, M. Kozek, and S. Jakubek, "Catenary emulation for hardware-in-the-loop pantograph testing with a model predictive energy-conserving control algorithm," *Mechatronics*, vol. 41, pp. 17 – 28, 2017.

[23] S. Gregori, M. Tur, A. Pedrosa, J. Tarancón, and F. Fuenmayor, "A modal coordinate catenary model for the real-time simulation of the pantograph-catenary dynamic interaction," *Finite Elem. Anal. Des.*, vol. 162, pp. 1–12, 2019.

[24] J. Gil, M. Tur, A. Correcher, S. Gregori, A. Pedrosa, and F. J. Fuenmayor, "Hardware-in-the-loop pantograph tests using analytical catenary models," *Veh. Syst. Dyn.*, pp. 1–15, 2021.

[25] S. Gregori, M. Tur, E. Nadal, J. V. Aguado, F. J. Fuenmayor, and F. Chinesta, "Fast simulation of the pantograph–catenary dynamic interaction," *Finite Elem. Anal. Des.*, vol. 129, pp. 1 – 13, 2017.

[26] H. Chebli, R. Othman, and D. Clouteau, "Response of periodic structures due to moving loads," *Comptes Rendus Mécanique*, vol. 334, no. 6, pp. 347 – 352, 2006.

[27] H. M. Hilber, T. J. Hughes, and R. L. Taylor, "Improved numerical dissipation for time integration algorithms in structural dynamics," *Earthq. Eng. Struct. Dyn.*, vol. 5, no. 3, pp. 283–292, 1977.

Appendix A

Demonstrative example

In order to illustrate the method and facilitate the reproducibility of the numerical results, a HIL simulation is described in this appendix by using a linear small-size FE model. The procedure described in the paper is thoroughly followed and some numerical results are provided at each step.

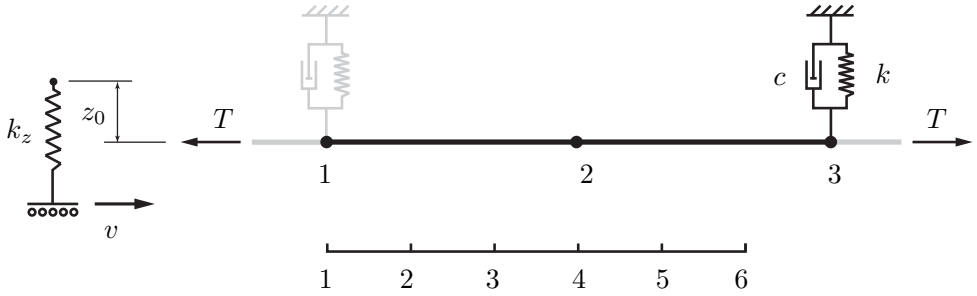

Figure A.1: *Academic periodic FE model.*

The infinite periodic model chosen is composed of a tensioned string periodically supported as shown in Fig. A.1. The repeated block consists of a piece of string modelled with two elements (3 nodes) and a spring-damper system on the right end. A given element of the string has two nodes and two degrees of freedom, the

vertical displacement of each node. The dynamic equation of an element e with tension T, linear density μ and length L_e is:

$$\mathbf{m}\ddot{\mathbf{u}}^{\mathrm{e}} + \mathbf{k}\mathbf{u}^{\mathrm{e}} = \mathbf{F}^{\mathrm{e}} \tag{A.1}$$

in which the mass and stiffness matrices and the vector of degrees of freedom are:

$$\mathbf{m} = \frac{\mu L_e}{6}\begin{bmatrix} 2 & 1 \\ 1 & 2 \end{bmatrix}; \quad \mathbf{k} = \frac{T}{L_e}\begin{bmatrix} 1 & -1 \\ -1 & 1 \end{bmatrix}; \quad \mathbf{u}^{\mathrm{e}} = \begin{bmatrix} u_1 \\ u_2 \end{bmatrix} \tag{A.2}$$

The FE model of the whole block is obtained by assembling the two string elements and the spring-damper system, which results in:

$$\mathbf{M} = \begin{bmatrix} \frac{\mu L_e}{3} & \frac{\mu L_e}{6} & 0 \\ \frac{\mu L_e}{6} & 2\frac{\mu L_e}{3} & \frac{\mu L_e}{6} \\ 0 & \frac{\mu L_e}{6} & \frac{\mu L_e}{3} \end{bmatrix}; \quad \mathbf{C} = \begin{bmatrix} 0 & 0 & 0 \\ 0 & 0 & 0 \\ 0 & 0 & c \end{bmatrix}; \tag{A.3}$$

$$\mathbf{K} = \begin{bmatrix} \frac{T}{L_e} & -\frac{T}{L_e} & 0 \\ -\frac{T}{L_e} & 2\frac{T}{L_e} & -\frac{T}{L_e} \\ 0 & -\frac{T}{L_e} & \frac{T}{L_e} + k \end{bmatrix}; \quad \mathbf{U} = \begin{bmatrix} u_1 \\ u_2 \\ u_3 \end{bmatrix}; \tag{A.4}$$

The numerical values of the parameters that define the model are shown in Table A.1. The time and frequency discretization is made with $\Delta t = 5$ ms and $\Delta\omega = 2\pi/(N\Delta t)$ rad/s, being $N = 10000$ and the number of harmonics $N_f = 5969$, which leads to a maximum frequency of ≈ 750 rad/s.

Table A.1: *Parameters of the academic model.*

T(N)	μ(kg/m)	L_e(m)	k(N/m)	c(Ns/m)	v(m/s)
22000	1.3	0.75	300	10	50

The dynamic stiffness matrix $\mathbf{D}(\omega_k)$ can be computed with Eq. (6) and, by using Eqs. (12) and (14), the Frequency Response Function $\mathbf{H}(\omega_k)$ is obtained considering that node 1 is the left node, node 2 is the inner node and node 3 is the right node. For each frequency ω_k, $\mathbf{H}(\omega_k)$ is a matrix with two columns related to the excitation on the inner and the right nodes and three rows that match to

the displacement of each of the three nodes. For example, the matrix $\mathbf{H}(\omega_k)$ for the frequency index $k = 3000$ (60 Hz) is:

$$\mathbf{H}(\omega_{k=3000}) = 10^{-4} \begin{bmatrix} -0.1113 + 0.0845\,\mathrm{i} & 0.0161 - 0.0532\,\mathrm{i} \\ 0.0549 - 0.0074\,\mathrm{i} & -0.1113 + 0.0845\,\mathrm{i} \\ -0.1147 - 0.0797\,\mathrm{i} & 0.0555 - 0.0012\,\mathrm{i} \end{bmatrix}$$

Additionally, the norm of the different elements in $\mathbf{H}(\omega_k)$ are depicted in Fig. A.2, in which $|\mathbf{H}_{12}(\omega_k)| = |\mathbf{H}_{32}(\omega_k)|$ and $|\mathbf{H}_{11}(\omega_k)| = |\mathbf{H}_{22}(\omega_k)| = |\mathbf{H}_{31}(\omega_k)|$ due to the properties of the receptance and the periodic boundary conditions.

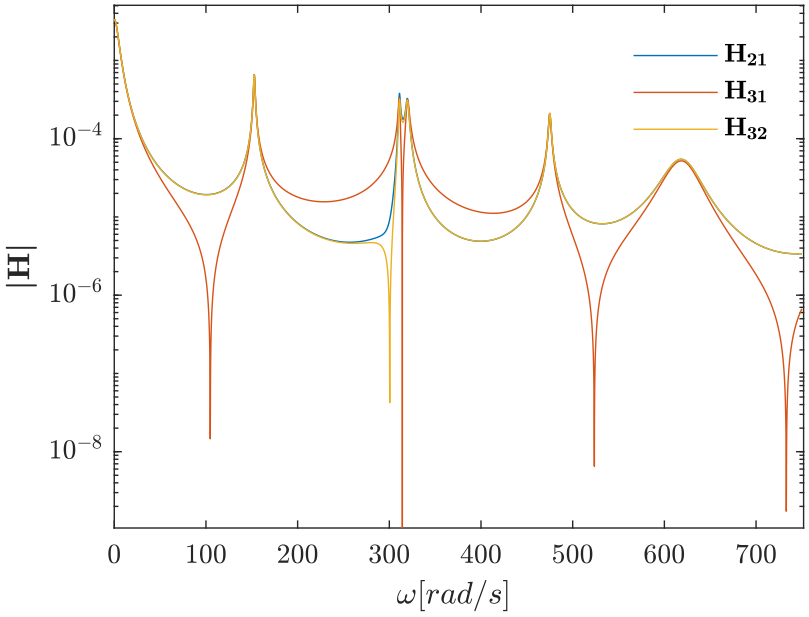

Figure A.2: *Norm of the receptance $H(\omega)$.*

The velocity of the moving load used in this example is $v = 50$ m/s. According to this value, the length of the block and Δt, there are $N_c = 6$ different discrete contact points along the block as depicted in Fig. A.1. The dynamic behaviour of the PFEM with a moving load is collected in the operator $\mathbb{I}(n, \hat{n})$. This operator is obtained with the evaluation of the discrete impulse function defined in Eq. (19) for all the combinations of $n \in [1, N_c]$ and $\hat{n} \in [1, N_c]$ as stated in Eq. (22). As the continuous operator $I(\omega, \mathbf{x}, \mathbf{y})$ appears in the discrete impulse function (Eq. (19)), it also must be evaluated for all combinations of n and $\hat{n}$ considering that the

observation point $\mathbf{x}$ is related to n and the excitation point $\mathbf{y}$ is related to $\hat{n}$. Thus, $I(\omega, n, \hat{n}) = I(\omega, \mathbf{x}_n, \mathbf{y}_{\hat{n}})$ is computed for every frequency ω_k, with 6 points of excitation and 6 points of observation, by means of Eq. (16).

To compute $I(\omega, n, \hat{n})$, the shape functions are arranged in a matrix that relates the forces of discrete points $\hat{n}$ (rows) to the three degrees of freedom (columns):

$$\mathbf{N} = \begin{bmatrix} 1 & 0 & 0 \\ 0.6667 & 0.3333 & 0 \\ 0.3333 & 0.6667 & 0 \\ 0 & 1 & 0 \\ 0 & 0.6667 & 0.3333 \\ 0 & 0.3333 & 0.6667 \end{bmatrix}$$

The operator $I(\omega, n, \hat{n})$ is organised in a matrix $\mathbf{I}$, referring the rows to n and the columns to $\hat{n}$. For example, the values of this operator for the frequency defined by $k = 3000$ are:

$$\mathrm{Re}(\mathbf{I}(\omega_{k=3000})) = 10^{-4} \cdot \begin{bmatrix} 0.0555 & -0.0001 & -0.0557 & -0.1113 & -0.0688 & -0.0264 \\ -0.0012 & -0.0195 & -0.0377 & -0.0559 & -0.0461 & -0.0362 \\ -0.0580 & -0.0388 & -0.0197 & -0.0005 & -0.0233 & -0.0461 \\ -0.1147 & -0.0582 & -0.0016 & 0.0549 & -0.0005 & -0.0559 \\ -0.0704 & -0.0475 & -0.0246 & -0.0016 & -0.0197 & -0.0377 \\ -0.0261 & -0.0368 & -0.0475 & -0.0582 & -0.0388 & -0.0195 \end{bmatrix}$$

$$\mathrm{Im}(\mathbf{I}(\omega_{k=3000})) = 10^{-5} \cdot \begin{bmatrix} 0.0116 & -0.2738 & -0.5593 & -0.8448 & -0.3860 & 0.0728 \\ 0.2736 & 0.0028 & -0.2679 & -0.5387 & -0.3348 & -0.1310 \\ 0.5355 & 0.2795 & 0.0235 & -0.2325 & -0.2837 & -0.3348 \\ 0.7975 & 0.5562 & 0.3149 & 0.0736 & -0.2325 & -0.5387 \\ 0.3568 & 0.3429 & 0.3289 & 0.3149 & 0.0235 & -0.2679 \\ -0.0838 & 0.1295 & 0.3429 & 0.5562 & 0.2795 & 0.0028 \end{bmatrix}$$

To show more information of this operator, the elements of the first column are plotted in Fig. A.3 for every frequency. In this case, $|\mathbb{I}_{51}| = |\mathbb{I}_{31}|$ and $|\mathbb{I}_{61}| = |\mathbb{I}_{21}|$ due to the periodicity condition and the symmetry of the model.

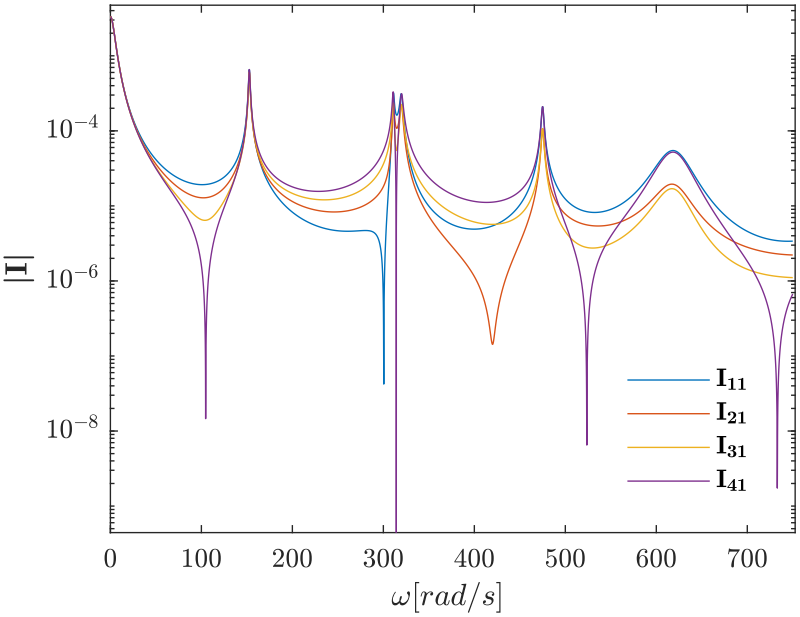

Figure A.3: *Harmonic response of discrete points of the block when the excitation is applied on point number 1.*

Finally, with Eq. (19) and Eq. (22), $\mathbb{I}(n, \hat{n})$ can be computed from $I(\omega, n, \hat{n})$. In this case, it results in:

$$\mathbb{I} = 10^{-4} \begin{bmatrix} 0.3804 & 0.3934 & 0.4126 & 0.3758 & 0.4676 & 0.4853 \\ 0.4853 & 0.3735 & 0.3778 & 0.4197 & 0.4216 & 0.4319 \\ 0.4676 & 0.4439 & 0.3676 & 0.3934 & 0.4029 & 0.4216 \\ 0.3758 & 0.4750 & 0.4902 & 0.3627 & 0.3934 & 0.4197 \\ 0.4126 & 0.4200 & 0.4437 & 0.4902 & 0.3676 & 0.3778 \\ 0.3934 & 0.3913 & 0.4200 & 0.4750 & 0.4439 & 0.3735 \end{bmatrix}$$

Once the former operator is obtained, a simulation of a HIL test can be carried out. To simplify the process, the model in contact (which replaces the real pantograph) is a single spring as shown in Fig. A.1. This spring applies a vertical force f_c on the contact point, which is proportional to the difference between the contact point height z_c and a reference value z_0, so that $f_c = k_z(z_c - z_0)$. In this example we use a spring with stiffness $k_z = 10000$ N/m and $z_0 = 5$ mm.

Given a contact force f_c, Eq. (25) provides the contact point height. In the first step of the simulation, the displacement of the contact point is initialised to 0 and the contact force is therefore $f_c(1) = k_z z_0 = 50$ N. By multiplying the first column of $\mathbb{I}(n, \hat{n})$ by this force, we obtain:

$$z_c^1 = 10^{-3} \cdot [1.9022 \quad 2.4265 \quad 2.3380 \quad 1.8791 \quad 2.0630 \quad 1.9668] \text{ m}$$

for all $n \in [1, 6]$. In the next step, the displacement of the contact point is $z_c^1(2) = 2.4265 \cdot 10^{-3}$ m and the contact force is $f_c(2) = k_z(z_0 - 2.4265 \cdot 10^{-3}) = 25.7351$ N. This value is used to multiply the second column of $\mathbb{I}(n, \hat{n})$ and the result is added to z_c^1 to compute z_c^2, from which the third value $z_c^2(3) = 3.4803 \cdot 10^{-3}$ can be obtained for the next step.

In the 7-th step, the block number 2 starts and hereinafter, instead of using the force value $f_c(7)$, we use the increment respect to the force on the former block, $f_c(7) - f_c(1)$, to multiply the first column of $\mathbb{I}(n, \hat{n})$. Following this procedure, the contact force obtained is shown in Fig. A.4. The contact force is finally repeated in every block as seen in the figure since the steady-state regime has been achieved. This periodic contact force is:

$$f_c = [14.1319 \quad 14.2372 \quad 14.4190 \quad 14.1001 \quad 14.2078 \quad 14.4236] \text{ N}$$

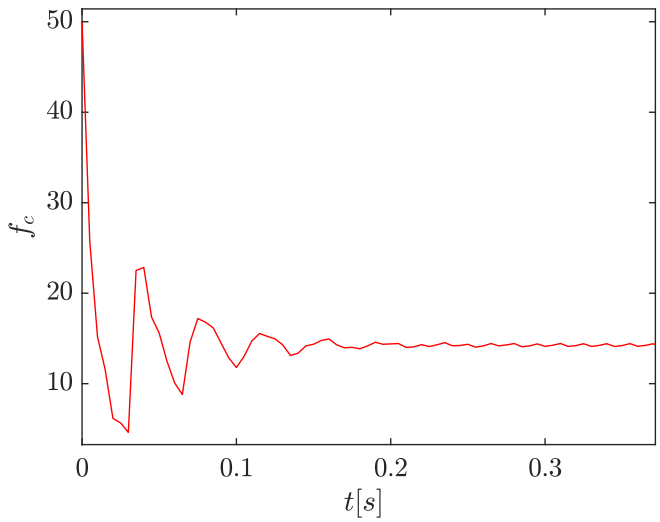

Figure A.4: *Contact force in a simulated HIL test with the academic model.*

PAPER D

Hardware-In-the-Loop simulations of a railway pantograph with a finite element periodic catenary model

J. Gil, M. Tur, S. Gregori, A. Correcher, A.M. Pedrosa and F. J. Fuenmayor

Submitted to Vehicle System Dynamics

Abstract

In this work, the pantograph-catenary dynamic interaction problem is addressed by Hardware-In-the-Loop (HIL) tests. This technique emulates the dynamic interaction between a numerical model (the catenary) and a physical device (the pantograph). The real-time simulation requires a computationally efficient numerical model and a time and accurate transference of the response to the pantograph. To this end, a Periodic Finite Element Model (PFEM) of the catenary is considered in this work for two main reasons. First, the low computation time required to solve it, makes it suitable for performing real-time simulations. Second, its ability for compensating the delay produced by the transference of the numerical model response.

The PFEM of the catenary used in this work considers the non-linear behaviour of dropper slackening, leading to high-accuracy HIL test results, which have been validated up to a frequency of 25 Hz.

Keywords

Hardware-In-the-Loop, Hybrid Simulation, Pantograph, Control, Periodic Catenary

Contents

1 Introduction

The current research on railway engineering, is now involved in multiple problems, one of which is the pantograph-catenary dynamic interaction problem. It is an established fact that, although there is still room for improvement, the performance of the pantograph-catenary couple limits the rolling stock speed. This is due to the apparent dynamic complexity of the system and the gap between the models and reality that hinders any attempt at improvement. This gap refers to the difficulty of reproducing experimental measurements by numerical simulations.

One of the solutions proposed to reduce the gap is the so-called Hardware-in-the-Loop (HIL) tests, also known as hybrid simulations (HS). These tests are used in multiple fields [1] and researchers have made great efforts to expand HIL boundaries. In the pantograph-catenary field, HIL tests consist of a pantograph loaded by an actuator that simulates the catenary response obtained from numerical simulations and can be considered midway between in-line experimental tests and pure numerical simulations.

Even though the use of HIL simulations is an appealing approach to avoid expensive in-line tests, their implementation presents certain challenges. HIL tests require very efficient models, advanced equipment and demanding electronic performance. One of the main requirements of HIL pantograph tests is thus a low computational cost of the catenary model as it needs to be integrated at a rate of 2 ms or less, which is high, considering the many degrees of freedom requiered of a catenary model to obtain accurate results. Another essential requirement is a short control loop delay to prevent an unstable response. To solve these two big problems, different efficient catenary models and techniques to mitigate the effect of the delay can be found in the literature.

The modal-truncated approach is used in [2, 3] to reduce the size of simplified catenary models as regards the computational cost. The same approach is also used in [4] but applied to a non-linear finite element catenary model. Another alternative is the sliding window method, which was first used in [5] with a simple catenary model composed of three spans. This model was upgraded in [6] by the inclusion of non-linear dropper slackening behaviour. In [7] a catenary model based on a moving mesh formulation in combination with absorbing boundary layers was used to perform catenary time integration in real-time. All these finite-length catenary models lead to a stationary response that is affected by the boundary conditions assumed.

Although the previously described catenary models can be computed in real-time, their response has to be faithfully transferred to the physical device, and

the presence of a delay prevents this. Some solutions have been proposed to address the negative effects of delays. In [8], the HIL technique is applied to the vehicle-bridge interaction and the work aims to compensate the HIL delay by using a recursive prediction optimal (RPO) compensator. This method has been shown to have better performance than other strategies such as polynomial extrapolation [9], inverse compensation [10] or differential feedforward [11]. The interaction between a real pantograph and a virtual catenary is dealt with in [12, 13]. This type of simulation is called a Dynamically Substructured System (DSS) as the interaction is conducted in a different way to that used in HIL. According to the authors, the HIL or HS labels are used when the interaction between the virtual and psysical substructure follows an open-loop strategy. In the HIL strategy, transferring the response of the virtual to the physical model therefore has to be ideal, implying rigorous requirements. On the other hand, DSS provides an interaction between the models by means of a closed loop in which the response of the virtual model is compared to the current status of the physical device and a control action is included. In [12], the control system is developed via Linear Substructuring Control (LSC) to perform DSS by a very elementary catenary model with one degree of freedom and variable stiffness. Experimental results can be achieved by replacing the pantograph with a shock absorber, which is good for the control field but is still far from accurate in representing the pantograph-catenary dynamic interaction. This approach was continued in [13] by applying a sliding window approach to model the catenary, but the test was performed with the same simplified pantograph model. The results obtained were compared with simulations but were seen to be significantly inaccurate. In [14], the DSS strategy was then tested with a real pantograph and the accuracy of the results was challenged. According to this terminology, the work conducted in [7] could be described as DSS, since they also developed a control algorithm based on the energy equation to limit the error in the controlled position of the catenary to avoid the instability produced by delays.

In the present work we adopted the periodic finite element model of the catenary proposed in [15]. This model provides highly accurate results, as demonstrated in [15], accounts for dropper slackening and has certain advantages for its practical implementation. Due to the infinite periodicity foundation, the steady-state solution provided by the PFEM is not influenced by the boundary-layer effects. The model is also suitable for a total delay compensation technique, which has shown good performance in virtual tests [15]. Our main aim was thus to describe the most important factors to be taken into account in performing HIL pantograph tests with the above-cited catenary PFEM. We also describe in detail the iterative algorithm used to achieve the steady-state regime and practical

measures to prevent test instability. The HIL test results were validated by a proposed method that can quantify the overall HIL-induced error.

The remainder of this paper is organised as follows: Section 2 gives a description of the test rig used in the HIL tests. Section 3 describes the two strategies used to perform HIL tests with the PFEM. Section 4 performs a stability parametric analysis of the two strategies proposed. Section 5 validates the HIL setup and presents some of the results of different catenaries and train speeds, while Section 6 sums up our main conclusions.

2 HIL test-rig

The test rig used for the real-time interaction of virtual catenaries and real pantographs is shown in Fig. 1. Its main elements are as follows:

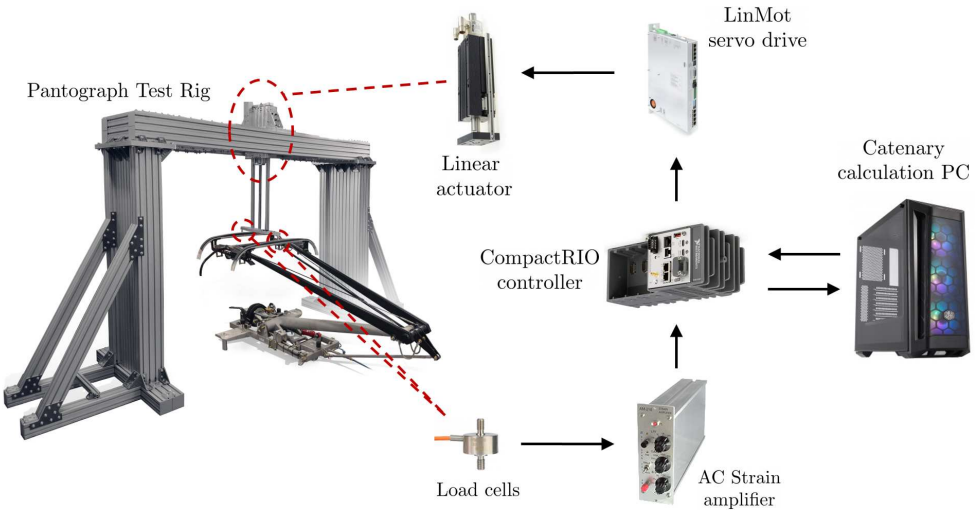

Figure 1: *Test-rig components and information flow.*

- **Actuator:** A linear magnetic motor (LINMOT PS10-70x240U) with a maximum velocity of 5.4 m/s and a maximum force of 1650 N.
- **Actuator Controller:** The E1450 motor drive controller receives position references by UDP communication via a LinUDP bespoke protocol. The controller generates intermediate sub-references using one of the several sub-reference generation modes. The selected working mode is a linear interpolation (ramp) between reference points to avoid generating parasite

frequencies and discrete steps that lead to instability. A closed-loop PID control strategy is used to follow all the sub-references generated. Since communications with the driver are non-deterministic, the sub-references are executed by a hardware trigger signal generated by the Real-Time Computer to guarantee periodic execution of the control commands.

- **Real-Time Computer:** A real-time *CompactRio* (CRIo-9040) device from National Instruments™ forms the system's brain, which carries out the main tasks. It includes a Dual Core 1.30 GHz processor, 2GB RAM, Ethernet communications, and several IO modules. The RT computer acquires the measured force. It also executes the main and control loops. The main loop has a rate of 2 ms in which it adquires the force value, sends the value to the computer and receives its response. The motor control loop has a rate of 10 ms in which it acquires the last displacement value of the main loop and sends it to the Actuator Controller.

- **PC:** This solves the virtual catenary PFEM implemented in Matlab™. As it is essential to have a flexible code to test different settings of the catenary in different experiments, this code runs on an Intel®Core™ i9, 3.6GHz, eight cores and 64Gb RAM PC high-speed processor.

- **Force measuring:** Two load cells measure the force of the pantograph on the actuator. These signals are conditioned by two AC Strain amplifiers (AS1201) that increase the signal levels and include a configurable filtering stage (10Hz, 30Hz, 100Hz, 300Hz, or no filter).

- **Pantograph:** The pantograph selected for this research is a DSA®380.03.

The test rig materialises the vertical displacement of the catenary contact point when a force is applied. The process carried out, since this force is measured until the actuator achieves the response given by the catenary model, follows the itinerary defined in Fig. 2. The time that this process takes has a great influence on the accuracy of the response. The process starts when the force is measured, then passes through a filter and the signal is converted into a digital value by the AD converter. The force value is picked by the RT computer at the beginning of the RT main loop. The following step in this main loop is to send the force to the PC, which after solving one time step of the catenary dynamics, answers with the displacement value of the catenary that is waiting to be sent at the beginning of the control loop. As the value is received by the motor driver that controls the actuator, the driver imposes intermediate values following a ramp between the former and the current references. The ramp finishes on receiving a new reference.

The different parts that account for the total delay can be identified by following the above-described path. The acquisition keeps getting values very quickly until the Main Loop of the RT computer picks one (negligible delay). 2 ms are spent until the iteration of the Main Loop is finished and the value enters the Control Loop. The force value is sent to the actuator controller, taking approximately 4 ms, and at this point a ramp of 10 ms (the time necessary to get the next reference) starts. The total delay is thus 16 ms.

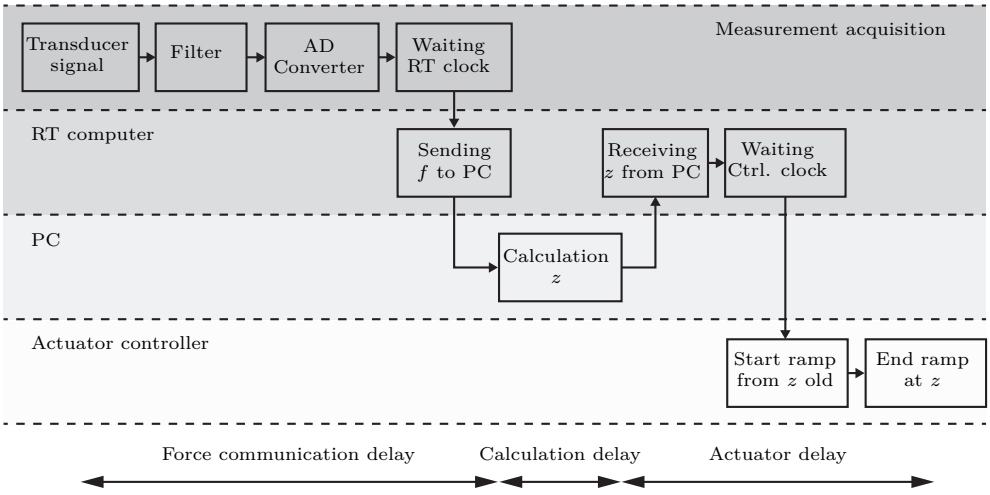

Figure 2: *Itinerary of the whole loop of the test rig*

3 Iterative algorithm of the HIL pantograph tests

The catenary model used for the pantograph-catenary HIL test consists of a periodic catenary modelled by the finite element method, which considers non-linear dropper slackening behaviour. This model reproduces the steady-state dynamic solution of the catenary under the action of a load moving at constant speed, which is representative of the central catenary spans of the pantograph-catenary interaction.

The method used aims to find the steady-state solution of the pantograph-catenary coupled system by means of the HIL rationale, in which the physical device (pantograph) and the virtual model (catenary) of both systems are coupled (the pantograph is governed by transient dynamics and the virtual model satisfies the steady-state equilibrium). To reach this stationary regime it is necessary to use

an iterative procedure to traverse the inevitable transient period. Both the catenary model and the iterative strategy used to guide the HIL test were proposed in [15].

In this section, the linear version of the catenary model and the iterative algorithm are first briefly described, emphasising the main differences required to implement them in a test environment. A new variant of the iterative algorithm is also proposed to tackle the stability issues that arise in practical implementations, and the strategy used to consider dropper non-linear behaviour is also introduced.

3.1 HIL tests with a linear PFEM of the catenary

This section briefly introduces the key ideas of the framework proposed in [15], although for further information the reader is referred to [15], which provides the steady-state response of an infinite periodic catenary subjected to a moving load for a discrete-time environment. The solution relates the periodic moving load vector $\mathbf{f}$ with the vertical position $\mathbf{z}$ due to the application of this load vector, as depicted in Fig. 3. Due to the existing periodicity, the time domain includes only the time taken by the load to travel across one span of the catenary and is discretised into N steps, so that the time step $n, \hat{n} \in [1, ..., N]$, n being the time step of a given displacement and $\hat{n}$ the time step of the load-application point. Given a complete set of contact forces $f(\hat{n})$ arranged in vector $\mathbf{f}$, the contact wire height $\mathbf{z}$ vector, which includes the contact points $z(n)$, can be directly obtained as:

$$\mathbf{z} = \mathbf{z}_0 + \mathbf{I}_{\mathrm{cc}}\mathbf{f} \tag{1}$$

$\mathbf{z_0}$ being the initial configuration contact point height (initial geometric catenary shape).

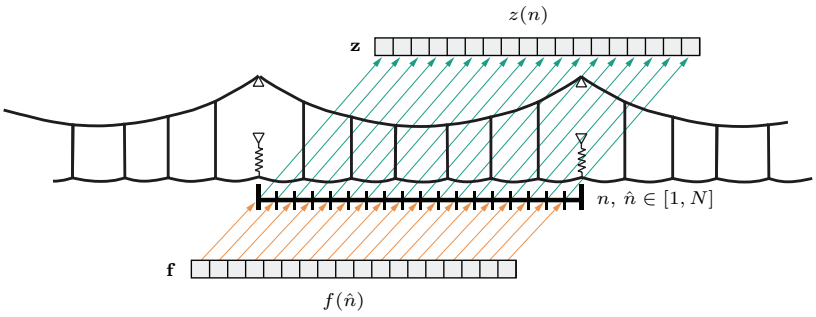

Figure 3: *Input* $\mathbf{f}$*, and output* $\mathbf{z}$*, of the PFEM of the catenary.*

With this scheme, the vertical displacement of the contact point $u(n)$, for all the time steps within the span, can be calculated by means of the product of the contact force $\mathbf{f}$ and matrix $\mathbf{I}_{cc}$ which contains the contribution of every load value (column index $\hat{n}$) to every displacement value (row index n).

The proposed model can give a response, provided the periodic contact force is known. This assumption does not apply to HIL tests, in which the force is measured and is not periodic (at least at the beginning of the test). The strategy of accomplishing HIL tests with a catenary PFEM was proposed in [15]. Roughly speaking, the goal is to measure the contact force along a span, compute the catenary response and impose this vertical position with a periodic assumption, even if the contact force is not periodic, assuming that an iterative process will reach the steady state.

HIL tests are performed following a discrete time scheme. In each global time step, denoted by index k, every contact point displacement is imposed and its contact force is measured. This global time is also organised in blocks of N samples in the form of the length of a period in the problem. The time is denoted in every block b by index $\bar{n}$, starting from 1 at the beginning of the block. The measured contact force in a given time step is denoted as $\bar{f}(k)$ and the vertical position of the actuator in this time step as $\bar{z}(k)$, which depends on the contact force of the previous time steps, as will be explained below. When the test reaches convergence, displacement and forces are repeated in every block and must satisfy Eq. (1). The measured contact force can also be referred to as $\bar{f}^b(\bar{n})$ and the position sent to the actuator as $\bar{z}^b(\bar{n})$, since every global time step k represents a a local time step $\bar{n}$ in block b.

Two alternatives are proposed in this paper for the iterative protocol of the HIL test, i.e. step-by-step and span-by-span updating. In the former we need to compute the displacement of the next step in every time step in which the force is measured, while the span-by-span updating strategy initially defines the position of the actuator along the whole span.

3.2 Step-by-step updating

The first version of the algorithm presented to perform HIL tests with the periodic catenary model is called step-by-step updating. The procedure is depicted in Fig. 4 through different elements. The physical pantograph is represented at the bottom. The horizontal bar moves toward the left and represents the time with the markers on the horizontal line, which can be grouped in blocks. The upper

part describes the mathematical procedure to compute the displacement using the measured force at every instant.

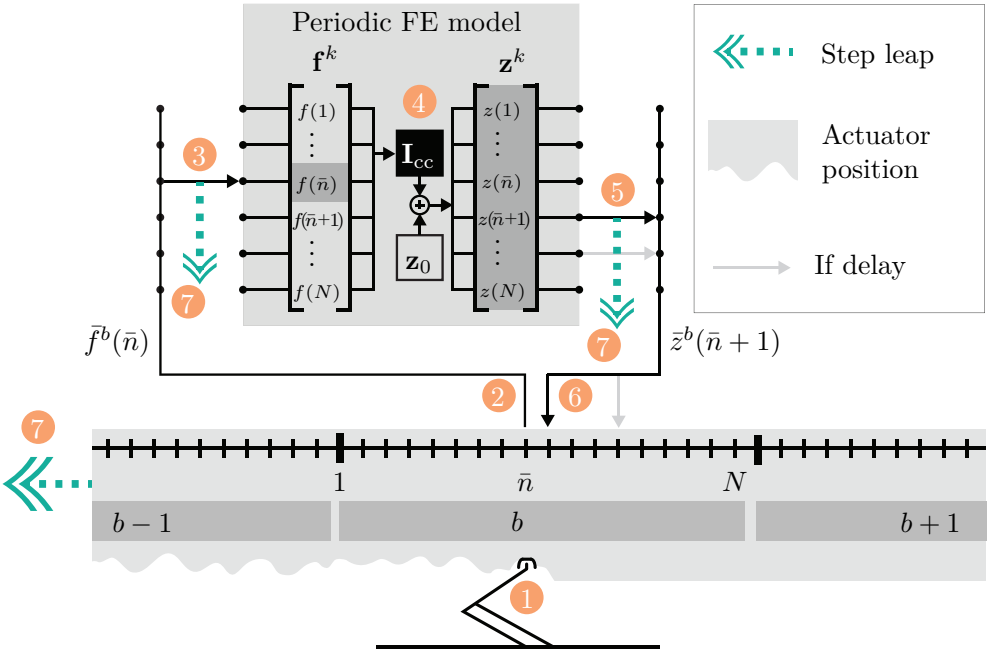

Figure 4: *Graphical description of the step-by-step HIL test architecture with a PFEM of the catenary.*

The different points of Fig. 4 are detailed as follows:

- Point 1: Let us say that the test is in the k global time step (or time step $\bar{n}$ within the block b, as represented in the bar over the pantograph illustration) and the pantograph has reached the displacement sent from the previous time step $k-1$.
- Point 2: The force $\bar{f}^b(\bar{n})$ is measured simultaneously to Point 1.
- Point 3: The measured force is placed in vector $\mathbf{f}^k$ (which changes every time step k, as denoted by the superscript) in the right position $\bar{n}$ while the other elements of this vector remain unaltered.

- Point 4: Eq. (1) is applied to compute the response of the periodic model with $\mathbf{f}^k$, producing the $\mathbf{z}^k$ vector which replaces the one in the previous step $k-1$. Note that in this case, all the components in vector $\mathbf{z}^k$ change.
- Point 5: The vertical position of the next step $\bar{n}+1$ is taken from $\mathbf{z}^k$ since this is the position that would be reached in the next step $k+1$. At this point, a more advanced position to $\bar{n}+1$ can be extracted from $\mathbf{z}^k$ in order to compensate for any possible delay.
- Point 6: The displacement is sent to the actuator.
- Point 7: It is time to move to the next step and the timeline depicted at the bottom of the figure moves one position to the left, so that the pantograph can reach the position sent from point 6. The indexes of Points 3 and 5 drop down a position to be ready to receive and give the right values in the next step $k+1$.

In Point 4, the PFEM's response is computed according to Eq. (1), but as explained in [15], a mathematically equivalent formulation can be used to reduce the computation time. Then, $\mathbf{z}^k$ can be equivalently obtained by considering the force increment in every time step:

$$\mathbf{z}^k = \mathbf{z}^{k-1} + \mathbf{I}_{\mathrm{cc}}(\bar{n})(\bar{f}^b(\bar{n}) - \bar{f}^{b-1}(\bar{n})) \tag{2}$$

due to the fact that only one element of vector $\mathbf{f}^k$ is changed in every time step.

3.3 Span-by-span updating

A different updating strategy is here proposed to circumvent some convergence issues. This new strategy follows the four first points listed in Section 3.2 and shown in Fig. 4, but the differences arise in Point 5. Whereas a single value of vector $\mathbf{z}^k$ was extracted in the step-by-step strategy and it would continue its way to Point 6, in the span-by-span updating strategy there is a memory rack between Points 5 and 6. Only at the time step $\bar{n} = N$ (at the end of each block) the whole vector $\mathbf{z}^k$ is extracted and its N values are stored in the memory. The stored vector is called $\mathbf{z}^b$ and it fulfils $\mathbf{z}^b = \mathbf{z}^k$ if $k = bN$. According to the proposed scheme, the displacement $\bar{z}^b(\bar{n})$ sent to the actuator in Point 6 is computed from the stored vectors $\mathbf{z}^b$ of the two previous blocks, combining both with linear shape functions to avoid lack of continuity at the beginning of a new block, i.e.:

$$\bar{z}^b(\bar{n}) = N_1(\bar{n}) z^{b-2}(\bar{n}) + N_2(\bar{n}) z^{b-1}(\bar{n}) \; ; \quad \bar{n} \in [1, N] \tag{3}$$

in which N_1 and N_2 are linear shape functions which go from 1 to 0 and from 0 to 1, respectively. This method has a different performance in terms of stability, which will be discussed in Section 4.

3.4 Delay compensation

As mentioned in Section 2, there is a consumed time in the test loop (see Fig. 2) that delays the response of the catenary. A delay of D time steps exists from the moment at which the contact force is measured in Point 2 (Fig. 4) until the pantograph reaches the position computed in Point 5. Fig. 4, represents the unavoidable delay of one step $D = 1$, but an extra delay is also considered in Point 6 of the figure by a grey arrow. If the position sent to the actuator takes the path defined by the grey arrow, it will be placed in a later position on the timeline because it will need more time steps to be achieved by the pantograph.

Note that this delay does not affect the rate of the loop, the pantograph will reach the sent position later but it does not prevent the next time step from starting. One of the main advantages of the catenary PFEM is that this delay can be easily allowed for because the contact wire height $\mathbf{z}^k$ includes the displacement values at all times n in the span. To compensate for a given delay, the position value extracted in Point 5 in Fig. 4 is thus the $n = \bar{n} + D$ indicated by the grey arrow. This procedure eliminates the error produced by the delay in the dynamic response, since at the end of the test, when convergence is achieved, $\mathbf{f}^k$ and $\mathbf{z}^k$ do not change and the value at time step $n = \bar{n} + D$ will be a perfect prediction.

3.5 Frequency content reduction

Another important aspect to consider is that we can limit the frequency content of the actuator displacement. As vector $\mathbf{z}$ is periodic, it can be shifted to the frequency domain by the discrete Fourier transform (DFT) and then the higher frequencies can be removed before being brought back to the time domain by the inverse discrete Fourier transform (IDFT).

A number of N_h frequencies (the zeroth harmonic included) are considered in this frequency reduction, f_{max} being the highest frequency included. This number plays an important role in the stability of the HIL test because if f_{max} is higher than the biggest frequency that the gear can control it will lead to deficient performance. The whole process can be done directly by applying matrix operations to $\mathbf{z}$. Let us define the DFT matrix operator as:

$$\mathbf{W} = e^{\frac{-2\pi i}{N}\mathbf{m}\mathbf{n}^\top} \qquad \text{for} \qquad \begin{matrix}\mathbf{m} = [0, 1, ..., N_\mathrm{h} - 1]^\top \\ \mathbf{n} = [0, 1, ..., N - 1]^\top\end{matrix} \tag{4}$$

With the same approach, the IDFT matrix can be obtained as:

$$\mathbf{V} = \frac{1}{N} e^{\frac{2\pi i}{N}\mathbf{n}\mathbf{m}^\top}\mathbf{A} \tag{5}$$

$\mathbf{A}$ being an $N_\mathrm{h} \times N_\mathrm{h}$ diagonal matrix with a 1 in the first element of the diagonal and a 2 in the other components, to duplicate the value of columns 2 to N_h of matrix $\mathbf{V}$ due to considering the unilateral representation of the DFT. These two operations defined in Eqs. (4) and (5) can be combined in a single matrix, i.e.:

$$\widetilde{\mathbf{W}} = \mathrm{Re}(\mathbf{V}\mathbf{W}) \tag{6}$$

Thus, to filter vector $\mathbf{z}$, Eq.(1) is multiplied by $\widetilde{\mathbf{W}}$:

$$\widetilde{\mathbf{z}} = \widetilde{\mathbf{W}}\left[\mathbf{z}_0 + \mathbf{I}_\mathrm{cc}\mathbf{f}\right] \tag{7}$$

This filtering operation can be precomputed by applying the operator $\widetilde{\mathbf{W}}$ to $\mathbf{I}_\mathrm{cc}$ and $\mathbf{z}_0$ so that Eq. (1) is rewritten as:

$$\widetilde{\mathbf{z}} = \widetilde{\mathbf{z}}_0 + \widetilde{\mathbf{I}}_{cc}\mathbf{f} \tag{8}$$

3.6 Relaxation coefficient and initial ramp

Another difference between the numerical algorithm proposed in [15] and that used to perform HIL tests relies on a relaxation coefficient μ_c to reduce the sharp change between the response of successive blocks during the iterative procedure. In Point 3 in Fig. 4, the measured force replaces the element $\bar{n}$ of $\mathbf{f}^k$, in which the measure of the previous block was previously allocated. If the relaxation is applied, the current measurement will be relaxed with the old one, resulting in:

$${}^\mathrm{r}\bar{f}^b(\bar{n}) = {}^\mathrm{r}\bar{f}^{b-1}(\bar{n}) + \mu_\mathrm{c}(\bar{f}^b(\bar{n}) - {}^\mathrm{r}\bar{f}^{b-1}(\bar{n})) \tag{9}$$

which will be allocated finally in the void. This relaxation can be included in Eq. (2)

$$\mathbf{z}^k = \mathbf{z}^{k-1} + \mu_\mathrm{c}\mathbf{I}_\mathrm{cc}(\bar{n})(\bar{f}^b(\bar{n}) - {}^\mathrm{r}\bar{f}^{b-1}(\bar{n})) \tag{10}$$

This coefficient is used to ensure convergence of the test and plays an important role in the stability of the iterative method, as explained in Section 4.

To avoid a sudden jump at the beginning of the HIL test, the height sent to the actuator is scaled by a factor that varies linearly from 0 to 1 step by step, thus defining an initial ramp that lasts N_r steps.

3.7 Considering dropper slackening

In Point 4 of the loop (see Fig. 4), Eq. (1) is used to compute the response of the catenary, given a contact force, although additional external actions can also be applied. Non-linear dropper slackening behaviour is essential to perform accurate simulations and can be considered by adding external correction forces, which depend on the elongation of the droppers, as explained in [15]. If matrix $\mathbf{I}_{cd}$ includes the stationary response of the contact point produced by a compressive force acting on both ends of dropper d, then Eq. (1) can be extended to:

$$\mathbf{z} = \mathbf{z}_0 + \mathbf{I}_{\mathrm{cc}}\mathbf{f} + \sum_{d=1}^{N_{\mathrm{d}}} \mathbf{I}_{\mathrm{c}d}\mathbf{f}_d \tag{11}$$

in which $\mathbf{f}_d$ is the correction force vector of dropper d, N_{d} is the total number of droppers. Note that $\mathbf{I}_{cd}$ rows indicate the time step of the contact point displacement and its columns are related to the time step of the dropper force application.

So far, the response of the catenary has been evaluated at the contact point only, but hereinafter the dropper elongation also needs to be computed. Let us define matrices $\mathbf{I}_{dc}$ and $\mathbf{I}_{dd}$, which account for the dropper elongation produced by the contact force and the other droppers' correction forces, respectively. The total elongation of dropper d can therefore be computed as:

$$\mathbf{\Delta L}_d = \mathbf{I}_{d\mathrm{c}}\mathbf{f} + \sum_{d=1}^{N_{\mathrm{d}}} \mathbf{I}_{dd}\mathbf{f}_d \tag{12}$$

As in $\mathbf{z}$, it is important to limit the frequency content of $\mathbf{\Delta L}_d$ in order to ease the convergence of the method. To this end, the terms involved in Eq. (12) are pre-multiplied by the matrix $\widetilde{\mathbf{W}}_d$, which is built like $\widetilde{\mathbf{W}}$ (see Section 3.5), but considering in this case a different number of harmonics N_{hd}.

In the same way that $\mathbf{f}^k$ is treated in Point 4 of the HIL loop, vector $\mathbf{f}_d^k$ is modified in each time step $\bar{n}$ by replacing the corresponding elements with the dropper forces computed in that step. As described in Section 3.6, relaxation can also be applied to $\mathbf{f}_d^k$ with a coefficient μ_{d} (See [15] for further information).

4 Stability parametric analysis

This section describes the stability of the proposed method, which depends on several factors: the catenary model, the pantograph, the frequencies included in the catenary response, the stiffness of the contact, the relaxation coefficient and the delay. For the sake of simplicity, stability is studied in a computational environment, replacing the real pantograph by a numerical model and using the *penalty* method as the contact model and performing a numerical time integration in what we call a virtual HIL test.

To study the stability it is necessary to express the problem as a linear iterative process in which the variables or state vector in any iteration can be written as a linear operation applied to the previous state. In the specific problem of a virtual HIL test, the iterative formulation has a certain complexity because the concept of iteration refers to an entire block iteration instead of a time-step iteration, so that every iteration includes the application of another iterative method to numerically integrate the dynamic response of the pantograph model.

The state vector of block b, $\mathbf{X}^b$, considers the necessary variables to compute the state vector of the next block, such as the displacement/force of the contact point in every time step, among others. This section mainly defines the iterative linear operation to analyse the stability of the method by means of the spectral radius, which can be written as:

$$\mathbf{X}^{b+1} = \mathbf{A}\mathbf{X}^b + \mathbf{B} \tag{13}$$

in which all the vectors and matrices depend on the HIL strategy followed (their definitions can be found in 6). Once the matrices in Eq. (13) are obtained, the virtual HIL test can be conducted by applying this linear operation iteratively, and the stability of the iterative procedure can be determined by the spectral radius of matrix $\mathbf{A}$.

Parametric studies are performed for the span-by-span and step-by-step approaches to analyse the stability of the proposed HIL strategy, including the influences of the number of harmonics considered in the catenary response N_h (related to the higher frequency f_{max}), and the contact stiffness k_c. We use a specific stitched catenary model (defined in Section 5) and a one-degree-of-freedom pantograph model, also considering the delay in our actual test rig. The pantograph model has a mass of 6.6 kg, a stiffness of 7000 N/m and a damping of 10 Ns/m and similar behaviour to the pantograph used in real HIL tests. The frequency of the loop is $\Delta t = 2$ ms and the delay is $D = 8$.

The spectral radius obtained by the span-by-span updating strategy is shown in Fig. 5 (a) for different f_{max} and k_c. Values bigger than 1, that indicate unstable behaviour, are hidden in white. At every point on the map, the value of the relaxation coefficient μ_c, which minimises the spectral radius, is chosen and plotted in Fig. 5 (b). The same information is shown in Fig. 6 for the step-by-step updating strategy. The solid red curve highlights the natural frequency of the pantograph model, including contact stiffness. The span-by-span approach results can be seen to be more stable, and the pantograph's natural frequency is a barrier to stability. Higher contact stiffness can therefore improve stability and it is required to reduce the number of frequencies involved in the response of the catenary model below the natural frequency related to the pantograph contact degree of freedom.

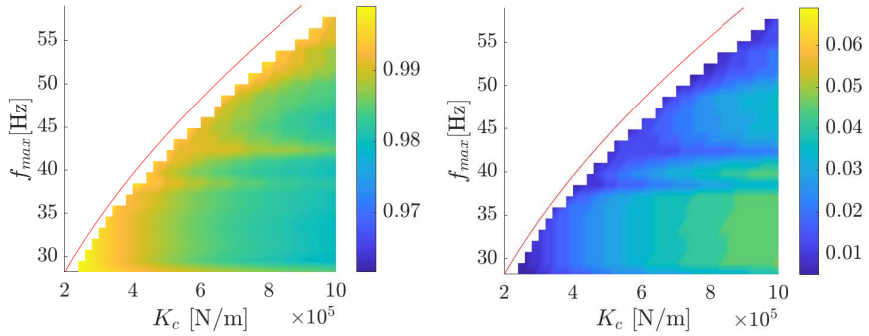

(a) *Spectral radius* **(b)** μ_c *optima*

Figure 5: *Stability analysis of the span-by-span updating scheme with delay* $D = 8$.

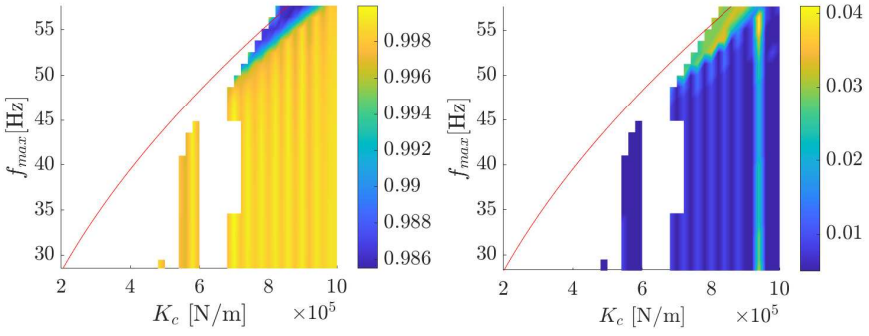

(a) *Spectral radius* **(b)** μ_c *optima*

Figure 6: *Stability analysis of the step-by-step updating scheme with delay* $D = 8$.

Unlike the span-by-span method, the delay plays a fundamental role in stability in the step-by-step strategy. Fig. 7 shows a similar representation but with a contact stiffness $k_c = 6 \cdot 10^5$ N/m and including the delay as a parameter. The figure shows a repetitive pattern of the delay, which makes possible including an additional delay to achieve a stable zone.

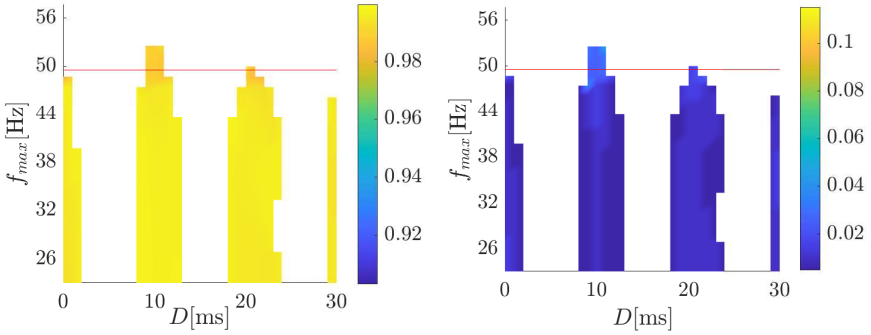

(a) *Spectral radius* **(b)** μ_c *optima*

Figure 7: *Stability analysis of the step-by-step updating scheme with contact stiffness* $k_c = 6 \cdot 10^5$ *N/m.*

5 HIL tests results

This section is devoted to the practical implementation of the HIL test and a discussion of the results. A stitched catenary [16] and a simple catenary [17] are modelled by PFEM for the numerical model, since they are the two most representative catenary types. A single span of each catenary model is depicted in Fig. 8. The time step used in all the examples studied is $\Delta t = 2$ ms and the span-by-span updating strategy was selected for stability reasons, as concluded in Section 4. Each HIL test is performed for 120 s, the initial ramp being active in the first 40 s, so that $N_r = 20000$. The relaxation coefficients are $\mu_c = 0.1$ and $\mu_d = 1$. The number of harmonics included in $\mathbf{z}$ and $\mathbf{\Delta L}$, N_h and N_{hd} respectively, are tuned to include the maximum frequency content that provides stable tests. All the results of the experimental HIL tests shown were obtained as the average of 10 spans in which the steady-state response was achieved.

Additional tests are performed to validate the accuracy of the results before the HIL tests on the pantograph.

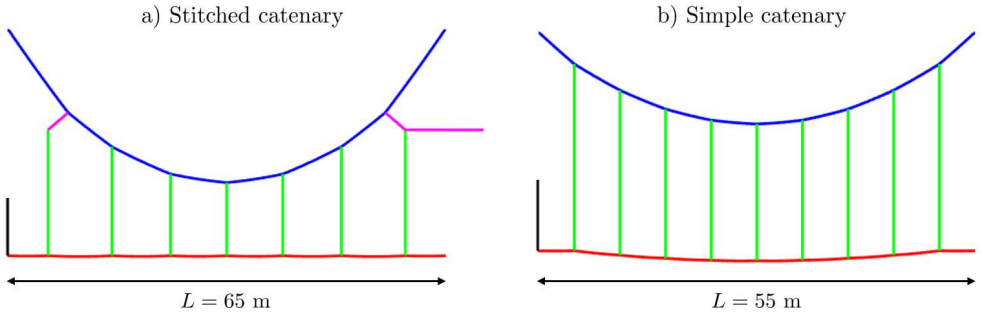

Figure 8: *a) Stitched and b) simple catenary spans for the PFEM catenary models.*

5.1 HIL test validation with an attached mass

To validate the results obtained from the HIL tests, we use the same strategy as that proposed in [18], which consists of attaching an aluminium mass directly to the load cells to take on the role of a hardware device replacing the pantograph. A photo of the assembly described with the attached mass is provided in Fig 9. The whole HIL test can be accurately simulated by computer for this scenario, which avoids the uncertainties of using a mathematical pantograph model. The results of these full HIL simulations can serve as a validation reference for the whole HIL setup (measurement, communication, computation time, delay, etc.).

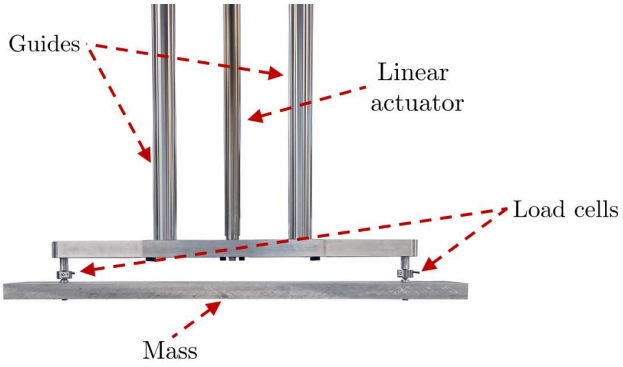

Figure 9: *Aluminium mass acting as hardware substructure for validation purposes.*

The contact force between the mass and the virtual catenary obtained from the HIL test and the simulated HIL are compared in Fig. 10. The forces represented are the mean of the ten last $\mathbf{f}^k$ when the steady state is achieved. In this example,

the simulated speed is $v = 250$ km/h (Fig. 10a) and $v = 300$ km/h (Fig. 10b) and the interaction takes place with the stitched catenary (see Fig. 8a). We used $N_\mathrm{h} = 25$ for 250 km/h and $N_\mathrm{h} = 21$ for 300 km/h to consider frequencies up to 25 Hz in both cases. A delay of $D = 8$ time steps (16 ms) was used to anticipate the reference position. The good agreement between both the experimental and simulated contact forces indicates that the HIL test rig is properly calibrated to provide accurate results.

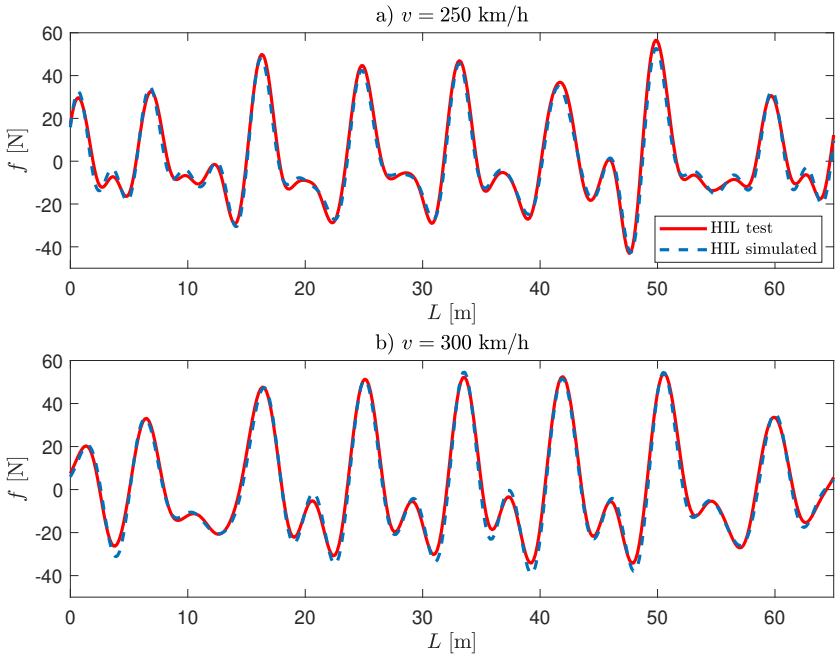

Figure 10: *Comparison of contact forces obtained from experimental HIL tests (solid line) and virtual HIL (dashed line) with the mass travelling at a) 250 km/h and b) 300 km/h.*

In the previous example any dropper could slacken, so that only the linear response of the catenary PFEM was active. To also validate the HIL test setup with nonlinear catenary behaviour, the HIL test with the mass virtually moving at 300 km/h was repeated, but now we added numerically 160 N to the force measured by the load cells. The resulting force was that applied to the virtual catenary. As can be seen in Fig. 11, not only does the contact force measured agree with that obtained from the pure simulated HIL, but the slackened dropper correction forces are also in very good agreement.

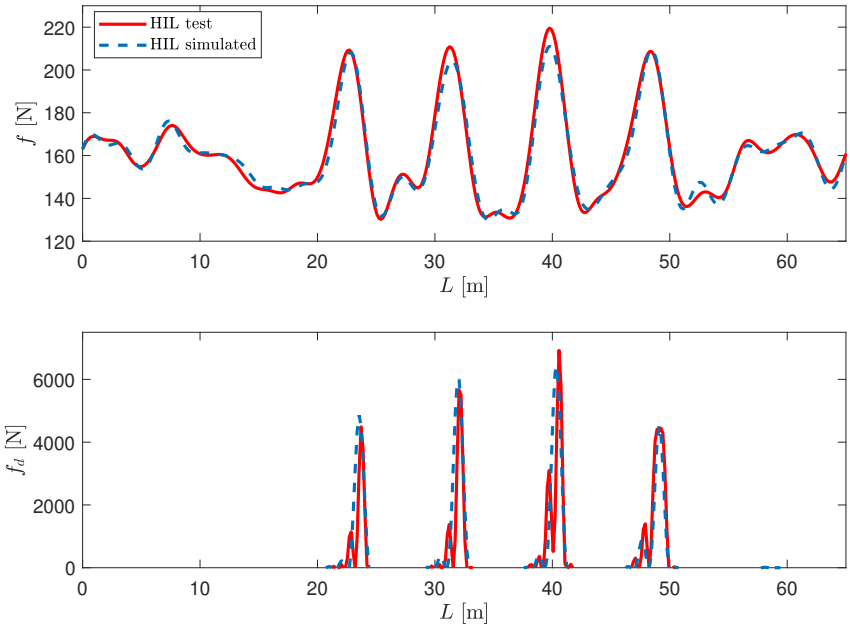

Figure 11: *Comparison of contact forces (top figure) and slackened dropper correction forces (bottom figure) obtained from experimental HIL tests (solid line) and virtual HIL simulations (dashed line) with the mass travelling at 300 km/h and a mean pushing force of 160 N.*

5.2 HIL tests with the pantograph DSA-380

This section gives the results of the HIL tests with the real pantograph DSA-380 interacting with a virtual periodic catenary. As previously mentioned, we use a PFEM of both the stitched and the simple catenaries shown in Fig. 8. The experimental results are compared in this case with the contact force obtained from a standard simulation of the pantograph-catenary dynamic interaction. We use PACDIN software [19] to perform these simulations, which participated in the benchmark exercise [17]. The catenary model simulated in PACDIN has repetitive spans and is long enough to guarantee a stationary response in its central spans to obtain comparable results. The contact force on 5 consecutive central spans is selected to make the comparisons, while the pantograph is simulated by a linear lumped mass model.

The pantograph-catenary contact force obtained from the HIL tests and PACDIN are compared in Figs. 12 and 13 with the pantograph running at 250 and 300 km/h, respectively, for both the simple and stitched catenaries. Although the HIL tests performed include the number of harmonics shown in Table 1, the contact force used in the comparisons is filtered to 25 Hz. This frequency exceeds the 20 Hz that must be considered for validation and comparison purposes in this type of simulations according to the standard [20]. The mean value of the contact force given in Table 1 is related to the train speed required to meet the criterion given in standard [21].

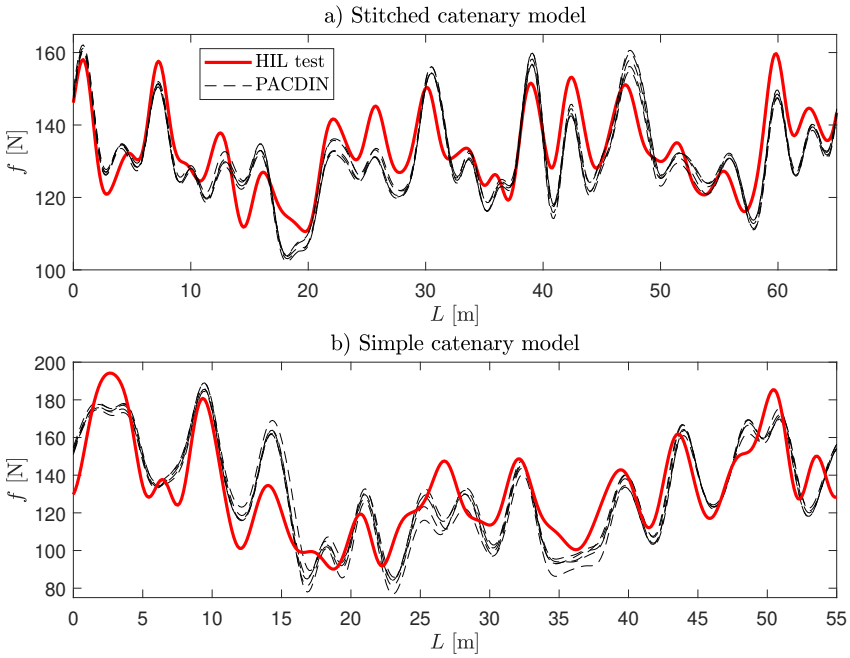

Figure 12: *Comparison of contact forces obtained from experimental HIL tests (solid line) and conventional simulation with PACDIN of the pantograph-catenary dynamic interaction (dashed line) with the pantograph running at 250 km/h and interacting with a) the stitched catenary model and b) the simple catenary model.*

Figs. 12 and 13 show that the contact forces computed on PACDIN for 5 consecutive spans overlap each other, indicating that the steady-state regime was achieved and this solution is suitable to be compared with the PFEM of the catenaries used in the HIL tests. The other important conclusion drawn from these

results is the notable similarity between the HIL tests and the standard simulation. As the HIL set-up was properly validated in Section 5.1, the discrepancies that can be seen in Figs. 12 and 13 are mainly due to the inability of the pantograph model used in PACDIN to accurately reproduce the dynamic behaviour of the real pantograph device because non-linear features such as dry friction or joint clearances are not accounted for in the model.

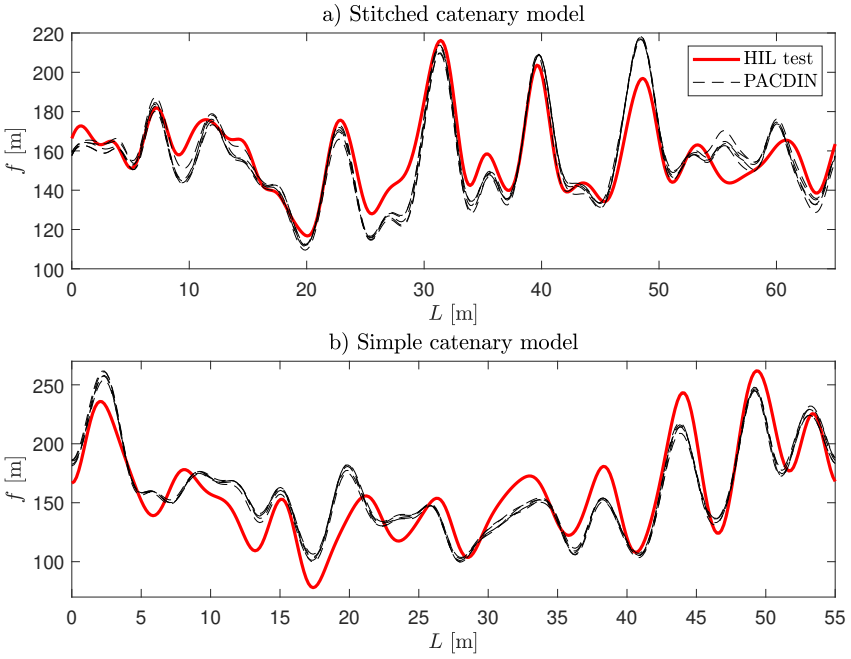

Figure 13: *Comparison of contact forces obtained from experimental HIL tests (solid line) and conventional simulation of the pantograph-catenary dynamic interaction (dashed line) with the pantograph running at 300 km/h and interacting with a) the stitched catenary model and b) the simple catenary model.*

Table 1: *Number of harmonics considered in HIL tests and mean value of contact force.*

	Stitched		Simple		
v [km/h]	N_h	N_hd	N_h	N_hd	Mean force [N]
250	31	107	25	90	≈ 130
300	27	90	22	40	≈ 157

5.3 HIL tests with optimised catenaries

HIL tests can also be applied to validate the dynamic behaviour of a given catenary model designed or tested only by numerical simulations. TeGreg2018Optim the authors proposed an optimisation of the catenary geometry to obtain the minimum standard deviation of the contact force and therefore to improve the current collection quality when the train travels at 300 km/h. However, the optimisation procedure was fully based on numerical simulations in which a lumped mass model of the pantograph was used. To remove the limitations of this simple pantograph model and validate the optimised catenary designs when interacting with a real pantograph, we perform HIL tests in this study using the catenary PFEMs derived from the optimised geometry obtained in [16]. The contact wire height at dropper connection points was optimised in the optimised catenary 1 (OC1) and dropper spacing was optimised in optimised catenary 2 (OC2) while keeping the symmetry of the span in both cases. These two optimised geometries can be seen in Fig. 14, in which the vertical scale of OC1 was tuned for a better appreciation of the contact wire height variation along the span.

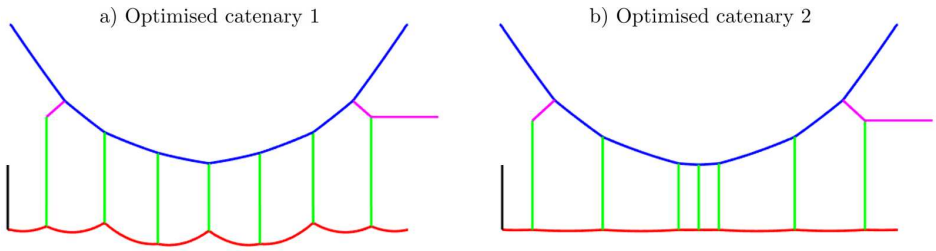

Figure 14: *PFEM models of optimised stitched catenaries at 300 km/h with a) optimal contact wire height and b) optimal dropper spacing.*

The pantograph-catenary contact force obtained in the HIL tests is plotted in Fig. 15 for both optimised catenaries and is compared with the results of numerical simulations performed with PACDIN, the software used to optimise the catenary geometry [16]. The inputs shown in Table 1 for $v = 300$ km/h are also applied in these HIL tests. The main conclusion of this section is drawn from analysing the results given in Table 2, in which the main statistical parameters of the contact force are compared in the nominal and optimised catenaries. The latter can be seen to greatly reduce the maximum value and considerably increase the minimum contact force. Furthermore, the contact force standard deviation, which is used as a current collection quality indicator, is 11.24 % and 21.87 % lower for OC1 and OC2 than that obtained from the nominal catenary. These catenary designs

therefore still behave better than the nominal design when interacting with a real pantograph, which is a further step towards the final implementation of these optimised overhead contact lines.

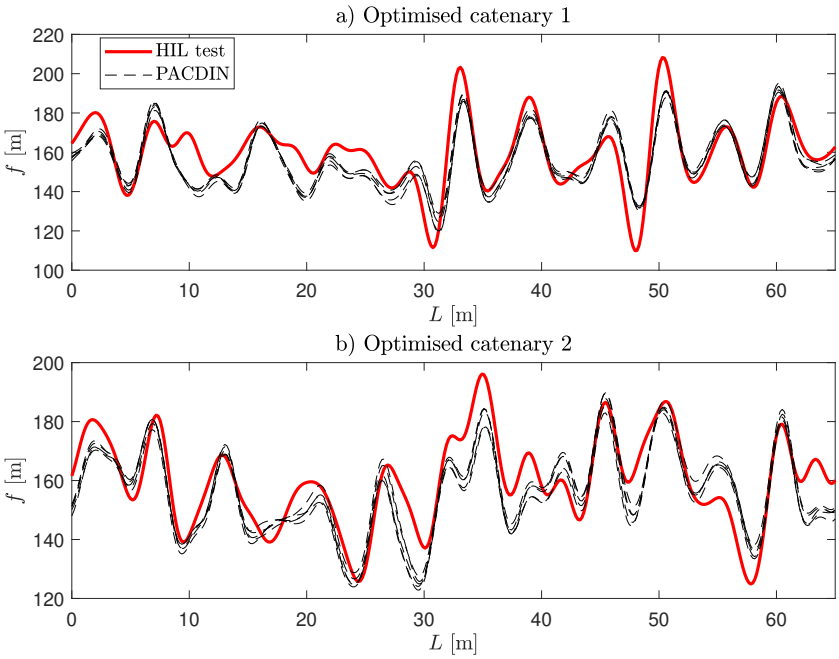

Figure 15: *Comparison of contact forces obtained from experimental HIL tests (solid line) and conventional simulation of the pantograph-catenary dynamic interaction (dashed line) with the pantograph running at 300 km/h and interacting with a) the optimised catenary model 1 and b) the optimised catenary model 2.*

Table 2: *Contact force statistical parameters obtained from HIL tests with the nominal and optimised stitched catenaries.*

	$\sigma(f)$ [N]	max(f) [N]	min(f) [N]
Nominal	19.3	261.9	78.0
Optimised 1	17.13	208.2	110.0
Optimised 2	15.08	196.1	124.9

6 Conclusions

The present work addressed the implementation of HIL pantograph tests with the use of a periodic finite element catenary model proposed in [15], although it is limited to the steady-state interaction regime, it incorporates non-linear dropper slackening behaviour and has some important advantages in performing stable HIL tests, such as the ease of tackling delays and limiting the frequency content of the response. Regarding the stability of the iterative scheme used to carry out the HIL tests, a span-by-span updating strategy was proposed and shown to be independent of delay and thus the most robust in practice.

The accuracy of the HIL setup was first validated by a mass block interacting with the virtual catenary with good agreement of the simulation and experimental results. The results of some HIL pantograph tests interacting with different catenaries and travelling at different speeds were then compared with the results of conventional dynamic simulations. The few discrepancies obtained in these comparisons can be attributed to the inability of the linear pantograph model used in the conventional simulations to reproduce the real dynamic pantograph behaviour.

Briefly, the results of the HIL pantograph tests described here offer:

- Accurate spatial discretisation of the catenary by means of the Finite Element Method.
- No boundary effects due to the periodicity condition applied.
- Ideal compensation for the delay.
- Incorporation of dropper slackening behaviour.

However, the proposed approach is limited to the steady-state regime and to considering certain particularities of actual catenaries in HIL tests, factors such as overlapping sections, local irregularities or curved paths are still a matter for further investigation.

Acknowledgements

The authors would like to acknowledge the financial support received from the State Research Agency of the Spanish Science and Innovation Ministry (PID2020-113458RB-I00) and from the Valencian Regional Government (PROMETEO/2021/046).

Bibliography

[1] W. Song, C.-M. Chang, and V. Dertimanis, "Editorial: Recent advances and applications of hybrid simulation," *Frontiers in Built Environment*, 11 2020.

[2] W. Zhang, G. Mei, X. Wu, and Z. Shen, "Hybrid simulation of dynamics for the pantograph-catenary system," *Veh. Syst. Dyn.*, vol. 38, no. 6, pp. 393–414, 2002.

[3] W. Zhang, G. Mei, X. Wu, and L. Chen, "A study on dynamic behaviour of pantographs by using hybrid simulation method," *Proc. Inst. Mech. Eng. F: J. Rail Rapid Transit*, vol. 219, no. 3, pp. 189–199, 2005.

[4] S. Gregori, M. Tur, A. Pedrosa, J. Tarancón, and F. Fuenmayor, "A modal coordinate catenary model for the real-time simulation of the pantograph-catenary dynamic interaction," *Finite Elem. Anal. Des.*, vol. 162, pp. 1–12, 2019.

[5] A. Collina, A. Facchinetti, F. Fossati, and F. Resta, "Hardware in the loop test-rig for identification and control application on high speed pantographs," *Shock Vib.*, vol. 11, pp. 445–456, 01 2004.

[6] F. Resta, A. Facchinetti, A. Collina, and G. Bucca, "On the use of a hardware in the loop set-up for pantograph dynamics evaluation," *Veh. Syst. Dyn,*, vol. 46, no. S1, pp. 1039–1052, 2008.

[7] A. Schirrer, G. Aschauer, E. Talic, M. Kozek, and S. Jakubek, "Catenary emulation for hardware-in-the-loop pantograph testing with a model predictive energy-conserving control algorithm," *Mechatronics*, vol. 41, pp. 17 – 28, 2017.

[8] H. Zhou, B. Zhang, X. Shao, Y. Tian, C. Zeng, W. Guo, and T. Wang, "Recursive predictive optimal control algorithm for real-time hybrid simulation of vehicle–bridge coupling system," *International Journal of Structural Stability and Dynamics*, vol. 22, 03 2022.

[9] T. Horiuchi, M. Inoue, T. Konno, and Y. Namita, "Real-time hybrid experimental system with actuator delay compensation and its application to a piping system with energy absorber," *Earthquake Engineering & Structural Dynamics*, vol. 28, no. 10, pp. 1121–1141, 1999.

[10] C. Chen and J. M. Ricles, "Analysis of actuator delay compensation methods for real-time testing," *Engineering Structures*, vol. 31, no. 11, pp. 2643–2655, 2009.

[11] R.-Y. Jung, P. Benson Shing, E. Stauffer, and B. Thoen, "Performance of a real-time pseudodynamic test system considering nonlinear structural response," *Earthquake Engineering & Structural Dynamics*, vol. 36, no. 12, pp. 1785–1809, 2007.

[12] D. P. Stoten, T. Yamaguchi, and Y. Yamashita, "Dynamically substructured system testing for railway vehicle pantographs," *Journal of Physics: Conference Series*, vol. 744, p. 012204, sep 2016.

[13] S. Kobayashi, D. P. Stoten, Y. Yamashita, and T. Usuda, "Dynamically substructured testing of railway pantograph/catenary systems," *Proceedings of the Institution of Mechanical Engineers, Part F: Journal of Rail and Rapid Transit*, vol. 233, no. 5, pp. 516–525, 2019.

[14] S. Kobayashi, Y. Yamashita, T. Usuda, and D. Stoten, "Hybrid simulation testing of a pantograph-catenary system using a dynamically substructured system framework and a mdof catenary model," *Quarterly Report of RTRI*, vol. 61, pp. 127–132, 05 2020.

[15] J. Gil, M. Tur, S. Gregori, A. Correcher, and F. J. Fuenmayor, "Finite element periodic catenary model to perform HIL pantograph tests considering non-linear dropper behaviour," *Submitted to Finite Elem Anal Des*, 2022.

[16] S. Gregori, M. Tur, E. Nadal, and F. J. Fuenmayor, "An approach to geometric optimisation of railway catenaries," *Vehicle System Dynamics*, vol. 56, no. 8, pp. 1162–1186, 2018.

[17] S. Bruni, J. Ambrosio, A. Carnicero, Y. H. Cho, L. Finner, M. Ikeda, S. Y. Kwon, J. P. Massat, S. Stichel, and M. Tur, "The results of the pantograph-catenary interaction benchmark," *Veh Syst. Dyn.*, vol. 53, no. 3, pp. 412–435, 2015.

[18] J. Gil, M. Tur, A. Correcher, S. Gregori, A. Pedrosa, and F. J. Fuenmayor, "Hardware-in-the-loop pantograph tests using analytical catenary models," *Veh Syst. Dyn.*, pp. 1–15, 2021.

[19] M. Tur, L. Baeza, F. Fuenmayor, and E. García, "PACDIN statement of methods," *Vehicle System Dynamics*, vol. 53, no. 3, pp. 402–411, 2015.

[20] EN 50318:2018, "Railway applications. Current collection systems. Validation of simulation of the dynamic interaction between pantograph and overhead contact line," *European Committee for Electrotechnical Standardization (CENELEC)*, 2018.

[21] EN 50367:2012, "Railway applications. Current collection systems. Technical criteria for the interaction between pantograph and overhead line," *European Committee for Electrotechnical Standardization (CENELEC)*, 2012.

Appendix A

Formulation for stability analysis

This appendix calculates the terms of Eq. (13) to carry out a virtual HIL simulation in a linear iterative process. The virtual HIL simulation is performed completely in a computational environment in which the pantograph is also simulated. As mentioned in Section 4, this is necessarily an intricate formulation as all the steps carried out for the time integration of a whole span have to be considered in the matrices of Eq. (13). The formulation changes for the two different approaches, the span-by-span and the step-by-step updating strategies.

1 Span-by-span state formulation

For the sake of simplicity and without any loss of generality, let us define the pantograph model as a single degree of freedom model, whose vertical displacement is defined as $y_{\bar{n}}^{b}$ (for a given span or block b and the time step $\bar{n}$ within this block) and arranged in vector $\mathbf{y}^{b}$. The state variables chosen for a block b are:

$$\mathbf{X}^{b} = [\mathbf{z}^{b-2} \qquad \mathbf{z}^{b-1} \qquad \dot{y}_{N}^{b-1} \qquad y_{N}^{b-1}]^{\top} \tag{A.1}$$

which includes the $\mathbf{z}^{b}$ values of the two previous spans and the displacement and velocity of the pantograph model in the last time step N of the span $b-1$. The

state variables for the next span can be computed according to Eq. (13) as:

$$\mathbf{X}^{b+1} = \mathbf{A}\mathbf{X}^{b} + \mathbf{B} \tag{A.2}$$

To build the matrices $\mathbf{A}$ and $\mathbf{B}$ it is necessary to assemble all the linear operations that happen in the block b. The vertical position $\bar{z}^b(\bar{n})$ or $\bar{z}^b_{\bar{n}}$ of the contact point which will be imposed throughout the block b can be computed from the state vector with Eq. (3). The displacement $\mathbf{y}^b$ of the pantograph model, excited by $\bar{z}^b_{\bar{n}}$, can be obtained using a discrete-time integration scheme. For example, if the Newmark method is chosen, it can be expressed as:

$$\left[\begin{array}{c} \dot{y} \\ y \end{array}\right]^b_{\bar{n}} = \hat{\mathbf{A}} \left[\begin{array}{c} \dot{y} \\ y \end{array}\right]^b_{\bar{n}-1} + \hat{\mathbf{B}}\ \bar{z}^b_{\bar{n}-1} + \hat{\mathbf{C}}\ \bar{z}^b_{\bar{n}} \tag{A.3}$$

If this iterative scheme is applied recursively from the first time step of the span until a given step $\bar{n}$, it results in:

$$\left[\begin{array}{c} \dot{y} \\ y \end{array}\right]^b_{\bar{n}} = \hat{\mathbf{A}}^{\bar{n}} \left[\begin{array}{c} \dot{y} \\ y \end{array}\right]^{b-1}_{N} + \sum_{j=1}^{\bar{n}} \hat{\mathbf{A}}^{\bar{n}-j} \left(\hat{\mathbf{B}}\ \bar{z}^b_{j-1} + \hat{\mathbf{C}}\ \bar{z}^b_{j}\right) \tag{A.4}$$

By rearranging Eq. (A.4), $\mathbf{y}^b$ can be obtained from the linear relation with the state vector:

$$\left[\begin{array}{c} \dot{\mathbf{y}}^b \\ \mathbf{y}^b \end{array}\right] = \left[\begin{array}{c} \mathbf{Q}_1 \\ \mathbf{Q}_2 \end{array}\right] \mathbf{X}^b \tag{A.5}$$

The measured contact force ($\bar{f}^b(\bar{n})$ arranged in the vector $\bar{\mathbf{f}}^b$) comes from the *penalty* method equation and again, a linear relation can be established:

$$\bar{\mathbf{f}}^b = k_c(\mathbf{y}^b - \bar{\mathbf{z}}^b) \equiv \mathbf{R}\mathbf{X}^b \tag{A.6}$$

As described in the span-by-span updating strategy (see Section 3.3), in point 5 of Fig. 4, the vector $\mathbf{z}^b$ is fully defined when $\bar{n} = N$, time step in which $\mathbf{f}^k = \bar{\mathbf{f}}^b$. Thus, according to Eq. (1):

$$\mathbf{z}^b = \mathbf{z}_0 + \mathbf{I}_{\mathrm{cc}}\bar{\mathbf{f}}^b \tag{A.7}$$

Additionally, as the force has not been included in the state vector, the relaxation coefficient can be applied here equivalently:

$$\mathbf{z}^b = \mu_{\mathrm{c}}(\mathbf{z}_0 + \mathbf{I}_{\mathrm{cc}}\bar{\mathbf{f}}^b) + (1-\mu_{\mathrm{c}})\mathbf{z}^{b-1} \equiv \mathbf{S}\mathbf{X}^b + \mu_{\mathrm{c}}\mathbf{z}_0 \tag{A.8}$$

The state vector of the next span can be built as:

$$\mathbf{X}^{b+1} = [\mathbf{z}^{b-1} \;\; \mathbf{z}^{b} \;\; \dot{y}_N^b \;\; y_N^b]^\top = [\mathbf{z}^{b-1} \;\; \mathbf{S}\mathbf{X}^b + \mu_c \mathbf{z}_0 \;\; \mathbf{Q}_1|_N \mathbf{X}^b \;\; \mathbf{Q}_2|_N \mathbf{X}^b]^\top \quad \text{(A.9)}$$

in which $|_N$ refers to the N row.

So far, the delay has not been considered but its unavoidable existence in a real HIL test affects its stability. The formulation can then be modified to consider a delay of D time steps in the imposed displacement $\bar{z}^b(\bar{n})$, affecting Eq. (3):

$$\bar{z}^b(\bar{n}) = \begin{cases} N_1(m) z^{b-3}(m) + N_2(m) z^{b-2}(m) & \text{if } \bar{n} \leq D \\ N_1(\bar{n}-D) z^{b-2}(\bar{n}-D) + N_2(\bar{n}-D) z^{b-1}(\bar{n}-D) & \text{if } \bar{n} > D \end{cases} \quad \text{(A.10)}$$

being $m = N + \bar{n} - D$ and therefore, at least the last D values of $\mathbf{z}^{b-3}$ should be included in the state. As the delay in the HIL test is known, the compensation can be applied by defining $\mathbf{z}^b$ as:

$$\mathbf{z}^b = [z(N-D+1) \;\; z(N-D+2) \;\; \ldots \;\; z(N) \;\; z(1) \;\; z(2) \;\; \ldots \;\; z(N-D)]^\top \quad \text{(A.11)}$$

2 Step-by-step state formulation

The stability of the HIL iterative procedure depends on the updating strategy followed. In this section, we describe the procedure to obtain the iterative linear operation that applies between consecutive spans for the step-by-step approach. In this case, the state variables vector includes the displacement imposed in the last step of the previous block, the relaxed force of the previous block and the velocity and displacement of the pantograph model in the last step of the previous block, respectively. That is:

$$\mathbf{X}^b = [\bar{z}_N^{b-1} \qquad {}^{\mathrm{r}}\bar{\mathbf{f}}^{b-1} \qquad \dot{y}_N^{b-1} \qquad y_N^{b-1}]^\top \quad \text{(A.12)}$$

Now the displacement $\bar{\mathbf{z}}^b$ of the contact point imposed comes from Eq. (1), taken by considering that the vector $\mathbf{f}^k$ is made up of values of the contact force from both the previous and the current block:

$$\bar{\mathbf{z}}^b = \mathbf{z}_0 + \mathbf{T}\bar{\mathbf{f}}^b + \mathbf{U}^{\mathrm{r}}\bar{\mathbf{f}}^{b-1} \equiv \mathbf{z}_0 + \mathbf{T}\bar{\mathbf{f}}^b + \mathbf{V}\mathbf{X}^b \quad \text{(A.13)}$$

in which $\mathbf{T} = \mu_c \mathbf{I}_{cc} \mathbf{W}$ and $\mathbf{U} = \mathbf{I}_{cc} - \mathbf{T}$ with:

$$\mathbf{W} = \begin{bmatrix} 0 & 0 & 0 & \cdots \\ 1 & 0 & 0 & \cdots \\ 1 & 1 & 0 & \cdots \\ \vdots & \vdots & \vdots & \ddots \end{bmatrix} \tag{A.14}$$

Eq. (A.4) provides the pantograph model displacement $\mathbf{y}^b$ produced by $\bar{\mathbf{z}}^b$ and this equation can be written as:

$$\mathbf{y}^b = \mathbf{Y}\bar{\mathbf{z}}^b + \mathbf{Z}\mathbf{X}^b \tag{A.15}$$

Eqs. (A.6), (A.13) and (A.15) form a linear system whose unknowns are $\bar{\mathbf{f}}^b$, $\bar{\mathbf{z}}^b$ and $\mathbf{y}^b$. Once solved, the state variables of the next span can be built as:

$$\mathbf{X}^{b+1} = [\bar{z}_N^b \quad {}^{\mathrm{r}}\bar{\mathbf{f}}^b \quad \dot{y}_N^b \quad y_N^b]^\top \tag{A.16}$$

in which ${}^{\mathrm{r}}\bar{\mathbf{f}}^b = \mu_c \bar{\mathbf{f}}^b + (1-\mu_c) {}^{\mathrm{r}}\bar{\mathbf{f}}^{b-1}$. A delay of D time steps and its compensation can be added to the formulation as in the span-by-span updating strategy.